MEASUREMENTS AND LINEAR WAVE THEORY BASED SIMULATIONS OF VEGETATED WAVE HYDRODYNAMICS FOR PRACTICAL APPLICATIONS

A Thesis

by

MARY ELIZABETH ANDERSON

Submitted to the Office of Graduate Studies of
Texas A&M University
in partial fulfillment of the requirements for the degree of

MASTER OF SCIENCE

August 2010

Major Subject: Ocean Engineering

MEASUREMENTS AND LINEAR WAVE THEORY BASED SIMULATIONS OF VEGETATED WAVE HYDRODYNAMICS FOR PRACTICAL APPLICATIONS

A Thesis

by

MARY ELIZABETH ANDERSON

Submitted to the Office of Graduate Studies of
Texas A&M University
in partial fulfillment of the requirements for the degree of

MASTER OF SCIENCE

Approved by:

Chair of Committee,	Jennifer Irish
Committee Members,	James Kaihatu
	Jane McKee Smith
	Daniel Thornton
Head of Department,	John Niedzwecki

August 2010

Major Subject: Ocean Engineering

ABSTRACT

Measurements and Linear Wave Theory Based Simulations of

Vegetated Wave Hydrodynamics for Practical Applications. (August 2010)

Mary Elizabeth Anderson, B.S., Mississippi State University

Chair of Advisory Committee: Dr. Jennifer Irish

Wave attenuation by vegetation is a highly dynamic process and its quantification is important for accurately understanding and predicting coastal hydrodynamics. However, the influence of vegetation on wave dissipation is not yet fully established nor implemented in current hydrodynamic models. A series of laboratory experiments were conducted at the Haynes Coastal Engineering Laboratory and in a two-dimensional flume at Texas A&M University to investigate the influence of relative vegetation height, stem density, and stem spacing uniformity on wave attenuation. Vegetation fields were represented as random cylinder arrays where the stem density and spatial variation were based on collected field specimens.

Experimental results indicate wave attenuation is dependent on relative vegetation height, stem density, and stem spacing standard deviation. As stems occupy more of the water column, an increase in attenuation occurred given that the highest wave particle velocities are being impeded. Sparse vegetation fields dissipated less wave energy than the intermediate density; however, the extremely dense fields dissipated very little, if any, wave energy and sometimes wave growth was observed.

This is possibly due to the highest density exceeding some threshold where maximum wave attenuation capabilities are exceeded and lowering of damping ensues. Additionally, wave attenuation increased with higher stem spatial variation due to less wake sheltering.

A one-dimensional model with an analytical vegetation dissipation term was developed and calibrated to these experimental results to capture the wave transformation over the vegetation beds and to investigate the behavior of the vegetation field bulk drag coefficient. The best fit between predicted and measured wave heights was obtained using the least squares method considering the bulk drag coefficient as the single calibration parameter.

The model was able to realistically capture the wave transformations over vegetation. Upon inspection, the bulk drag coefficient shared many of the dependencies of the total wave dissipation. The bulk drag coefficient increased with larger relative vegetation heights as well as with higher stem spacing standard deviation. Higher densities resulted in a lowering of the bulk drag coefficient but generally an increase in wave attenuation. These parameters and their influences help in identifying the important parameters for numerical studies to further our understanding of wave attenuation by wetlands.

ACKNOWLEDGEMENTS

First and foremost, I would like to thank my committee chair, Dr. Jennifer Irish, for providing me the opportunity to work as a graduate research assistant and introducing me to coastal engineering. It is because of her that my love for coastal engineering has grown and I look forward to applying this dedication to both experimental and modeling solutions for current coastal issues. Without her enthusiasm, dedication, guidance, and tolerance for numerous meetings, this project would not have been possible. I would also like to thank my committee members, Dr. James Kaihatu, Dr. Jane Smith, and Dr. Daniel Thornton for their guidance, support, and comments throughout the course of my graduate career. Special thanks are required for Cynthia Vittone and Charles Babbit for moving plywood, drilling hundreds of holes by hand, running numerous wave tests, and keeping me company in the laboratory. Without them, I would have never been able to reach my research goals in time and I appreciate them taking time out of their busy class schedules to help me. I would also like to thank Po-H. Yeh and John Reed for their technical guidance in both the Haynes Coastal Engineering Laboratory and Civil Laboratory. I would like to thank my parents for encouraging me to take risks, to stay strong, and to pursue what I love to do. Finally, I would like to express my utmost appreciation to all my friends in Ocean Engineering. They served as a solid foundation of support as well as encouraged me to enjoy my time in graduate school, and it is with them I have created fond memories for a lifetime.

NOMENCLATURE

$\tilde{k}$	Complex wave number
$\hat{\zeta}$	Amplitude of stem horizontal displacement
F_x^1	Force exerted by a single element
$\tilde{C}_D$	Individual stem drag coefficient
a	Cross-sectional area of body perpendicular to flow
A	Wave amplitude
A_0	Incident wave amplitude
ADV	Acoustic Doppler velocimeter
B	Breaking tuning parameter
C_D	Bulk drag coefficient
C_{Dcal}	Calibrated bulk drag coefficient
CFR	Codes of Federal Regulation
C_g	Group velocity
C_M	Inertia coefficient
C_P	Plant drag coefficient
d	Average stem diameter
E	Wave energy density
EI	Stem bending stiffness
f	Friction factor

F_a	Adjusted fetch length
F_D	Drag force
f_{DW}	Darcy-Weisbach friction factor
F_e	Equivalent fetch length
F_I	Inertia force
f_p	Peak frequency
F_{tot}	Total fetch length
F_x	Total horizontal force per unit volume
F_z	Total vertical force per unit volume
g	Gravitational acceleration
h	Water depth
H	Local wave height
H_0	Incident wave height
H_b	Breaking wave height
H_{rms}	Root-mean-square wave height
H_{rms0}	Incident root-mean-square wave height
H_s	Significant wave height
$H_{s,max}$	Maximum significant wave height
h_{veg}	Water depth at the beginning of the vegetation field
h_{wm}	Water depth at the wavemaker
k	Wavenumber
K	Keulegan-Carpenter number

K_f	Bottom friction coefficient
k_i	Exponential decay coefficient
K_p	Percolation coefficient
k_r	Real component of complex wave number
K_s	Shoaling coefficient
K_v	Viscous friction coefficient
L	Wavelength
l_s	Average stem length
m_0	Area under spectral curve
n	Ratio between group speed and celerity
N	Average stem density
OTRC	Offshore Technology Research Center
Q	Modified Keulegan-Carpenter number
Q_b	Fraction of broken waves
$\mathrm{Re_d}$	Stem Reynolds number
t	Time
T	Wave period
T_p	Peak period
t_v	Stem thickness
u	Horizontal particle velocity
u_b	Bottom orbital velocity
u_r	Relative velocity between particle and vegetation velocity

u_v	Stem swaying velocity
V	Body's volume
w	Vertical particle velocity
x	Horizontal coordinate
x_p	Total propagation distance
z	Vertical coordinate
γ_b	Breaking tuning parameter
Δs	Average stem spacing
Δx	Cross-shore width of vegetation field
δ_ζ	Phase shift
ε	Energy dissipation
ε_B	Wave breaking dissipation
ε_v	Time-averaged vegetation-induced energy dissipation
ζ	Stem horizontal displacement
κ	Breaker index
κ_{cal}	Calibrated breaker index
ρ	Fluid density
ρ_v	Plant material density
σ	Standard deviation of stem spacing
τ	Ensemble interaction coefficient
τ_0	Bed shear stress amplitude
υ	Kinematic viscosity

Φ	Velocity potential
ω	Wave angular frequency

TABLE OF CONTENTS

CHAPTER Page

LIST OF FIGURES

FIGURE Page

FIGURE Page

FIGURE Page

LIST OF TABLES

CHAPTER I

INTRODUCTION

1.1. Motivation and Objectives

Although describing flow in wetland vegetation is an important component of coastal hydrodynamics, the influence of vegetation is not fully quantified nor implemented in wave and hydrodynamic models. Standard practice in these models is to account for momentum loss and energy dissipation using a bottom friction term such as Manning's *n*. However, according to *Kadlec* (1990), the Manning formulation does not accurately describe flow through wetlands. The Manning equation is used to describe turbulent open-channel flow, but the flow in wetlands is generally transitional due to smaller slopes and water depths. Additionally, while Manning's *n* is appropriate in cases where bottom drag dominates, this approximation does not fully capture the impact of vegetation since vegetation drag impedes flow throughout the water column rather just along the sea bottom.

Due to the limitations of current modeling practices in describing vegetation-wave interactions, the objectives of this research are to investigate the influence of coastal vegetation on wave dynamics in the laboratory and develop a one-dimensional wave transformation model to simulate the experimental results. Laboratory flume experiments were used to gather data on monochromatic wave propagation through artificial vegetation. Vegetation fields were represented as random cylinder arrays where the density and spacing standard deviations were based on field specimens

---

This thesis follows the style of the *Journal of Geophysical Research*.

collected from wetlands in Galveston, Texas by *Feagin et al.* (in review). Following the experiments, an analytical wave dissipation formula for vegetation developed by *Dalrymple et al.* (1984) was implemented into a one-dimensional wave model based on linear wave theory in order to replicate the experimental results.

The equation derived by *Dalrymple et al.* (1984) for the time-average energy dissipation due to vegetation (ε_V) is the following:

$$\left\langle \varepsilon_V \right\rangle = \frac{2}{3\pi} \rho C_D N d \left(\frac{gk}{\omega} \right)^3 \frac{\left(\sinh^3 kl_s + 3\sinh kl_s \right)}{3k \cosh^3 kh} A^3 \tag{1.1}$$

where ρ is fluid density, C_D is the bulk or average drag coefficient within a vegetation field, N is average stem density, d is stem diameter, g is gravity, k is the wavenumber, ω is wave angular frequency, l_s is average stem length, and A is wave amplitude. This formulation was selected for a number of reasons. First, one of the derivation's inherent assumptions is approximating plant stems as rigid, vertical cylinders, which matches the artificial vegetation in the experiment. Secondly, the formulation is applicable to submerged as well as emergent vegetation conditions. Lastly, the *Dalrymple et al.* (1984) formulation is a reasonable representation of wave dissipation due to vegetation as well as being feasible for implementation.

1.2. Overview of Wetlands

In order to understand the motivation for the research herein, an overview of the wetland ecosystem must be provided. The United States Environmental Protection Agency defines wetlands under Title 40 of the Codes of Federal Regulation (CFR) as areas that are inundated or saturated by water all year or varying periods of the year that

sufficiently support vegetation suited for saturated soil conditions (*CFR*, 2010). In the United States, coastal or tidal wetlands serve as the interfaces between dry land and the Atlantic, Pacific, Alaskan, and Gulf coasts and are the focus of this discussion. A tidal wetland in Galveston Island State Park, Texas is shown below in Figure 1:

Figure 1. Example of a coastal wetland in Galveston, Texas (taken July 2008)

Typically, these wetlands experience varying local salinity levels due to tidal action and unsteady mixing between freshwater inflows and saltwater. While known by many other names, wetlands generally include bogs, fens, marshes, and swamp forests.

Wetlands are one of the most productive ecosystems, providing a variety of natural resources for animals and humans alike. In addition to providing shelter, migration destinations, and breeding grounds for many species, these areas are rich in coastal plants and small aquatic wildlife like insects, crustaceans, and fish that serve as food for larger predators such as birds and mammals. Many of the nation's industries

also benefit from the high productivity of coastal wetlands. These industries harvest annually shellfish, fish, timber, and fruit as well as pelts from mammals such as muskrats and beavers. In 2002, over 453,600 metric tons (1 billion pounds) of shellfish and fish valued at $343 million were harvested from Louisiana's coastal wetlands alone (*United States Environmental Protection Agency*, 2006). Wetlands also possess aesthetics and support recreational activities such as hunting, fishing, camping, bird watching, photography, and painting.

1.3. Benefits of Wetlands

In addition to economical and ecological benefits, wetlands offer at least three potential benefits relating to coastal engineering and coastal protection. These are the following: (1) surge reduction, (2) shoreline stabilization, and (3) damping of propagating water waves. Wave attenuation is the focus of this thesis and a complete literature review is presented herein in Chapter II.

Dangerous flooding resulting from hurricanes and other extreme storm impacts is an eminent risk in the coastal zones. These coastal areas are typically of low elevation and are relatively flat, making land and infrastructure highly susceptible to flooding. Although hard protection structures such as levees and floodwalls reduce the risk of flooding, these structures are typically located immediately outside the effected area. Since coastal wetlands often serve as transition zones from the open coasts to dry land, it is a general belief that wetlands could act as a substantial buffer by decreasing storm surge before it reaches coastal infrastructure. It is believed that wave setup, a main component of storm surge defined as the superelevation of the mean water level, would

decrease because of vegetation. Wave setup results from the transfer of wave momentum from breaking waves to the water column (*Dean and Dalrymple*, 2004). However, given that the leading edge of the storm would initially encounter the vegetation field, propagating waves would lose energy as they moved through the vegetation which inhibits wave breaking. *Dean and Bender* (2006) applied linear wave theory in the shallow water limit to show wave setup would be reduced by 2/3 due to vegetation. This decrease in wave setup directly translates to a smaller storm surge and, thus, lower flood levels. Unfortunately, the capability of wetlands to serve as soft protection for the coasts during extreme storms is not yet established though a moderate amount of publications exist documenting vegetation-induced wave attenuation as given in Chapter II.

Additionally, the coastal plants comprising wetlands assist in reducing erosion effects along oceans and bays. The roots of these coastal plants form a dense sediment/root matrix, stabilizing the sediment grains and reducing their transport (*Dean,* 1979). This stabilization process is directly observed in the formation of vegetative headlands along bays as seen below in Figure 2. These protruding headlands result from increased resistance to erosion due to being heavily vegetated. Additionally, *Dean* (1979) noted vegetation helps prevent the transport of sand inland by provided enhanced storage in nearshore dunes.

The capability of wetlands to alleviate erosion has been investigated by a number of researchers, two of which are *Neumeier and Ciavola* (2004) and *Türker et al.* (2006). *Neumeier and Ciavola* (2004) collected detailed velocity profiles within *Spartina*

alterniflora salt marshes to study the flow alterations caused by vegetation. *Neumeier and Ciavola* (2004) found the *Spartina* canopies served as substantial erosion protection during storms. In controlled laboratory flume experiments, *Türker et al.* (2006) examined the morphological changes of a beach profile under the protection of emergent vegetation. *Türker et al.* (2006) concluded that, in general, as the area of the beach profile occupied by vegetation increased, the area of erosion decreased considerably.

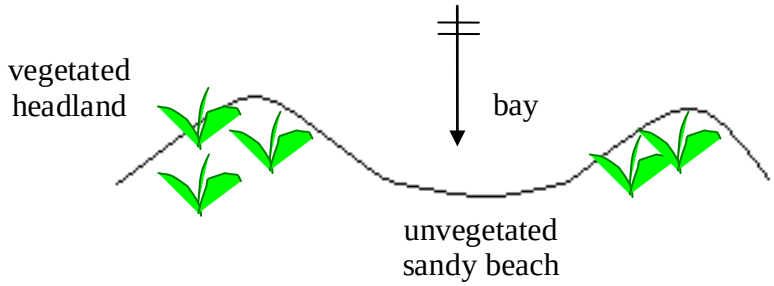

Figure 2. Formation of vegetative headlands (modified from *Dean*, 1979)

The context of this thesis focuses on wave attenuation. Wave attenuation occurs as waves propagate through a vegetation field due to the drag force exerted on the waves by individual stems. At the marsh-scale, the interaction between waves and vegetation is dependent on wave conditions, such as incident wave height, period, and water depth, and vegetation parameters, such as stem density, stem length, and rigidity. The vegetation-wave problem also exists at the stem-scale such that stem spatial variation alters flow patterns due to wakes generated by individual stems and branches (*Nepf*, 2004). The interaction between waves and vegetation is highly dynamic and better understanding and modeling of wave transformation over vegetation is highly desirable

in coastal engineering practices.

1.4. Thesis Content

The thesis is divided into six chapters. Chapter I presents the motivations behind this research and the importance of wetlands in coastal engineering. The motivations and objectives for this thesis are presented in Section 1.1 while Section 1.2 and 1.3 introduce wetlands and the potential benefits of wetlands to serve as coastal protection, respectively. Chapter II contains an extensive literature review whereby the first section presents experimental studies of wave attenuation over vegetation and the second section contains vegetation dissipation equations for water waves. Chapter III presents the experimental methods for this thesis. Section 1.1 provides a brief overview of the methodology with details of the constructed vegetation fields in Section 2.1. Section 3.1 details the physical model setups in the Haynes Coastal Engineering Laboratory and the two-dimensional wave flume, and Section 4.1 focuses on instrumentation and data acquisition. Chapter IV presents the experimental results for both studies and addresses the influence of relative vegetation height, stem density, and stem spacing standard deviation on wave attenuation. Chapter V introduces the governing equations of the one-dimensional model in Section 1.1 with model sensitivity and calibrated values of the bulk drag coefficient presented in Section 2.1 and 3.1, in that order. The dependence of the bulk drag coefficient on vegetation parameters is included in this section. Finally, conclusions and recommendations for future research are presented in Chapter VI.

CHAPTER II

BACKGROUND AND LITERATURE REVIEW

2.1. Introduction

Coastal vegetation is known to dissipate wave energy as documented and quantified in numerous field and laboratory studies (*Knutson et al., 1*982; *Fonseca and Cahalan,* 1992; *Løvås and Tørum,* 2000*; Möller and Spencer,* 2002; *Cooper,* 2005*; Möller,* 2006, *Augustin,* 2007*).* As gravity waves propagate through submerged and emergent vegetation, they lose energy by performing work on the vegetation stems, resulting in a reduced wave height (*Dalrymple et al.,* 1984). Wave attenuation by vegetation is a function of vegetation characteristics such as geometry, buoyancy, density, stiffness, and spatial coverage as well as hydrodynamic conditions such as incident wave height, wave period, and direction. Vegetation-wave interactions are highly dynamic in that the vegetation field is exposed to variable wave forcing and changes with time as stems bend or flatten to the bed. As evidenced by these many dependencies and the extensive variety of coastal plants, the variability of wave damping by vegetation is large (*Mendez and Losada,* 2004).

Numerous models and extensions of these models exist attempting to link the interactions between vegetation and waves (*Camfield,* 1977; *Dean,* 1979; *Knutson et al.,* 1982; *Dalrymple et al.,* 1984; *Asano et al.,* 1992; *Kobayashi et al.,* 1993; *Mendez and Losada,* 1999; *Möller et al.,* 1999, *Mendez and Losada,* 2004; *Lima et al.,* 2006). Figure 3 below is a diagram of typically used parameters in vegetation modeling where Δs is average stem spacing, d is average stem diameter, l_s is average stem length, N is the

average number of stems per unit area (average stem density), F_x is total horizontal force per unit volume on a stem array, and h is water depth.

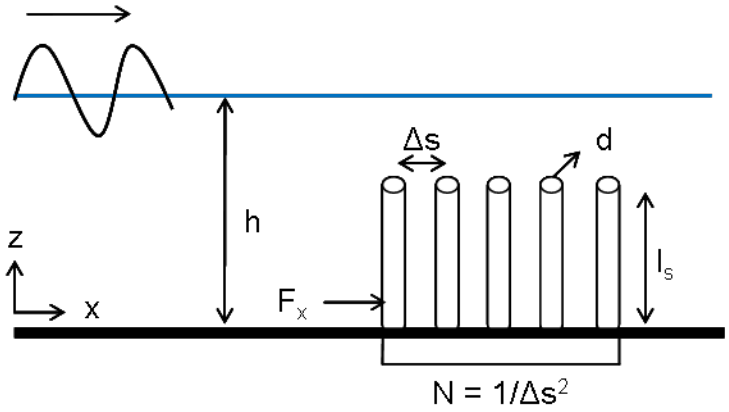

Figure 3. Vegetation modeling parameters (modified from *Dean and Bender*, 2006)

To provide a background of vegetation-induced wave attenuation, experimental results of wave damping by coastal and artificial vegetation (Section 2.2), vegetation-wave model formulations (Section 2.3), a focus on the physical properties of the bulk drag coefficient (Section 2.4), and a summary of the literature review and how it pertains to the context of this thesis (Section 2.5) are presented in this chapter.

2.2. Experimental Results of Wave Dissipation by Coastal and Artificial Vegetation

The effects of vegetation on wave-induced flows have been investigated in field and laboratory flume studies with natural vegetation and artificial vegetation simulated by various elements. *Knutson et al.* (1982) quantified wave damping in two smooth cordgrass (*Spartina alterniflora*) marshes in the Chesapeake Bay. For both locations, transects perpendicular to the shoreline were established and wave data was collected for

10 minutes along these transects at two gauges, one gauge located offshore of the marsh and the second located at a distance of 2.5, 5, 10, 20, or 30 m landward of the first. Shore parallel waves were generated by a research vessel, and wave heights ranging from 0.06 to 0.30 m were determined by averaging the three highest waves for each boat passing. Experimental results showed a substantial decrease in wave height as the waves propagated through the smooth cordgrass with 50% of the wave height dissipated within the first 2.5 m and a 94% wave height reduction at the end of the considered 30 m length. These damped waves impacted the shoreline with less energy, potentially altering coastal processes, such as sedimentation rather than erosion. *Knutson et al.* (1982) acknowledged emergent vegetation was most effective, as it impeded flow throughout the entire water column, noting in the case of extreme storms such as hurricanes, vegetation-induced dissipation will be considerably smaller as water depth exceeds canopy height.

The ability of four common North American seagrass species (*Halodule wrightii*, *Syringodium filiforme*, *Thalassia testudinum*, and *Zostera marina*) to dissipate wave energy was investigated by *Fonseca and Cahalan* (1992) in a laboratory flume study. Sods were harvested from natural habitats, and each species' density was based on field conditions. Relatively independent of plant species and density, a 40% wave energy reduction was observed over the 1 m transect when the water depth approximately equaled the plant height. As the water depth increased and the plants became submerged, the effectiveness of all the considered seagrass species to dissipate wave energy decreased.

Although coastal vegetation is shown by *Knutson et al.* (1982) and *Fonseca and Cahalan* (1992) to be effective in damping waves, an extensive field study conducted in southern California by *Elwany et al.* (1995) with giant kelp (*Macrocystis pyrifera*) suggested shoreward propagating waves were unaffected by these giant kelp beds. The measurable difference between wave height dissipation at the control and kelp locations was insignificant. Numerical modeling of the control and kelp sites indicated bathymetry-induced wave transformations were similar at both locations, eliminating the coincidence that kelp-induced wave damping compensated for bathymetry differences between sites. A further discussion provided by *Seymour* (1996) suggested the velocity difference between the kelp and the waves was very small because the flexible plants approximately followed the orbital motion of the waves. This motion reduced the drag exerted on the waves by the plants, and thus, reduced the giant kelp's effectiveness to attenuate propagating waves.

Using a laboratory flume, *Løvås and Tørum* (2000) investigated the effects of submerged, simulated *Laminaria hyperborea* kelp on wave damping and run-up for random waves. The physical model was constructed with a 1:30 sloping bottom, and a stem density of 12 stems per m^2 with uniform distribution was considered for the 7.27 m kelp field. From visual observations, the kelp field suppressed wave breaking and lowered wave celerity. When kelp was present, maximum wave height reduction initiated in deeper water and spectral zero-moment wave energy was reduced as much as 40%. Wave setup, a component of runup which is defined by *Sorensen* (2006) as the maximum vertical extent of wave uprush on a shoreline or structure, was significantly

smaller with kelp in the flume, and maximum runup with kelp was 53 to 66% of the value without kelp. Kelp also reduced the highest runup uprush velocities. Though not addressed in this study, by reducing runup elevation and velocities, *Løvås and Tørum* (2000) proposed swash forces leading to dune erosion and overtopping may be reduced when kelp is present.

Möller and Spencer (2002) investigated spatial and temporal variability in wave height dissipation by unvegetated mudflats and saltmarshes on the Dengie Peninsula in Essex, UK by assessing differences in dissipation along the marsh fringe, within the marsh interior, and due to seasonal changes in vegetation growth and structure. Two marsh sites were considered for 10 months, Tillingham and Bridgewick. Tillingham was characterized by a sloping bottom while Bridgewick was characterized by a mudflat with an abrupt transition to a vegetated cliff 1.5-2.0 m high. At Tillingham, significant wave height (H_s) attenuation was 0.14% per m over the mudflat and 0.54% per m over the saltmarsh, translating to 0.3% per m for the entire 310 m transect. While the saltmarsh at Bridgewick reduced wave heights by 4.38% per m, the mudflat experienced a negative attenuation of -0.23% per m in front of the marsh cliff, resulting in an increased wave height of 0.52% per m across the entire 112 m transect. After resolving the attenuation further, the most rapid reduction in wave energy, and thus wave height, occurred within the first 10 m of permanent vegetation cover with values of 2.12% per m and 1.14% per m at Tillingham and Bridgewick, respectively. Due to this rapid attenuation at the marsh fringe, *Möller and Spencer* (2002) proposed the water depth at these transition zones was more crucial to the wave damping process than within the marsh interior where the

effect of water depth on wave attenuation was reduced. At both sites, average wave attenuation variations reflected seasonal changes where vegetation density and wave attenuation was highest in September-November and lowest in March-July.

Cooper (2005) reported results from a year-long data collection study investigating the wave dissipation ability of Wash Inlet intertidal zone along the eastern UK coasts. Changes in wave height and energy were calculated among a lower, mid, and upper station along three shore-normal transects located at Wrangle Flats, Butterwick Low, and Breast Sand. Field results indicated wave height dissipation was significantly larger across the upper saltmarsh than the lower mudflat for all three transects. At Wrangle Flats, average wave height dissipation across the mudflat and saltmarsh were 10% and 91%, respectively. The mudflat at Butterwick Low resulted in an average wave height dissipation of 23% while the saltmarsh reduced the average wave height by 64%. An average wave height dissipation of 36% was observed over the mudflat and 78% observed over the saltmarsh at Breast Sands. Due to differences between transect characteristics such as incident wave height and location of wave recording stations, *Cooper* (2005) was unable to make direct comparisons of wave height dissipation effectiveness between transects. However, *Cooper* (2005) suggested intertidal elevation, intertidal zone width, and saltmarsh vegetation characteristics were the most critical parameters affecting wave dissipation.

Similar to the study conducted in 2002, *Möller* (2006) investigated wave height damping over a Dengie Peninsula saltmarsh. Three 10 m transects with little topographic variation but with different combinations of vegetation cover were

considered. Wave attenuation was highly variable, ranging from 0.08% to 33%, and *Möller* (2006) suggested hydrodynamic conditions such as significant wave height to depth ratio (H_s/h) may dominate over vegetation characteristics such as density or structure. For transects with the greatest proportion of *Spartina anglica*, when H_s/h exceeded 0.55, further increase in maximum observed wave attenuation ceased, suggesting the attenuation capability of the vegetation was achieved. Expanding upon this idea, *Möller* (2006) suggested this threshold may indicate a transition from deposition ($H_s/h<0.55$, where maximum wave attenuation can occur) to erosion ($H_s/h>0.55$, where maximum wave attenuation potential was reached and excess energy became available to transport sediment).

In a three-dimensional wave basin and two-dimensional wave flume, *Augustin* (2007) investigated the effects of numerous wave and vegetation characteristics on wave attenuation, such as incident wave height, stem density, stem flexibility and vegetation height to water depth ratios. The waves considered had periods representative of wind waves (1.0-2.0 s) and vegetation fields were simulated using wooden dowels and polyethylene foam tubing. *Augustin* (2007) observed a linear increase in wave attenuation as incident wave height increased. The experimental data showed denser arrays of 194 stems/m^2 attenuated waves 12-17% more than 97 stem/m^2 arrays, and the attenuation under emergent conditions was 50 to 200% greater per wavelength than under near-emergent conditions considering the same hydrodynamic conditions. Additionally, wave attenuation demonstrated a slight dependence on plant flexibility with flexible elements dissipating an additional 1-4% when compared to rigid elements.

2.3. Modeling Vegetation-wave Interactions

Various models exist for simulating the interaction between waves and vegetation. While some models account for vegetation simply with higher bottom friction factors (*Camfield*, 1977; *Möller et al.*, 1999), the majority of models approach this phenomenon by estimating the wave-induced drag forces along the plant stem (*Dalrymple et al.*, 1984; *Asano et al.*, 1992; *Kobayashi et al.*, 1993; *Mendez and Losada*, 1999; *Mendez and Losada*, 2004; *Lima et al.*, 2006). However, the validity of each model depends on its application to appropriate physical conditions, mainly the biomechanics of the considered species. For example, reed plants such as *Spartina alterniflora* can be simulated as rigid, vertical cylinders whereas flexible vegetation such as kelp requires a more complex drag formulation.

Camfield (1977) developed a preliminary approach for determining wave height transformations over vegetation by modeling vegetative areas with high Darcy-Weisbach friction factors (f_{DW}). Higher bottom friction was accounted for by adjusting the propagation distance using already existing shallow water wave forecasting curves (e.g. the wave decay over 914 m of tall grass is equal to the wave decay over 4,099 m for a water depth of 3.05 m and wind speed of 40.2 m per second). The total propagation fetch length (F_{tot}) was given as:

$$F_{tot} = F_e + F_a \tag{2.1}$$

where F_e is the equivalent fetch length for the initial wave obtained from shallow water forecasting curves and F_a is the adjusted fetch length. Depending on the seaward incident wave height (H_0) at the beginning edge of the fetch and its comparison to the

maximum significant wave height ($H_{s,max}$), *Camfield* (1977) proposed two wave transformation conditions. If $H_0<H_{s,max}$, wave growth was expected. The increase in wave height for a wave traveling over $f_{DW}>0.01$ is lower for than for a wave height propagating over $f_{DW}=0.01$ considering the same total propagation distance (x_p) in both cases. Thus, an adjusted fetch length of $F_a<x_p$, was used to describe the wave growth condition. For the second condition where $H_0>H_{s,max}$, wave decay was expected. A value of $f_{DW}>0.01$ would cause the wave to decay faster than if propagation occurred over $f_{DW}=0.01$, and therefore, an adjusted fetch $F_a>x_p$ was selected.

Möller et al. (1999) developed a one-dimensional numerical model accounting for the combined effects of shoaling, viscous friction, percolation, and bottom friction roughness on wave height dissipation. The one-dimensional model was expressed in the form below:

$$\frac{H}{H_0} = K_S K_v K_f K_p \tag{2.2}$$

where K_s is a shoaling coefficient, K_v is a viscous friction coefficient, K_f is a bottom friction coefficient, and K_p is a percolation coefficient. Numerical results were compared to observed wave heights across a saltmarsh and mudflat in Stiffkey, North Norfolk, UK. Initially, modeled results did not include the bottom roughness coefficient K_f, and this coefficient served as an adjusting parameter to account for any discrepancies between the experimental and numerical results. Without the bed roughness coefficient, the model underestimated wave attenuation over the saltmarsh and all but three mudflat locations, indicating the total energy dissipation was not accounted for by shoaling,

viscous friction, and percolation alone. Assuming the remaining energy dissipation was due only to surface friction, K_f and the corresponding friction factor (f) was calculated according to the following equation:

$$K_f = \left[1 + \frac{64\pi^3}{3g^2}\frac{fH_0\Delta x}{h^2}\frac{h^2}{T^4}\frac{K_s^{\,2}}{\sinh^3(2\pi h/L)}\right]^{-1} \text{ where } f = \frac{\tau_0}{\frac{1}{2}\rho u_b^2} \tag{2.3}$$

and τ_0 is amplitude of bed shear stress, Δx is the cross-shore width of the vegetation field over which propagation occurs, L is wavelength, T is wave period, and u_b is bottom orbital velocity. The friction factor values corresponding to the saltmarsh were found to be at least one order of magnitude higher than those corresponding to the mudflat (average of 0.2 for the saltmarsh and 0.01 for the mudflat). *Möller et al.* (1999) proposed this increase in bed friction factor for saltmarshes was responsible for the observed higher wave attenuation.

Based on empirical estimates of fluid drag forces acting on vertical, rigid cylinders, *Dean* (1979) was one of the first to propose a simple hydrodynamic model for wave attenuation due to vegetation. The proposed model for the damping of incoming water waves by coastal plants was the following:

$$\frac{H}{H_0} = \frac{1}{1 + R\Delta x} \text{ where } R = \frac{C_D d}{6\pi\Delta s^2 h}H_0 \tag{2.4}$$

and H is the local wave height. The bulk or average drag coefficient C_D for the plant field is assumed constant over the depth and was approximated as 1.0 to describe drag forces associated with smooth, rigid vertical cylinders.

However, *Knutson et al.* (1982) recognized the Dean Model, described above,

did not account for the responses of real plants to wave forcing, such as swaying. As a result, *Knutson et al.* (1982) slightly modified the Dean Model to include an empirical vegetation adjustment parameter C_P, the plant drag coefficient. The modified Dean Model was the following:

$$\frac{H}{H_0} = \frac{1}{1 + R'\Delta x} \text{ where } R' = \frac{C_D C_P d}{3\pi \Delta s^2 h} H_0 \tag{2.5}$$

Utilizing wave data gathered from two *Spartina alterniflora* marshes in the Chesapeake Bay, *Knutson et al.* (1982) found a calibrated value of C_p=5 resulted in the smallest root-mean-square error between observed and predicted wave heights.

The dissipation equation considered within this thesis is that of *Dalrymple et al.* (1984). *Dalrymple et al.* (1984) formulated an algebraic wave dissipation equation using linear theory and conservation of wave energy by approximating a vegetation field as an array of rigid, vertical cylinders. The derivation considered a flat bottom and arbitrary water depth and stem length, allowing for both submerged and emergent vegetation. The general form of the conservation of energy equation is the following:

$$\frac{\partial \left(EC_g \right)}{\partial x} = -\left\langle \varepsilon \right\rangle \tag{2.6}$$

where E is wave energy density, C_g is group velocity, ε is energy dissipation, and x is the horizontal coordinate. Assuming ε was only a function of the drag force, the horizontal force per unit volume (F_x) induced by a stem array was expressed as a Morison-type equation with the inertia force component neglected:

$$F_x = \frac{1}{2} \rho C_D N d u \left| u \right| \tag{2.7}$$

where u is horizontal particle velocity given by linear theory. The time-averaged vegetation-induced energy dissipation (ε_v) was the following:

$$\left\langle \varepsilon_V \right\rangle = F_x u \tag{2.8}$$

Evaluating ε_v over the stem length, the formulation for the energy dissipation due to a vegetation array was given by:

$$\left\langle \varepsilon_V \right\rangle = \frac{2}{3\pi}\rho C_D N d \left(\frac{gk}{\omega}\right)^3 \frac{\left(\sinh^3 kl_s + 3\sinh kl_s\right)}{3k\cosh^3 kh} A^3 \tag{2.9}$$

Substituting equation 2.9 into 2.6, the solution for wave amplitude decay due to a vegetation field was the following:

$$\frac{A}{A_0} = \frac{1}{1+\alpha x} \tag{2.10}$$

where A_0 is incident amplitude and α is the wave damping factor given by:

$$\alpha = \frac{2}{3\pi} C_D N d \left(\sinh^3 kl_s + 3\sinh kl_s\right)\left[\frac{4k}{3\sinh kh\left(\sinh 2kh + 2kh\right)}\right] A_0 \tag{2.11}$$

The bulk drag coefficient is assumed constant over the depth in this formulation. However, unlike the Dean Model where C_D=1, *Dalrymple et al.* (1984) allows for calibration of the bulk drag coefficient in order to account for the varying reactions of different plant species to wave forcing.

The equation developed by *Dalrymple et al*. (1984) served as the foundation for an empirical model developed by *Mendez and Losada* (2004) to estimate monochromatic and random wave transformations over variable depth vegetation fields under both breaking and nonbreaking conditions. The model neglected plant motion and depended

on the drag coefficient as the single calibration parameter. For a sloping bottom, the conservation of energy equation was modified to include a linear summation of breaking dissipation (ε_B) and vegetation-induced dissipation:

$$\frac{\partial\left(EC_g\right)}{\partial x} = -\left\langle \varepsilon_B \right\rangle - \left\langle \varepsilon_V \right\rangle \tag{2.12}$$

The average rate of energy dissipation by wave breaking is that proposed by *Thornton et al.* (1983):

$$\left\langle \varepsilon_B \right\rangle = \frac{3\sqrt{\pi}}{16}\rho g \frac{B^3 f_p}{\gamma_b h^5} H_{rms}^7 \tag{2.13}$$

where B and γ_b are tuning parameters, f_p is peak frequency, and H_{rms} is root-mean-square wave height. The variation in wave height was modeled assuming an unmodified Raleigh distribution and the dissipation due to vegetation was formulated as:

$$\left\langle \varepsilon_V \right\rangle = \frac{1}{2\sqrt{\pi}}\rho C_D N d \left(\frac{kg}{2\omega}\right)^3 \frac{\left(\sinh^3 kl_s + 3\sinh kl_s\right)}{3k\cosh^3 kh} H_{rms}^3 \tag{2.14}$$

The experimental results of *Dubi* (1995) and *Løvås* (2000) validated this empirical model for an artificial *Laminaria hyperborea* kelp field subjected to nonbreaking and breaking conditions, respectively.

Kobayashi et al. (1993) derived a solution for wave attenuation by submerged vegetation in terms of exponential decay based on the continuity and linearized momentum equations rather than the conventional conservation of wave energy approach. The method approximated plants as rigid, vertical cylinders and analyzed the wave field regions above and within the vegetation while satisfying boundary conditions at the interface. Within the vegetation, the continuity equation was given by:

$$\frac{\partial u}{\partial x} + \frac{\partial w}{\partial z} = 0 \tag{2.15}$$

and the linearized momentum equations per unit water volume were expressed as:

$$\rho \frac{\partial w}{\partial t} = -\frac{\partial p}{\partial z} - F_z \tag{2.16}$$

$$\rho \frac{\partial u}{\partial t} = -\frac{\partial p}{\partial x} - F_x \tag{2.17}$$

where w is vertical particle velocity, z is the vertical coordinate, t is time, and F_z is the total vertical force per unit volume acting on a stem array. The horizontal force F_x was approximated according to equation 2.7, while the vertical force F_z was assumed negligible when compared to F_x and approximated as $F_z \cong 0$. The local wave height was assumed to decay exponentially with propagation distance through the plant field according to the following form:

$$H = H_0 \exp(-k_i x) \tag{2.18}$$

where k_i is the exponential decay coefficient and a component of the complex wave number $\tilde{k}$ given by:

$$\tilde{k} = k_r + ik_i \tag{2.19}$$

in which k_r is the real component of the wave number. The analytical solution herein formulated by *Kobayashi et al.* (1993) was compared with the results of an artificial kelp experiment conducted by *Asano et al.* (1988). The measured wave heights were fitted to the exponential decay expression using the method of least squares to calibrate the drag coefficient until the calculated values of k_i equaled the measured values of k_i. The exponential decay model adequately captured the trend in observed wave heights.

Asano et al. (1992) extended the analytical model developed above by *Kobayashi et al.* (1993) to include vegetation motion. While *Kobayashi et al.* (1993) used horizontal particle velocity in the force formulation, *Asano et al.* (1992) modified the solution of the flow field to include the relative velocity (u_r) between the horizontal particle velocity and swaying velocity of the stem (u_v). The horizontal and vertical forces per unit volume on the vegetation stems were assumed as:

$$F_x = \frac{1}{2}\rho C_D N d u_r |u_r| \text{ where } u_r = (u - u_v) \tag{2.20}$$

$$F_z \cong 0 \tag{2.21}$$

Asano et al. (1992) assumed the magnitude of vegetation motion was small and treated it as horizontal swaying; however, each stem was treated independently and the interaction between stems ignored. This swaying was modeled as a forced vibration with one degree of freedom where buoyancy and stem stiffness were considered restoring forces. Each individual stem was modeled as a cantilever beam, fixed at the bottom, and the simplified horizontal displacement for each stem (ζ) with respect to the vertical z-axis given as:

$$\frac{1}{2}\left\{\rho(C_M - 1) + \rho_v\right\} V \frac{\partial^2 \zeta}{\partial t^2} + \frac{1}{2}\rho C_D |u| R \frac{\partial \zeta}{\partial t} + \left\{\frac{8EI}{D^3} + (\rho - \rho_v) g \frac{V}{D}\right\} \zeta \tag{2.22}$$

$$= \frac{1}{2}\rho C_D R u |u| + \rho C_M V \frac{\partial u}{\partial t}$$

where V, R, and D are given as:

$$V = dDt_v \tag{2.23}$$

$$R = dD \tag{2.24}$$

$$D = \frac{l_s + \sqrt{l_s^2 - \hat{\zeta}^2}}{2} \tag{2.25}$$

and ρ_v is density of the plant material, t_v is stem thickness, EI is stem bending stiffness, C_M is the inertia coefficient of the stem, and $\hat{\zeta}$ is the amplitude of the stem horizontal displacement. Like *Kobayashi et al.* (1993), the model results were compared to the experimental results of *Asano et al.* (1988) using the least squares method, and the present model including the swaying motion of the vegetation yielded a better agreement with the same data set. Since the present model does not account for turbulence stress, *Asano et al.* (1992) suggested the extension may begin to break down when the swaying motion of the vegetation becomes large and able to generate turbulence.

Mendez and Losada (1999) extended the existing wave decay solutions of *Kobayashi et al.* (1993) and *Asano et al.* (1992) to include random waves along a flat bottom. Unlike the methods of *Kobayashi et al.* (1993) and *Asano et al.* (1992), which solved for the wave field only within the vegetation, *Mendez and Losada* (1999) analyzed the complete wave field by considering the vegetation field as well as the vicinity of the field by separating the problem into four regions and defining in each region a velocity potential. The four defined velocity potentials are diagramed below in Figure 4 and were defined as: seaward region of the vegetation field (Φ_1), region above the vegetation field (Φ_2), region behind the vegetation field (Φ_3), and within the vegetation field (Φ_4).

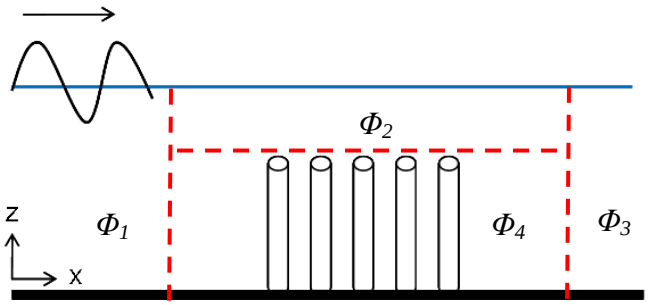

Figure 4. Definition sketch of *Mendez and Losada* (1999)

In the case of emergent plants, the region above the vegetation field was omitted. The solution accounts for reflection and transmission of waves as they encounter the interfaces between the seaward region, vegetation field, and leeward region. Unlike the previously discussed models where the horizontal force was dominated by the drag force as in equation 2.7, *Mendez and Losada* (1999) defined F_x as a linear summation of the drag force and inertia force, which is caused by the fluid and vegetation accelerations:

$$F_x = \frac{1}{2}\rho C_D N d u_r \left|u_r\right| + \rho N d t_v \left[C_M \frac{\partial u}{\partial t} - (C_M - 1)\frac{\partial^2 \zeta}{\partial t^2} \right] \tag{2.26}$$

The vertical force F_z is given by 2.21. The swaying of an individual stem was defined according to equation 2.22, whose analytic solution for a given location of the vegetation was given by:

$$\zeta = \hat{\zeta}\cos(\sigma t + \delta_\zeta) \tag{2.27}$$

where δ_ζ is the phase shift with respect to the forcing. The interaction between the fluid and vegetation was solved iteratively until the plant motion velocity converged with the fluid velocity. Since the model is linear, the extension to random waves was achieved by introducing an incident unidirectional frequency spectrum and dividing this spectrum

into a finite number of wave frequencies. The linear model was then used to obtain a solution for each of the wave frequencies in a given vegetation field. The model was compared to the experimental results of *Dubi* (1995). Using C_D as the calibration parameter, the theoretical results compared well to the experimental results and accurately captured the modulations in observed wave height resulting from reflection at the front and back of the vegetation field.

While the previous models reviewed herein are formulated based on linear wave theory, *Lima et al.* (2006) formulated a model for wave damping over highly flexible vegetation using nonlinear stream function wave theory. Buoyant vegetation stems were simulated by fixed length, flexible nylon rope to allow for large displacements. Unlike previous models, where total resistance was a summation of the drag contributed by individual stems, *Lima et al.* (2006) allowed for resistances resulting from interactions between stems, such as entanglement, by including an ensemble interaction coefficient (τ). The total horizontal drag force was defined as a function of the force exerted by a single element on the fluid (F_x^1), the stem density, and the ensemble coefficient given by:

$$F_x = \tau N F_x^1 \tag{2.28}$$

Each nylon stem was treated as a string of equally-spaced nodes, and each n^{th} segment was described using a system of equations consisting of a constitutive equation that established the stem's fixed length and a momentum balance in the horizontal and vertical directions. The solution of this system of equations provided the connecting forces between nodes and the horizontal and vertical displacement of each node. Using

observations of a single stem and dimensional analysis, the drag force for an individual element was the following:

$$F_x^1 = 0.133 \frac{\rho_v d (l_s/h)^4 H^3}{T^2} \tag{2.29}$$

where l_s/h is the portion of the water column occupied by the stem and T is wave period. An expression for wave height decay in terms of the ensemble coefficient was obtained as:

$$\frac{H}{H_0} = \frac{1}{1+\beta x} \text{ where } \beta = 1.064 \frac{\tau N d (l_s/h)^4}{g T^2 (4n-1)} \frac{\rho_v}{\rho} H_0 \tag{2.30}$$

and n is the ratio between wave group speed and celerity given as (*Dean and Dalrymple*, 1984):

$$n = 1 + \frac{2kh}{\sinh 2kh} \tag{2.31}$$

All parameters in equation 2.30 except for τ were known, and this parameter was estimated for each experiment by minimizing the average quadratic error between theoretical and observed wave heights. By multivariate regression, the equation for τ was obtained as:

$$\tau = 7.44 \frac{L^2 d^{3/2}}{H_0 l_s \Delta s^{1/2}} \tag{2.32}$$

Substituting equation 2.32 into equation 2.30, the wave decay model for waves traveling through a vegetation field with flexible elements was proposed as:

$$\frac{H}{H_0} = \frac{1}{1+\beta x} \text{ where } \beta = 7.916 \frac{L^2 (l_s/h)^4 d^{5/2} N^{5/4}}{g T^2 (4n-1) l_s^2} \frac{\rho_v}{\rho} \tag{2.33}$$

Lima et al. (2006) concluded the resistance imposed by a group of stems was on average four times higher than merely summing individual forces of all the stems, and suggested stem interactions were a greater importance than previously considered.

2.4. Physical Properties of the Bulk Drag Coefficient

If a vegetation stem is considered stiff and the magnitude of swaying small, the forces induced in stem-wave interactions can be described using the Morison equation. The Morison equation describes the forces induced by a solid body in oscillatory flow and is made up of two components: a drag force (F_D) proportional to the square of the instantaneous velocity and an inertia force (F_I) proportional to the horizontal accelerative force. The Morison equation is the following:

$$F = F_D + F_I = \rho \tilde{C}_D a u |u| + \rho C_m V \frac{\partial u}{\partial t} \tag{2.34}$$

where $\tilde{C}_D$ is the drag coefficient for a singular element, V is the body's volume, and a is the cross-sectional area of the body perpendicular to the flow (*Morison et al.*, 1950). The drag and inertia coefficients are determined empirically. In the majority of the above models, only the drag force is considered. Rather than determining the drag coefficient for each individual stem, the average or bulk drag coefficient C_D within the plant field is considered and served as the calibration parameter to minimize error between measured and predicted wave heights. Defining a generalized value to describe all plant-induced dissipation is impossible since the drag coefficient is a function of

hydrodynamic and plant biomechanical characteristics. However, the physical properties of the bulk drag coefficient in a vegetation field can be understood by examining empirical formulas. These empirical formulas attempt to formulate relationships between the bulk drag coefficient C_D and nondimensional flow parameters to predict appropriate bulk drag coefficient values for specific plant types.

The bulk drag coefficient was found to be dependent on the stem Reynolds number given by:

$$\mathrm{Re}_d = \frac{ud}{\nu} \tag{2.35}$$

where υ is kinematic viscosity of the fluid. *Kobayashi et al.* (1993) investigated the large variation of the bulk drag coefficient by plotting the C_D values calibrated for the artificial kelp experiments of *Asano et al.* (1988) against the corresponding stem Reynolds number. The bulk drag coefficient was found to decrease with increasing Re_d and approached the order of 0.1 for large Re_d. *Kobayashi et al.* (1993) formulated the following empirical relationship between C_D and Re_d for $2{,}200<\mathrm{Re}_d<18{,}000$:

$$C_D = 0.08 + \left(\frac{2{,}200}{\mathrm{Re}_d}\right)^{2.4} \tag{2.36}$$

Mendez and Losada (1999) also validated their model extension for regular waves with the experimental of *Asano et al* (1988). However, *Mendez and Losada* (1999) reported different empirical relationships between C_D and Re_d than *Kobayashi et al.* (1993):

No swaying: $$C_D = 0.08 + \left(\frac{2,200}{\mathrm{Re_d}} \right)^{2.2} \quad \text{for } 200<\mathrm{Re_d}<15,500 \tag{2.37}$$

Swaying: $$C_D = 0.40 + \left(\frac{4,600}{\mathrm{Re_d}} \right)^{2.9} \quad \text{for } 2,300<\mathrm{Re_d}<20,000 \tag{2.38}$$

For the no swaying condition, the varying of the C_D values was smaller than *Kobayashi et al.* (1993) with a 20% improvement in the correlation coefficient. Given the same stem Reynolds number, the inclusion of plant motion resulted in a higher bulk drag coefficient. By including plant motion, u_r was reduced and, thus, a higher C_D was required to maintain the same amount of wave attenuation. These trends as well as the comparison with *Kobayashi et al.* (1993) can be seen in Figure 5.

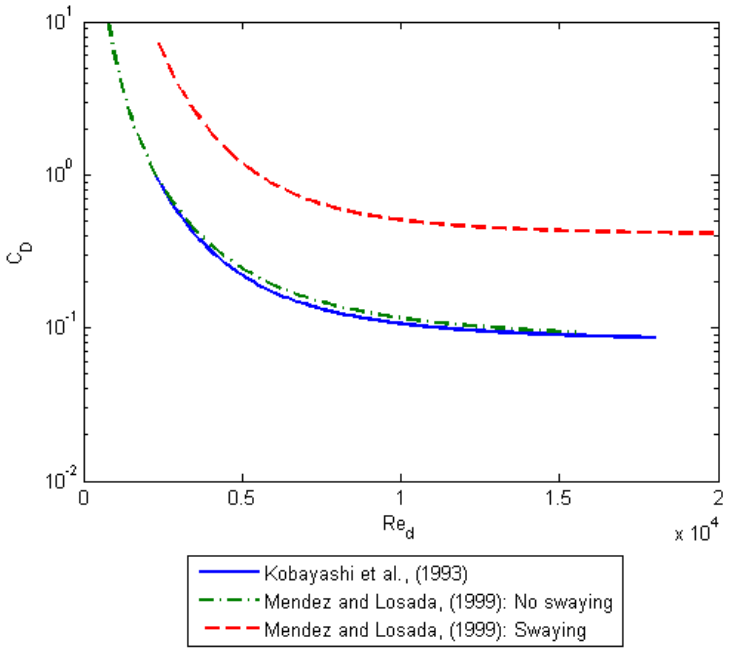

Figure 5. Different empirical relationships between C_D and $\mathrm{Re_d}$

The bulk drag coefficient was also found to be dependent on wave properties. *Mendez and Losada* (2004) parameterized C_D for the artificial kelp experiments of *Dubi* (1995) as a function of the local Keulegan-Carpenter number, K, defined as:

$$\mathrm{K} = \frac{uT_p}{d} \tag{2.39}$$

where T_p is peak period. *Mendez and Losada* (2004) observed scattering when C_D was considered a function of K alone, and, after considering other parameters, found this relationship was also dependent on l_s/h, the relative vegetation height. A modified Keulegan-Carpenter number (Q) was defined to account for differences in l_s/h. The empirical relationship between C_D and Q was defined as the following for $7 \leq Q \leq 172$ and is illustrated below in Figure 6:

$$C_D = \frac{\exp(-0.0138\mathrm{Q})}{\mathrm{Q}^{0.3}} \text{ where } \mathrm{Q} = \frac{\mathrm{K}}{(l_s/h)^{0.76}} \tag{2.40}$$

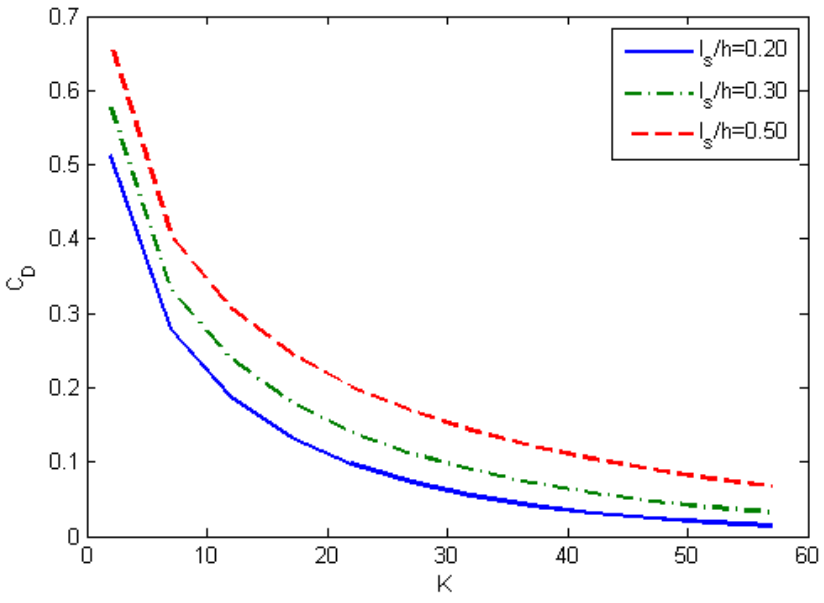

Figure 6. Relationship between C_D and K for different l_s/h values

The bulk drag coefficient decreased with an increasing K, and as the relative vegetation height increased (i.e., the stem occupied more of the water column), the bulk drag coefficient increased.

When a vegetation field is simulated by a cylinder array, other processes resulting from interactions between cylinders influence the bulk drag coefficient. A convenient way to approach an array of cylinders is that taken by *Nepf* (1999), who studied the effect of stem density on the bulk drag coefficient in steady, unidirectional flow by defining the nondimensional fractional volume of the flow occupied by the stems as:

$$\boldsymbol{a}\, d = \frac{d^2}{\Delta s^2} \text{ where } \boldsymbol{a} = Nd = \frac{d}{\Delta s^2} \tag{2.41}$$

Nepf (1999) found the drag coefficient decreased with an increase in stem density **a**d for $Re_d > \approx 200$. This reduction in drag for high density vegetation is attributed to wake sheltering. Wake sheltering is an interaction among upstream and downstream cylinders where upstream stem wakes reduce the drag on downstream stems. The reduction in drag on downstream stems arises from the following two effects. First, some downstream cylinders may lie in the wake of upstream cylinders and these cylinders experience a lower impact velocity due to the velocity reduction in the wake of the upstream cylinder. Secondly, wake turbulence from the upstream cylinder lowers the pressure differential, and thus the drag, around the downstream cylinder by delaying the point of separation of the boundary layer. In emergent canopies, the impact of sheltering was significant for **a**d$\geq$0.03, and for lower stem densities the drag coefficient can be

approximated as that for individual cylinders at the same Re_d. In submerged canopies, the bulk drag coefficient is further lowered from standard cylinder values (*Nepf*, 2004).

2.5. Summary of Literature Review

The background information provided herein is directly related to the research objective of this thesis. Although highly variable and dynamic, the ability of coastal plants to dissipate wave energy, and thus wave heights, is verified and documented by several sources. Numerous hydrodynamic models attempting to explain these interactions between waves and vegetation are presented as well as their methods of formulation and inherent assumptions. Typically, vegetation stems are simulated by numerous rigid, vertical cylinders and drag forces induced on these stems by waves are described using the Morison equation. An empirical vegetation field bulk drag coefficient, C_D, is required in this description and often serves as the calibration parameter to minimize error between predicted and observed wave heights.

The quantification of vegetation-induced dissipation is pertinent for accurately predicting coastal hydrodynamics and has led to an increasing demand for numerical models that adequately predict wave transformations over vegetation fields. This thesis focuses on integrating the hydrodynamic derivation of *Dalrymple et al.* (1984) into a one-dimensional wave transformation model in order to predict wave attenuation over coastal vegetation. The model is calibrated using experimental data where vegetation fields are simulated by random cylinder arrays composed of wooden dowels. Improvement of existing models to account for this random placement may be required due the influence of stem-scale interactions, such as wake effects, on wave dissipation.

CHAPTER III

EXPERIMENTAL METHODS

3.1. Overview

Samples of *Spartina alterniflora* (smooth cordgrass) were obtained from Galveston Island State Park, Texas in July 2008 by *Feagin et al.* (in review). Samples were selected from both healthy and sparse portions of the wetland in order to obtain simple biophysical parameters, including stem density, standard deviation of spacing, modulus of elasticity, and bending stress, of a common wetland plant species. Stem density and uniformity of stem spacing are the primary parameters of interest within this thesis.

After collecting field data, experiments were conducted in the three-dimensional wave basin at the Haynes Coastal Engineering Laboratory to assess the influence of relative vegetation height, stem density, and stem spatial variation on wave transformations through artificial vegetation fields. Subsequent experiments using specifically selected vegetation fields were conducted in the two-dimensional wave flume at Texas A&M University to verify the wave trends observed in the Haynes Coastal Engineering Laboratory. For both experiments, vegetation fields, represented by random cylinder arrays, were constructed from 6.4 mm (0.25 in) diameter wooden dowels embedded into plywood sheets. These cylinder arrays varied in stem density as well as randomness of stem spacing. Emergent and near-emergent vegetation conditions were investigated, and monochromatic wave conditions with periods between 1.0 s and 2.0 s were chosen for both sets of experiments. Details of the vegetation arrays (Section

3.2), the physical models (Section 3.3), the instrumentation and data acquisition (Section 3.4), and data preprocessing (Section 3.5 and 3.6) for the Haynes Coastal Engineering Laboratory basin and the two-dimensional wave flume are presented in this chapter.

3.2. Artificial Vegetation Construction

Considering the practical limitations of using real plants, plant stems were simulated using 6.4 mm (0.25 in) diameter rigid wooden dowel rods. Wooden dowel rods were selected due to the morphological similarities of shape between the rods and *S. alterniflora* (*Nepf*, 2004). *S. alterniflora* is a common wetland species along coastal wetlands of the Atlantic and Gulf coasts, and is typically 0.30 to 2.4 m (1 ft to 8 ft) tall and has hollow, stout stems up to 13 mm (0.50 in) in diameter (*National Resources Conservation Service*, 2002). Figure 7 shows a scientific drawing as well as a photo of *S. alterniflora* in Galveston Island State Park, Texas.

Figure 7. *S. alterniflora* rendering (*Tiner*, 1993) and photo (*Feagin et al.*, in review)

Unlike the majority of previous literature which focuses on cylinders spaced on a grid, random cylinder arrays were selected to represent the conditions observed by *Feagin et al.* (in review). The parameters of interest in constructing the vegetation fields were the average stem density and standard deviation of spacing per m^2 (σ) for a healthy and an unhealthy section of the wetland. To calculate these quantities, the spatial distribution of plant stems within each 1 m^2 plot was photographed and x-y coordinates located for each emerged stem using ArcGIS. Next, these coordinates were imported into MATLAB and the average distances between stems as well as the standard deviation of this distance were calculated. For healthy plots, Δs=8.1 cm with σ=3.1 cm or 38% of the average distance while for unhealthy plots, Δs=9.6 cm with σ=5.1 cm or 53% of the average distance between stems. An example of these 1 m^2 plots provided by *Feagin et al.* (in review) for a healthy and unhealthy sample is shown in Figure 8.

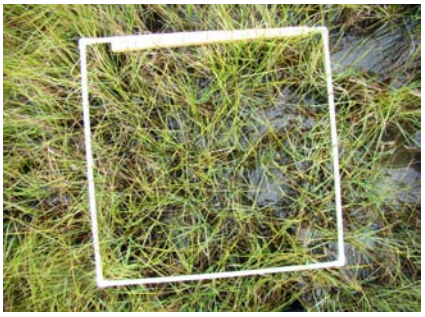
(a)

(b)

Figure 8. Healthy (a) and unhealthy (b) *S. alterniflora* samples

Using the data gathered from *Feagin et al*. (in review) as a basis, MATLAB was used to generate nine random array patterns with average stem spacings of 4 cm, 7 cm,

and 11 cm, and standard deviations of 20%, 40%, and 60% of these spacings. For clarification, the "randomness" of the stems' positions increases with increasing standard deviation. The plots of the constructed arrays are presented in Figure 9 with a summary of array properties, including the **a**d parameter, following in Table 1. The control case, which lacked vegetation, is identified as array 0. The Δs=7 cm, σ=40% case is the array that most closely resembles the conditions of the healthy wetland and Δs=11 cm, σ=60% is the array most closely resembling the conditions of the unhealthy wetland.

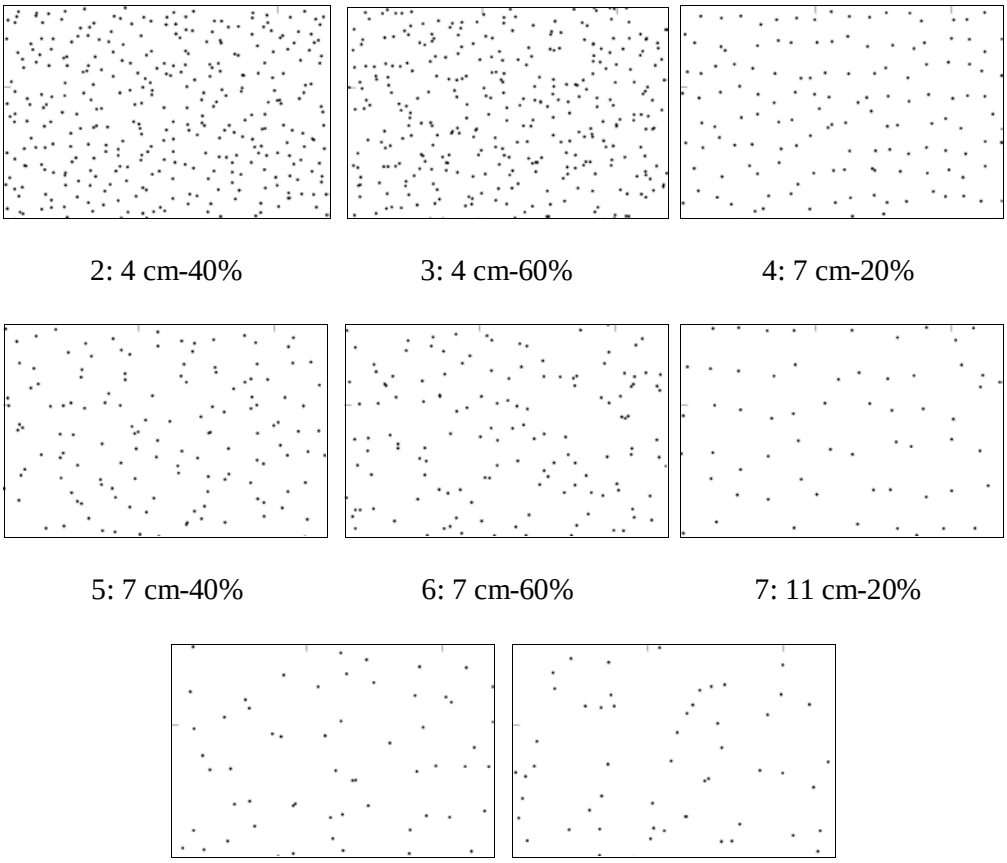

Figure 9. Vegetation array patterns

In order to construct the vegetation fields, the above plots were used to construct lab-scale templates to overlay the 0.02 m (0.75 in) thick plywood sheets after being printed by a plotter. Holes corresponding to the templates were drilled using hand drills, and then dowels were embedded and secured in the plywood using Liquid Nails™. The length of the dowels after being embedded was 30.5 cm (1 ft) for the Haynes Coastal Engineering Laboratory but was slightly shorter at 25.4 cm (0.83 ft) to accommodate water depth limitations in the flume. Figure 10 shows a completed vegetation field in the two-dimensional wave flume.

Figure 10. Installed vegetation field in wave flume

Table 1. Properties of constructed vegetation fields

Array Number	Δs (cm)	N (stems/m^2)	σ (cm, % of Δs)	**a**d
0	-	-	-	-
2	4	625	1.6 (40%)	0.0256
3	4	625	2.4 (60%)	0.0256
4	7	204	1.4 (20%)	0.0084
5	7	204	2.8 (40%)	0.0084
6	7	204	4.2 (60%)	0.0084
7	11	83	2.2 (20%)	0.0034
8	11	83	4.4 (40%)	0.0034
9	11	83	6.6 (60%)	0.0034

3.3. Physical Models

3.3.1. Haynes Coastal Engineering Laboratory

The shallow-water three-dimensional wave basin at the Haynes Coastal Engineering Laboratory is 22.9 m (75 ft) wide, 36.6 m (120 ft) long, and 1.5 m (4 ft) deep with a rock beach at the end opposite of the wavemaker to absorb wave energy. The wave generator is a 42 segmented piston type wavemaker with directional capabilities able to produce wave periods ranging from 0.5 s to 5.0 s (*Texas A&M University*, 2004).

Three neighboring, individual flumes with dimensions of 12.2 m (40 ft) long and 1.2 m (4 ft) wide with a slope of 1:40 were constructed inside the basin using an steel ramp and 0.02 m (0.75 in) thick plywood sheets. A photo of the physical setup illustrating the individual flumes is shown below in Figure 11.

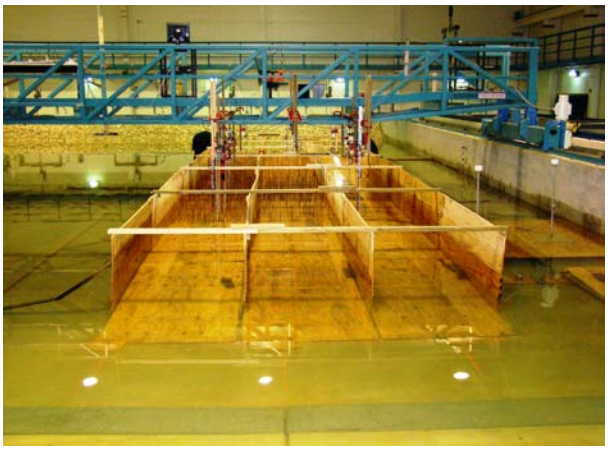

Figure 11. Individual flumes of Haynes Coastal Engineering Laboratory model setup

A secondary smaller 2.4 m (8 ft) long ramp with a slope of 1:8 was constructed flush to the beginning of the flumes in order to shoal incoming waves. In case waves broke as they propagated up the smaller ramp, the vegetation field started 2.4 m (8 ft) from the beginning of the flume to allow turbulence dissipation and reformation of the waves before encountering the beginning of the vegetation field. The total length of the vegetation field measured 9.8 m (32 ft). A side view of the physical model setup is shown below in Figure 12.

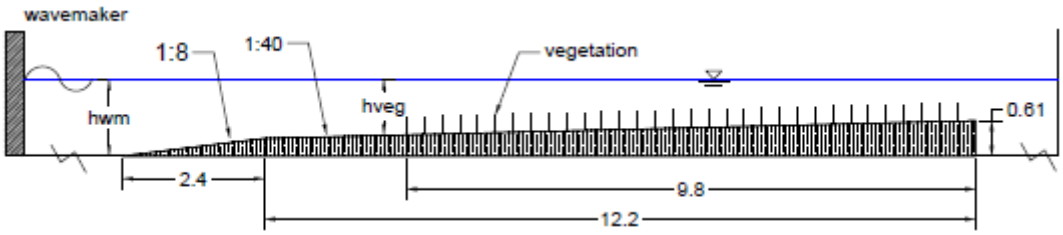

Figure 12. Side view of Haynes Coastal Engineering Laboratory physical model setup

The selected water depths at the wavemaker (h_{wm}) were 96.5 cm, 76.5 cm, and 56.5 cm, corresponding to water depths of 60 cm, 40 cm, and 20 cm, respectively, at the beginning of the vegetation field (h_{veg}). These water depths at the beginning of the vegetation field represent relative vegetation heights of near-emergent (l_s/h=0.51 and 0.76) and emergent (l_s/h=1.0) conditions, in that order. A simple diagram illustrating these ratios is shown below in Figure 13.

Only wave paddles within the flume region were used for wave generation to minimize large-scale circulation and reflection throughout the basin. Nine monochromatic wave conditions with wave periods representative of wind waves (1.0 s to 2.0 s) were generated normal to the physical model. The tests for the deepest and intermediate water depths were repeated three times and twice, respectively. Wave conditions on the shallowest depths were only sampled once. A summary of wave conditions is provided below in Table 2 where H_{wm} is wave height at the wavemaker.

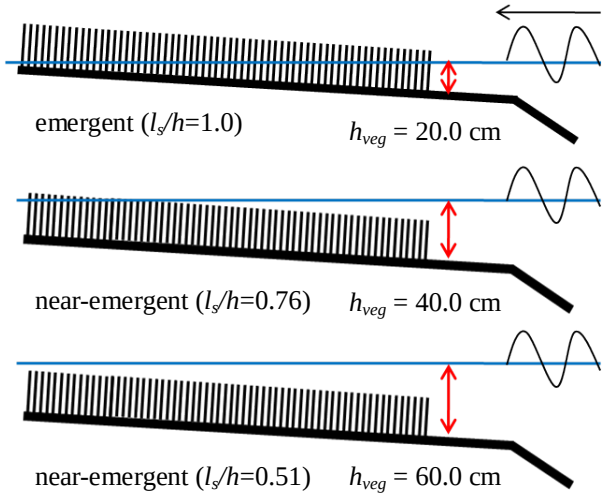

Figure 13. Illustration of emergent and near-emergent conditions (diagram not to scale)

Table 2. Summary of wave conditions for Haynes Coastal Engineering Laboratory

h_{veg} (cm)	H_{wm} (cm)	T (s)
60.0	28.0	1.2
	28.0	2.0
40.0	28.0	1.0
	28.0	2.0
20.0	17.0	1.0
	13.0	2.0
	10.0	2.0
	14.0	1.5
	13.0	1.0

Instrumentation consisted of 21 capacitance wave gauges to measure free surface fluctuations and four acoustic Doppler velocimeters to measure orbital velocity. Seven wave gauges were installed in each flume, and data was sampled at 25 Hz for 300 s. More detailed information regarding the instrumentation and data acquisition methodology for both experiments will be presented in Section 3.4.

Of the above nine constructed vegetation fields with stem lengths of 0.30 m, eight, including the control case, were tested in the Haynes Coastal Engineering Laboratory. Due to the construction of individual flumes, wave data could be acquired for three different vegetation arrays simultaneously per wave forcing. The vegetation arrays selected for the Haynes Coastal Engineering Laboratory are summarized below in Table 3.

Table 3. Vegetation arrays tested in Haynes Coastal Engineering Laboratory

Array Number	Δs (cm)	N (stems/m^2)	σ (cm, % of Δs)	**a**d
0	-	-	-	-
2	4	625	1.6 (40%)	0.0256
3	4	625	2.4 (60%)	0.0256
4	7	204	1.4 (20%)	0.0084
5	7	204	2.8 (40%)	0.0084
6	7	204	4.2 (60%)	0.0084
7	11	83	2.2 (20%)	0.0034
8	11	83	4.4 (40%)	0.0034

3.3.2. Two-dimensional Wave Flume

In order to verify the wave trends observed in the Haynes Coastal Engineering Laboratory, similar experiments were conducted in a two-dimensional wave flume, allowing for a more controlled environment. The glass-walled wave flume is found in Texas A&M's Civil Engineering Laboratory. The flume is 35.0 m (115 ft) long, 0.91 m (3 ft) wide, and 1.22 m (4 ft) deep with a Seasim Rolling Seal absorbing hinged flap wavemaker (RSW 90-85) at one end and a rubber horsehair beach at the other to dissipate energy and reduce wave reflection. This wavemaker is capable of making wave heights of 25.4 cm (10 in) in 91.4 cm (3 ft) of water (*Texas A&M University*, 1981).

Due to limitations of the wavemaker, a false bottom was constructed to obtain the desired water depths. However, unlike the physical model in the Haynes Coastal Engineering Laboratory that had a 1:40 sloping bottom, the wave flume false bottom

was chosen to be flat to remove shoaling effects. This false bottom was 9.8 m (32 ft) long and constructed using 0.02 m (0.75 in) thick plywood sheets supported by a galvanized angle iron frame. This bottom consisted of an initial 1.6 m (5.1 ft) long blank piece of plywood to allow for turbulence dissipation and reformation of waves before the vegetation field, resulting in the total length of the vegetation field measuring 8.2 m (approximately 27 ft). A 2.4 m long ramp with a slope of 1:8 was placed at the beginning of the setup in order to shoal waves up to the flat bottom. The plywood with the cylinder arrays were installed on top of the false bottom plywood, resulting in a total elevation of 30.2 cm above the bottom of the flume. A side view of the two-dimensional wave flume physical model is shown below in Figure 14.

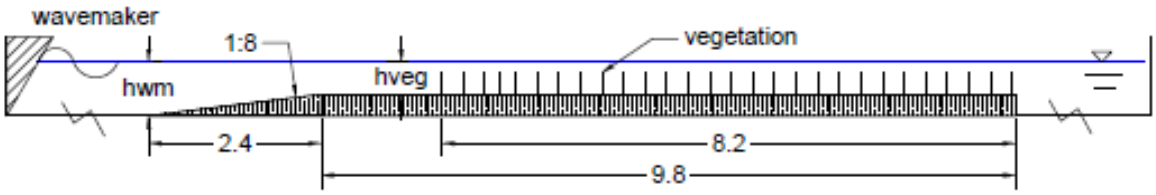

Figure 14. Side view of two-dimensional flume physical model

Two water depths of h_{wm}=47.4 cm and 59.4 cm were selected, corresponding to water depths at the beginning of the vegetation of h_{veg}=17.2 cm and h_{veg}=29.2 cm, respectively. These water depths represent emergent (l_s/h=1.0) and near-emergent (l_s/h=0.87) conditions. The near-emergent conditions in the Haynes Coastal Engineering Laboratory were unable to be represented due to the presence of another experimental setup in the flume.

Monochromatic waves with periods of 1.0 s, 1.6 s, and 2.0 s were selected, and data was sampled for 60 s at 25 Hz at eleven points in the flume using resistance wave gauges. A photo of a wave test for T=2.0 s is shown below in Figure 15. Shorter wave signals were required in order to reduce reflection in the flume; however, tests were repeated multiple times until at least 200 waves were sampled in achieve datasets suitable for spectral analysis. Wave conditions tested in the two-dimensional wave flume are presented below in Table 4.

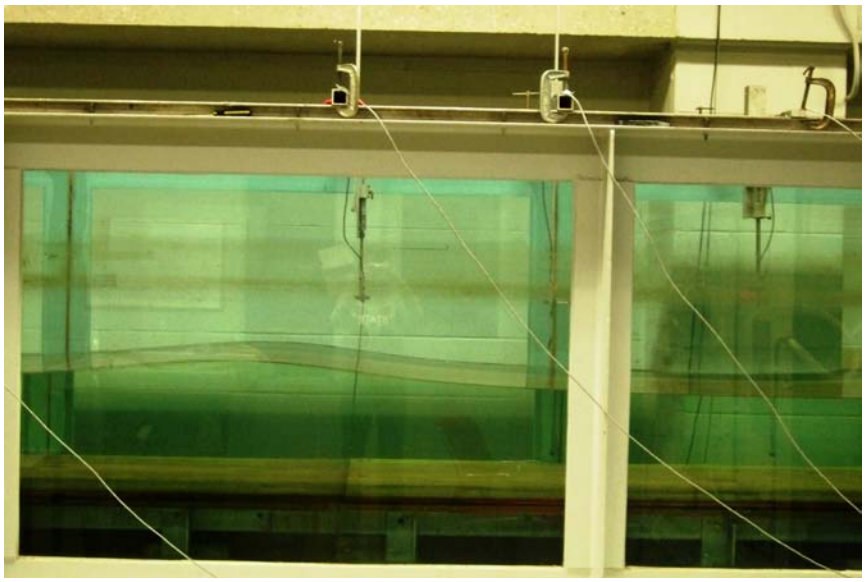

Figure 15. T=2.0 s wave signal in flume

Table 4. Summary of wave conditions for two-dimensional flume

h_{veg} (cm)	H_{wm} (cm)	T (s)
29.2	7.4	1.0
	6.8	1.6
	5.3	2.0
17.2	5.2	1.0
	4.8	1.6
	3.9	2.0

Only three of the vegetation configurations, including the control, were installed in the two-dimensional flume due to time constraints. The stem lengths for these vegetation fields were slightly shorter at 25.4 cm due to water depth restrictions. The vegetation fields tested in the two-dimensional wave flume are shown below in Table 5. Previous studies have been conducted investigating the affect of stem density on wave attenuation (i.e. *Augustin*, 2007); however, few, if any, literature addresses the affects of spacing uniformity. Of the two arrays selected, one is representative of the healthy wetland and the other is a variation with the same density but a lower standard deviation.

Table 5. Selected vegetation fields for wave flume experiments

Array Number	Δs (cm)	N (stems/m^2)	σ (cm, % of Δs)	**a**d
0	-	-	-	-
4	7	204	1.4 (20%)	0.0084
5	7	204	2.8 (40%)	0.0084

3.4. Instrumentation and Data Acquisition

3.4.1. Haynes Coastal Engineering Laboratory

Four acoustic Doppler velocimeters and 21 capacitance wave gauges (7 in each flume) were used for data collection in the Haynes Coastal Engineering Laboratory basin. Of these 21 capacitance wave gauges, eight were wireless gauges from the Haynes Coastal Engineering Laboratory and 13 were wired gauges borrowed from the Offshore Technology Research Center (OTRC). These gauges consist of a white wire that is held taunt by a metal rod and connected via a coaxial cable to a transducer box. The wireless gauges were charged prior to each set of experiments while the OTRC gauges were wired into a data acquisition board on the bridge. These gauges were calibrated using the LabVIEW Multiple Channel Data Acquisition System. The calibration process consisted of displacing the gauges a known distance into and out of the water column and acquiring a sample at each position to obtain a linear relationship between output voltage and wave height. The displacements were selected so the wave heights would always be bounded by the calibrated area.

Four Nortek Vectrino acoustic Doppler velocimeters (ADV), three down-looking and one side-looking, were used to measure wave orbital velocity. Two ADVs were paired with wave gauges in two of the three flumes. To gather data for velocity profiles, the ADVs were displaced a certain percentage of the water depth with each repeat. For example, the ADVs would be at 80% and 60% of the water depth for the first and second repeat, respectively. The datum was defined at the still water level so samples at smaller percentages of the total water depth were taken deeper in the water column than higher

percentages. For the deepest water depth (h_{veg}=60 cm), ADV measurements were gathered at 40%, 60%, and 80% of the water depth while for the intermediate depth (h_{veg}=40 cm), samples were only taken at 40% and 60%. The ADVs were not displaced in the lowest water depth (h_{veg}=20 cm) due to the water being too shallow. Although velocity data was obtained, the focus of this thesis is free surface fluctuations and ADV analysis will not be addressed in this thesis. A diagram of the instrumentation configuration within the vegetation field for the Haynes Coastal Engineering Laboratory is shown below in Figure 16.

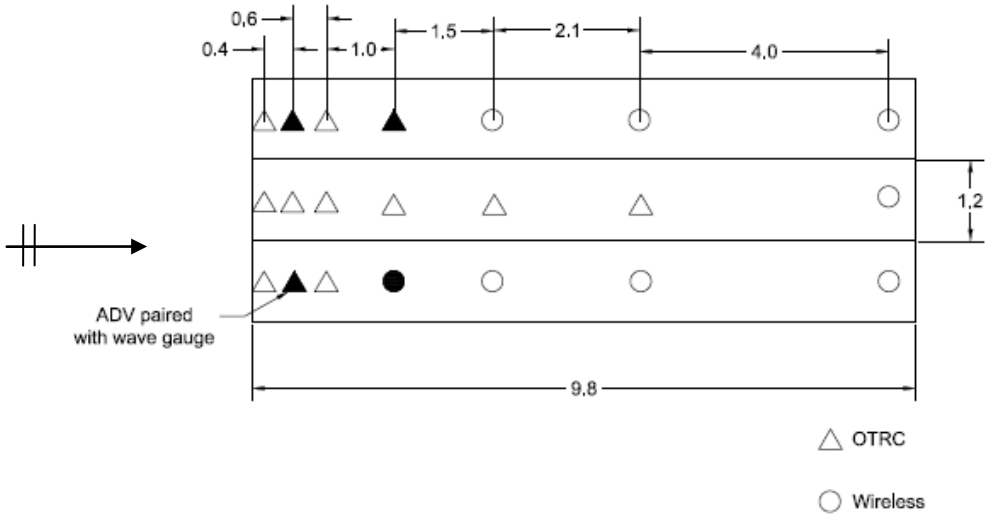

Figure 16. Instrumentation placement for Haynes Coastal Engineering Laboratory

The LabVIEW Multiple Channel Data Acquisition System was utilized to collect free surface fluctuation timeseries for all the wave gauges while velocity timeseries were obtained and converted to ASCII using Nortek's Vectrino Plus program. All instrumentation was wired to receive a trigger from the wavemaker to ensure sampling

began at the same time. Data was sampled at 25 Hz for 300 s to ensure an acceptable length wave record for spectral analysis.

3.4.2. Two-dimensional Wave Flume

Eight Seasim resistance wave gauges were used for data collection in the two-dimensional wave flume. Two sets of gauge locations were completed, allowing for 11 sampled locations inside the flume. The gauges were installed in the approximate center of flume in order to avoid edge effects. Each resistance gauge consists of two stainless steel probes 400 mm long. These gauges were then wired into an amplifier and the amplitude adjusted until a displacement of 1.0 cm registered approximately a 0.5 v change. Like the capacitance gauges, these gauges were calibrated in order to obtain a correlation between voltage and surface fluctuations, and a calibration was accepted only when the correlation error was below 0.005. The measured locations in the wave flume are presented below in Figure 17. In addition to obtaining free surface fluctuations from the gauges, visual measurements were recorded using a ruler to verify inaccurate points.

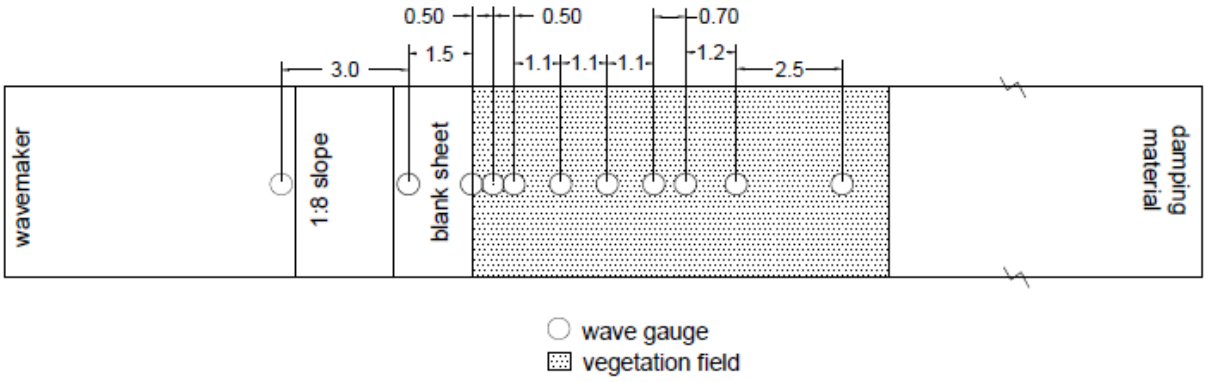

Figure 17. Location of sample points in the wave flume

Data was sampled at 25 Hz for 60 s for all tests using the LabVIEW Multiple Channel Data Acquisition program. Shorter wave signals than those in the Haynes Coastal Engineering Laboratory were required in order to reduce wave reflection interference; however, the tests were repeated multiple times until at least 200 waves were sampled to allow adequate length for spectral analysis. To obtain 200 waves, the T=2.0 s wave was repeated 12 times, the T=1.6 s wave was repeated 9 times, and the T=1.0 s wave was repeated 7 times.

3.5. Data Preprocessing

In order to ensure accurate data processing, raw timeseries from the capacitance wave gauges were filtered to remove large spikes from the wave records. These spikes were excluded by applying the phase-space thresholding method developed by *Goring and Nikora* (2002), which was available as a MATLAB subroutine written by Nobuhito Mori as part of the free MACE toolbox for coastal engineers. Originally intended to despike ADV data, the phase-space thresholding method uses the concept of a three-dimensional Poincaré map where the considered variable and its derivatives are plotted against each other. An ellipsoid is then defined using the Universal criterion, which defines the expected absolute maximum of a sequence of n independent, random numbers. The accurate data tends to cluster within this ellipsoid cloud while the outlying points are designated as spikes. An example a phase-space plot is presented below in Figure 18.

This despiking process was iterated until the number of outliners either remained constant or reduced to zero. After these points are identified as spikes, they are replaced

using a cubic interpolation. An example of a measured timeseries with the spike locations identified is presented below in Figure 19.

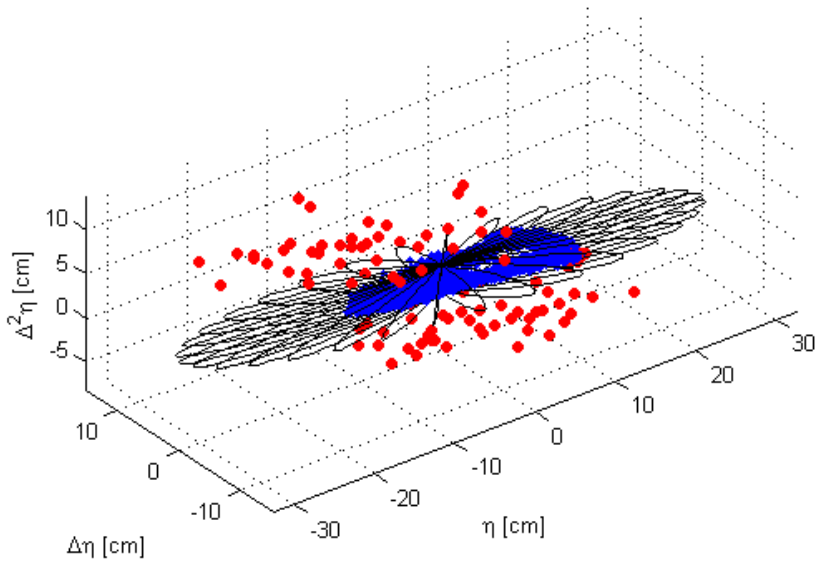

Figure 18. Phase-space plot (red points indicate outliers while blue indicates kept data)

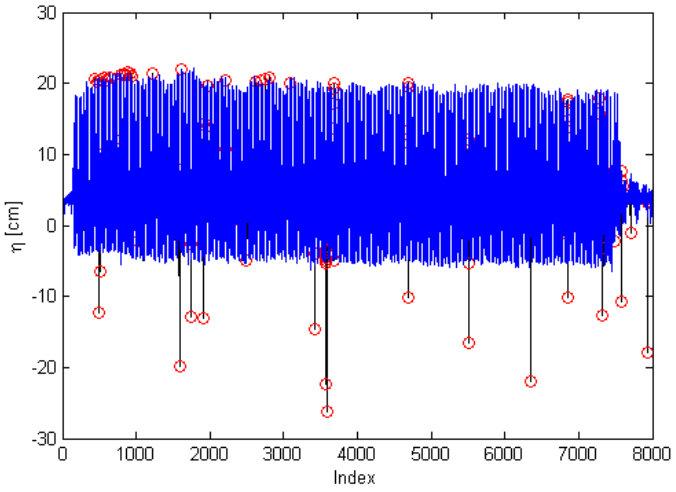

Figure 19. Example of a measured timeseries with identified spikes (spikes indicated by circles)

The data acquisition in the Haynes Coastal Engineering Laboratory was started approximately 15 s before wave generation commenced so a small portion at the beginning of each timeseries was truncated to eliminate possible errors in the analysis. The data acquisition system in the two-dimensional wave flume was started approximately 105 s before wave generation in order to sample the mean water level before wave propagation to calculate possible changes in the mean water level, such as setup. As a result, the portion of the timeseries for analysis was selected using a threshold whereby waves were identified as the top 6% of the points in the timeseries. An example of this method is shown below in Figure 20.

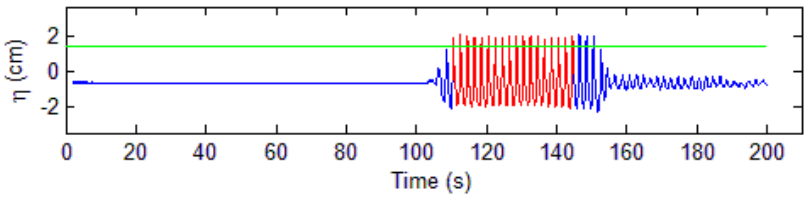

Figure 20. Threshold to identify analyzed portion (red) of measured timeseries

After removing spikes from the timeseries, wave heights were extracted from the timeseries in order to investigate the influence of relative vegetation height, stem density, and stem spatial variation on wave attenuation. The method of obtaining wave heights and the experimental results are presented in Chapter IV.

CHAPTER IV

EXPERIMENTAL RESULTS

4.1. Spectral Analysis

Initially, a wave-by-wave analysis using the zero-upcrossing method was considered to extract wave heights from the measured timeseries obtained in the wave basin and flume. However, after transforming the timeseries to the frequency domain using a fast Fourier transformation, it became evident energy was being nonlinearly transferred amongst frequencies, particularly in the case of the longer waves and shallower water depths. The spectral energy density for a wave with a period of T=2.0 s where h_{veg}=20 cm is shown below in Figure 21. While most of the energy is present at the base frequency, energy is also present at frequencies two and three times the base frequency, which are coupled to the base frequency.

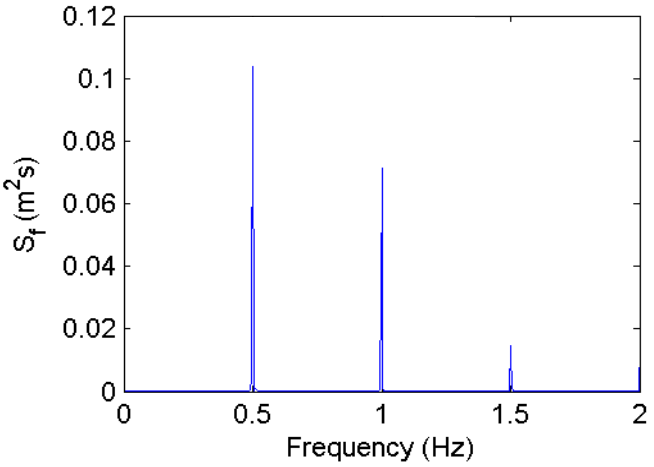

Figure 21. Spectral energy density of T=2.0 s wave

The zero-upcrossing method is incapable of capturing these nonlinearities, and as a result, the root-mean-square wave height was calculated using the total energy in the spectrum as follows:

$$H_{rms} = \sqrt{8m_0} \tag{4.1}$$

where m_0 is the zeroeth-order spectral moment or the area under the spectral curve. For the two-dimensional flume, each repeat served as a separate realization and was Bartlett averaged to generate a smoothed spectrum.

4.2. Haynes Coastal Engineering Laboratory

In a three-dimensional wave basin, monochromatic waves with periods ranging from 1.0 s to 2.0 s were investigated over eight vegetation arrays varying in stem spacing and uniformity of spacing. Three water depths of h_{veg}=60 cm, 40 cm, and 20 cm allowed for both submerged and emergent conditions. In order to describe the vegetation arrays, a convenient naming convention will be adopted from this point forward where the stem spacing and standard deviation will be described in the following stem spacing-standard deviation format. For example, random array 5 which has a stem spacing Δs=7 cm and a standard deviation σ=2.8 cm will from this point be referred to as 7 cm-40% where spacing standard deviation is represented as a percentage of Δs (e.g. σ=0.4*Δs=2.8 cm).

To eliminate small discrepancies between tests of the same wave conditions, wave heights are normalized by the incident wave height (H_{rms0}) for each individual test, ensuring all the plots start at H_{rms}/H_{rms0}=1.0. Distances are normalized by the local linear theory wave length L, which was calculated by substituting the peak period and water depth at the gauge location into the linear wave theory dispersion relation in the

absence of vegetation given as:

$$\omega^2 = gk\tanh(kh) \text{ where } \omega = \frac{2\pi}{T} \tag{4.2}$$

and the relationship between wavelength and wavenumber k is the following:

$$k = \frac{2\pi}{L} \tag{4.3}$$

In order to determine the influence of stem density on wave transformation, vegetation arrays 2, 5, and 8, corresponding to 4 cm-40%, 7 cm-40%, and 11 cm-40%, were considered. The affect of stem spacing standard deviation on wave transformation was evaluated by comparing arrays 4, 5, and 6, corresponding to 7 cm-20%, 7 cm-40%, and 7 cm-60%, respectively. Although additional vegetation arrays were tested, their analysis is not within the scope of this thesis. Unfortunately, the failure of multiple gauges during the control tests as well the vegetation arrays prevented the analysis of the shallowest water depth h_{veg}=20 cm as many subsequent points would have to be eliminated and the wave trends could not be accurately represented.

The average percent reductions in wave height per wavelength for all densities in the basin experiments, including the control, are summarized below in Table 6. As anticipated, dissipation of the incident wave through a given vegetation field was larger for the 40 cm water depth than for the 60 cm under the same wave conditions, as can be seen in Figure 22 for T=2.0 s. The l_s/h ratio for h_{veg}=40 cm and for h_{veg}=60 cm were approximately 0.76 and 0.51, respectively, meaning the stems occupied more of the water column for the 40 cm water depth than the 60 cm. A dependence of wave attenuation on the ratio between stem length and water depth is expected given that wave

particle velocities vary with depth.

Table 6. Average percent reduction in wave height due to different stem spacings

h_{veg} (cm)	T (s)	H_{wm} (cm)	Δs (cm)	N (stems/m^2)	Average percent reduction in wave height per wavelength
60	1.2	28.0	-*	-	2.6%
			11	83	-8.5%
			7	204	5.2%
			4	625	-0.60%
	2.0	28.0	-	-	22.8%
			11	83	3.4%
			7	204	4.9%
			4	625	4.9%
40	1.0	28.0	-	-	0.95%
			11	83	3.8%
			7	204	6.1%
			4	625	2.3%
	2.0	28.0	-	-	8.1%
			11	83	9.1%
			7	204	18.2%
			4	625	6.5%

* indicates control, which lacked vegetation

As seen in Figure 23, wave particles velocities are highest near the crest of the wave with lower velocities near the bed. As stems occupy more of the water column, it is these highest velocities that are further impeded, causing an increase in the amount of drag. This higher drag causes greater energy reductions through the vegetation field, which directly translates into a larger wave height decrease.

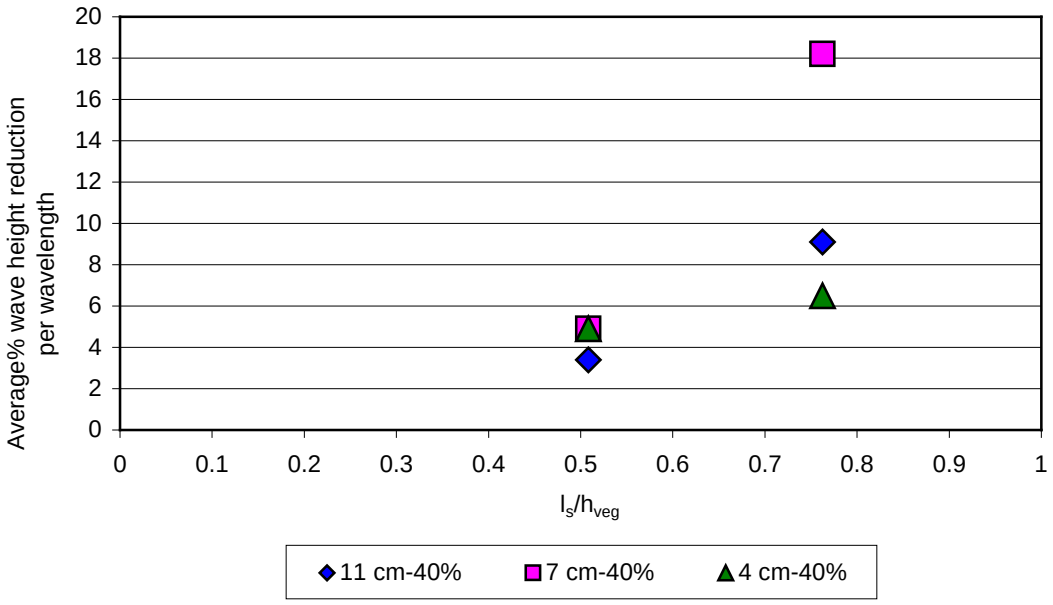

Figure 22. Average percent wave height reduction versus l_s/h for basin, [T=2.0 s]

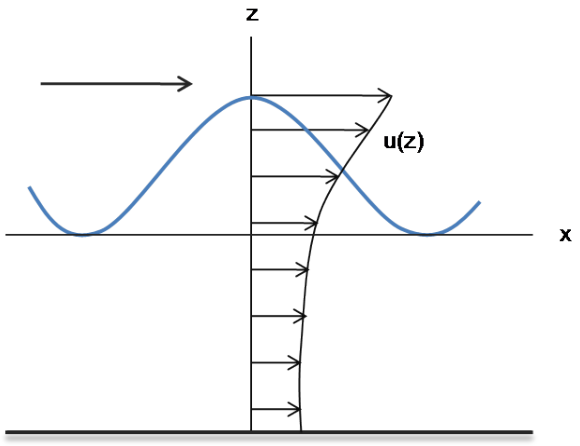

Figure 23. Wave particle velocities

For h_{veg}=60 cm, the influence of stem density on wave transformation for the group of experimental conditions is shown below in Figures 24-25. Significant

fluctuations in the wave trend are present, specifically within the first and second wave length, so percent differences were calculated at the last measured location. Although these fluctuations are sometimes dramatic, they were selected to remain in the dataset in order to demonstrate the dynamic processes that occur as the initial wave impacts the vegetation stems. Of particular interest is the presence of a peak that usually occurs at the second or third point within the vegetation field. This peak may occur as a result of the waves beginning to shoal as they encounter the vegetation field.

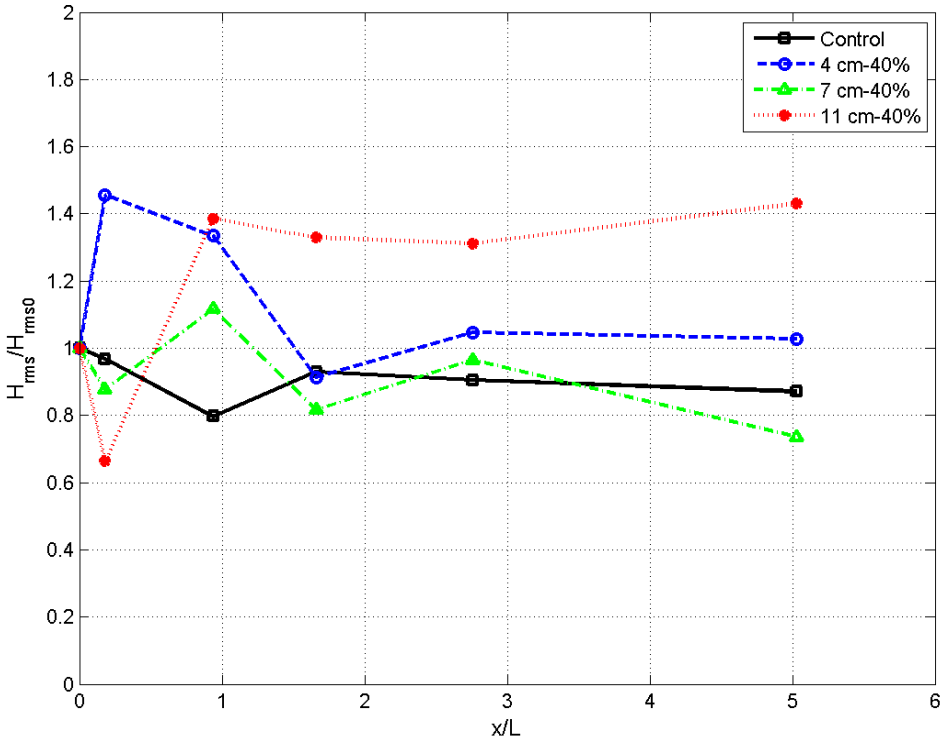

Figure 24. Normalized wave heights for different stem spacings, [h_{veg}=60 cm, T=1.2 s]

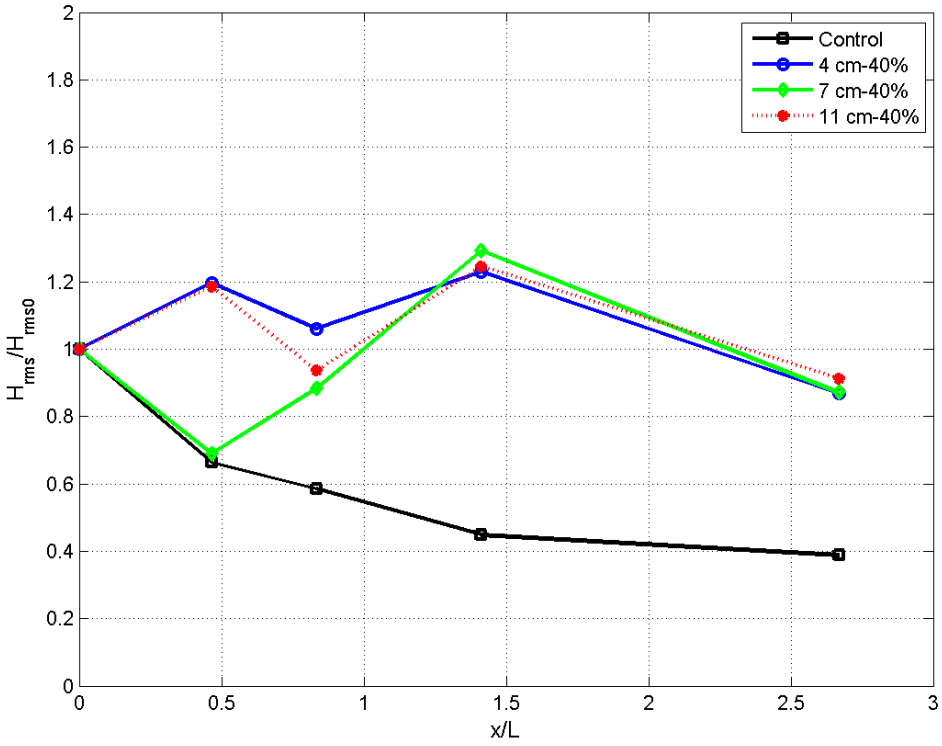

Figure 25. Normalized wave heights for different stem spacings, [h_{veg}=60 cm, T=2.0 s]

The results of the h_{veg}=60 cm cases indicate the vegetation fields for all the tests dissipated less energy than the control, except the 7 cm-40% array for T=1.2 s. In some cases, there was actually an increase in wave height, presented in Table 6 as a negative reduction. These results are presented graphically below in Figure 26. Although the exact reason for this occurrence is unknown, a possible explanation is the presence of some shoaling effect. Vegetation-induced wave attenuation was initially limited due to h_{veg}=60 cm being the most submerged condition with l_s/h=0.51, and possibly shoaling due to the sloping bottom could counteract any vegetation-induced wave attenuation further. Additionally, the higher density vegetation fields could induce lower damping

by behaving as a "pseudo" impermeable step. This possibility is supported by *Mendez and Losada* (1999) as they investigated the sensitivity of a derived model to plant density. *Mendez and Losada* (1999) found that increasing the stem density up to a certain point (between 100 and 5000 stems/m^2) caused lower wave damping, suggesting wave dissipation is limited and cannot increase above a given density. However, it is unknown as to why the lowest density had the largest increase in wave height for T=1.2 s or behaved similar to the medium and high density for T=2.0 s; these results could be due to persisting gauge errors since these wave conditions were conducted consecutively. The interaction between shoaling waves and vegetation is highly dynamic and complex, and additional experiments should be conducted to verify the wave trends presented herein.

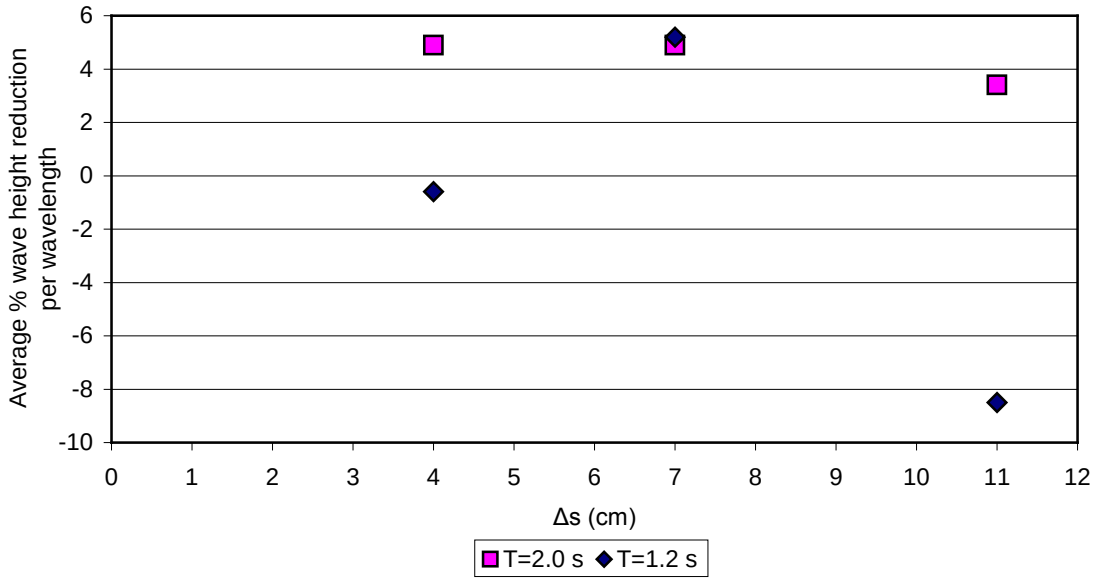

Figure 26. Average percent wave height reduction versus stem spacing, [h_{veg}=60 cm]

The influence of stem density on the amount of wave attenuation was more evident for h_{veg}=40 cm as seen in Figure 27 and Figure 28.

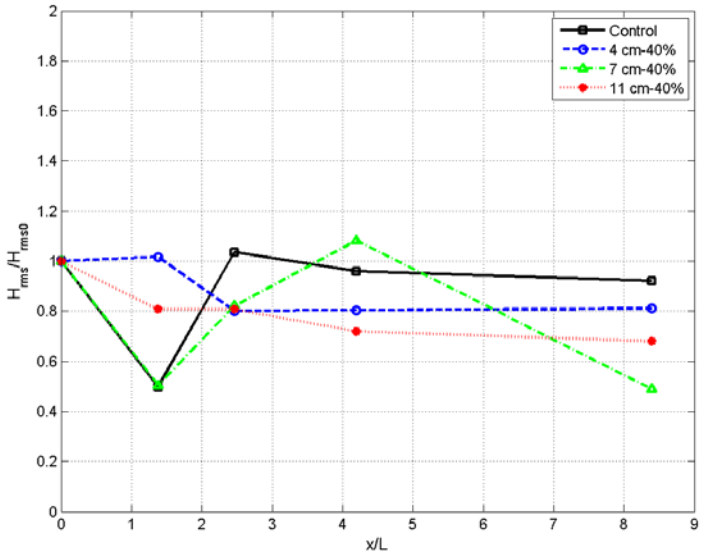

Figure 27. Normalized wave heights for different stem spacings, [h_{veg}=40 cm, T=1.0 s]

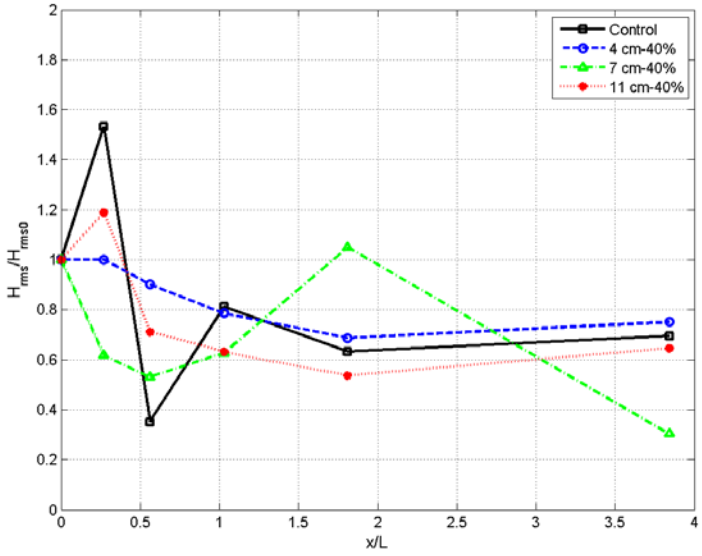

Figure 28. Normalized wave heights for different stem spacings, [h_{veg}=40 cm, T=2.0 s]

Contrary to h_{veg}=60 cm, the results indicate the vegetation arrays dissipated more energy than the control for all wave conditions except the 4 cm-40% for T=2.0 s. The medium stem density (Δs=7 cm) dissipated the most wave energy followed by the lowest stem density (Δs=11 cm) and the highest stem density (Δs=4 cm), respectively, for all wave conditions, as can be seen in Figure 29.

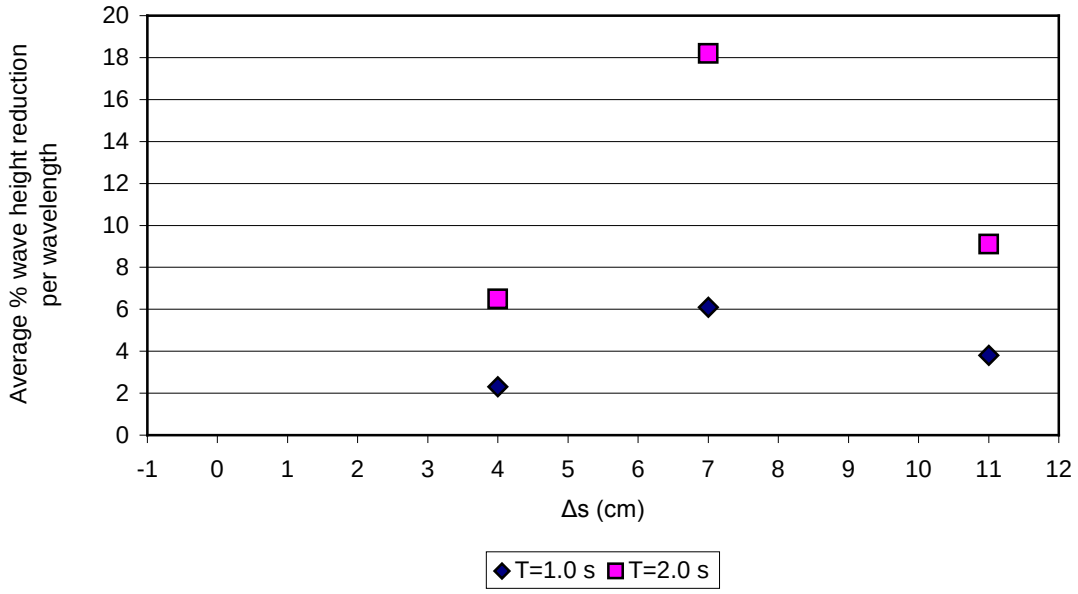

Figure 29. Average percent wave height reduction versus stem spacing, [h_{veg}=40 cm]

The medium stem density dissipated more energy than the lowest stem density, as expected. Remembering these stem spacings are representative of a healthy and unhealthy wetland, it becomes apparent a healthy wetland has higher wave attenuation capabilities than an unhealthy wetland due to a higher stem density. While it may be expected wave attenuation would continue to increase with increasing density, the

unnaturally highest density case (Δs=4 cm, N=625 stems/m^2) might dissipate the least amount of wave energy, and could actually cause wave shoaling, if the vegetation acted as an impermeable step and diverted flow over rather than through it.

The effect of stem spacing uniformity on wave transformation for h_{veg}=60 cm and 40 cm is also investigated. Table 7 summarizes the average percent reduction in wave height per wavelength for different standard deviations of stem spacing. Data for the 7 cm-60% vegetation array was obtained at fewer locations in the flume, so the percent difference in wave height was calculated at the last point where all three vegetation arrays were sampled. Interestingly, wave attenuation appears to have a slight dependence on stem spatial variation.

Table 7. Average percent reduction in wave height for varying stem spacing standard deviations

h_{veg} (cm)	T (s)	H_{wm} (cm)	Δs (cm)	σ (cm, % of Δs)	Average percent reduction in wave height per wavelength
60	1.2	28.0	7	1.4 (20%)	-3.3%
				2.8 (40%)	1.4%
				4.2 (60%)	-0.36%
	2.0	28.0	7	1.4 (20%)	-63.1%
				2.8 (40%)	-20.6%
				4.2 (60%)	-0.71%
40	1.0	28.0	7	1.4 (20%)	-8.3%
				2.8 (40%)	-1.9%
				4.2 (60%)	2.6%
	2.0	28.0	7	1.4 (20%)	-13.8%
				2.8 (40%)	-2.8%
				4.2 (60%)	18.2%

The total percent reduction in wave height for h_{veg}=60 cm and 40 cm are graphically presented in Figures 30-33.

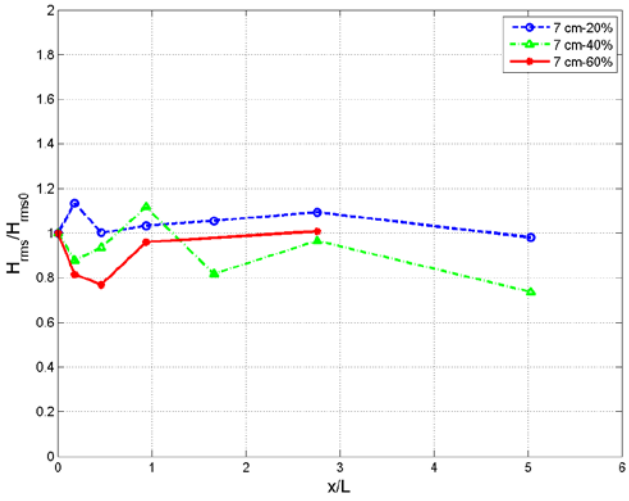

Figure 30. Normalized wave heights for different stem spacing standard deviations, [h_{veg}=60 cm, T=1.2 s]

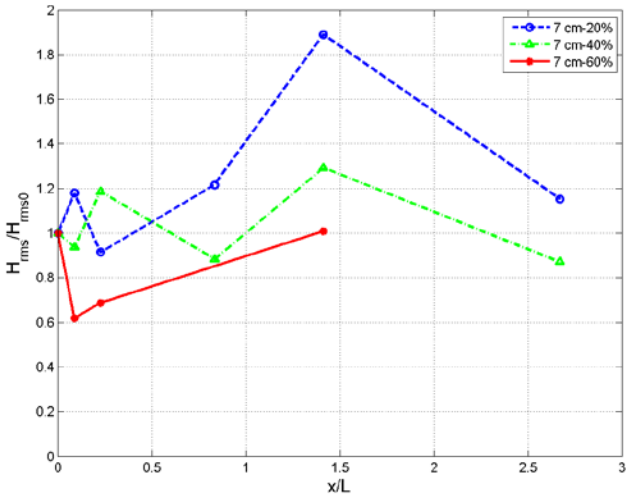

Figure 31. Normalized wave heights for different stem spacing standard deviations, [h_{veg}=60 cm, T=2.0 s]

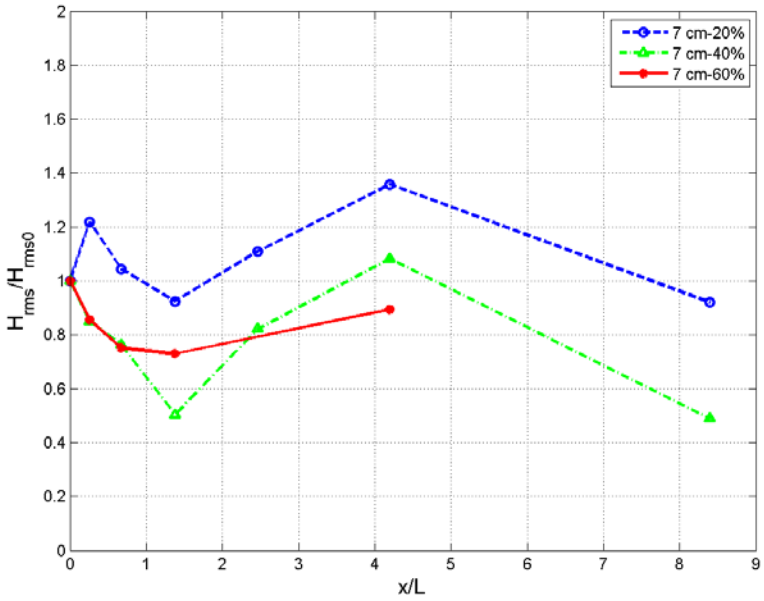

Figure 32. Normalized wave heights for different stem spacing standard deviations, [h_{veg}=40 cm, T=1.0 s]

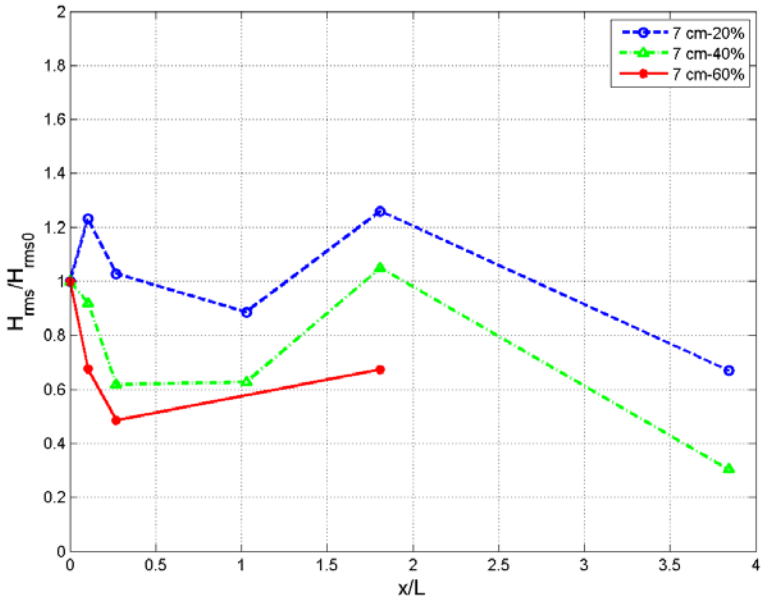

Figure 33. Normalized wave heights for different stem spacing standard deviations, [h_{veg}=40 cm, T=2.0 s]

For all wave conditions except for one, the 60% standard deviation yielded the highest wave attenuation followed by the 40% and 20% standard deviations, in that order. Essentially, wave dissipation increased as the randomness of stem spacing increased. This relationship can be seen in Figure 34.

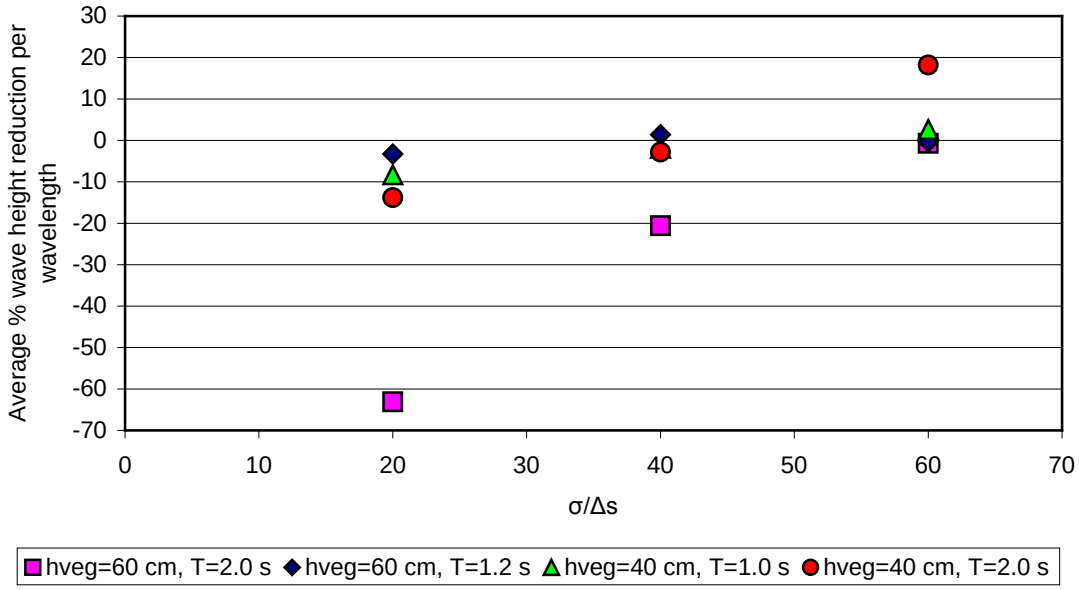

Figure 34. Average percent wave height reduction versus normalized spatial variation for basin

This dependence can be attributed to wake sheltering, an interaction between upstream and downstream cylinders. During wake sheltering, upstream stems are impacted by higher wave energy, slowing the fluid flow velocity behind them which reduces drag on nearby cylinders further down the field. *Nepf* (1999) documented an increase in wake sheltering as stem density increased. Logically, this is expected given that as the number of stems increases, the probability of having stems inline also increases. If this thought process is further applied to standard deviation, less uniformity

in spacing means the chances of stems being aligned is smaller than if the spacing standard deviation is small, as in a grid. As higher standard deviations result in smaller wake sheltering effects, the drag on downstream cylinders is greater than if stems were aligned, directly resulting in more wave dissipation. Additionally, the grouping of cylinders could change the scale of turbulence such that the wake sheltering principle is valid but stem clumps generate larger-scale wakes on the order of the clump diameter rather than the stem diameter.

In order to verify this dependence of wave dissipation on spacing uniformity, experiments were conducted afterwards in a two-dimensional wave flume. This wave flume provided a more controlled environment by allowing a more stable setup as well as more control over the wave conditions, such as limiting breaking. Additionally, these experiments allowed the shoaling element to be removed in order to return to a more simplified problem.

4.3. Two-dimensional Wave Flume

Monochromatic waves with periods ranging from 1.0 s to 2.0 s were investigated over two vegetation arrays varying in stem spacing standard deviation, 7 cm-20% and 7 cm-40%. Two considered water depths of h_{veg}= 17.2 cm and 29.2 cm, corresponding to l_s/h=1.0 and 0.87, represent emergent and near-emergent conditions, respectively. Local root-mean-square wave heights obtained from spectral analysis are nondimensionalized by the incident root-mean-square wave height and distances are normalized by the local wavelength at that gauge location to maintain analysis similarity between the two experiments. The incident wave height was taken as the wave immediately outside of

the vegetation field since the primary purpose of the offshore gauges was to confirm repeatability of the wave signal.

Since multiple repeats were required to obtain the 200 waves suitable for spectral analysis, it was pertinent to verify the repeatability of the wave maker. Twelve repeats of a T=2.0 s wave is shown below in Figure 35 with a closer view of the farthest offshore gauge. The variation in offshore wave height is approximately 0.1 cm, which is acceptable given the produced wave heights are at least one order of magnitude higher.

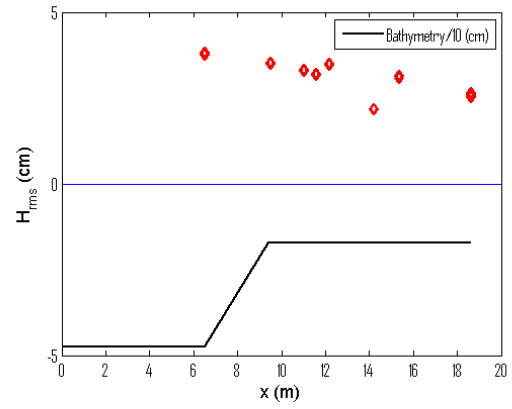

(a)

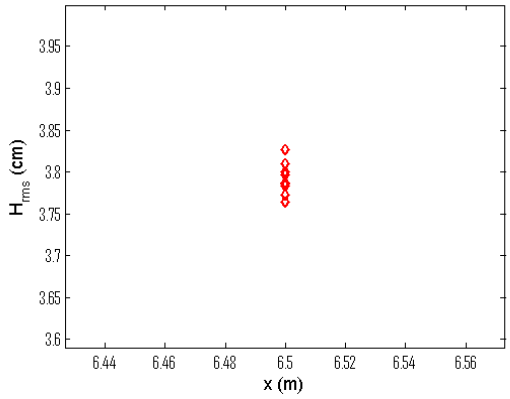

(b)

Figure 35. Accuracy of wavemaker (a) with closeup of offshore gauge (b)

The results of h_{veg}=29.2 cm and 17.2 cm for all considered wave conditions are shown below in Figures 36-41.

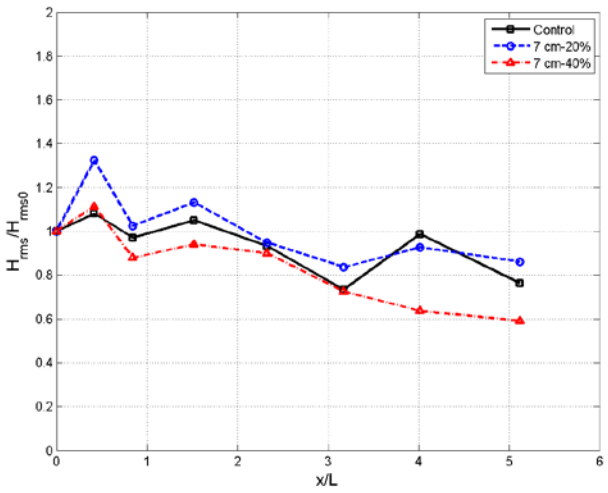

Figure 36. Normalized wave heights for different stem spacing standard deviations, [h_{veg}=29.2 cm, T=1.0 s]

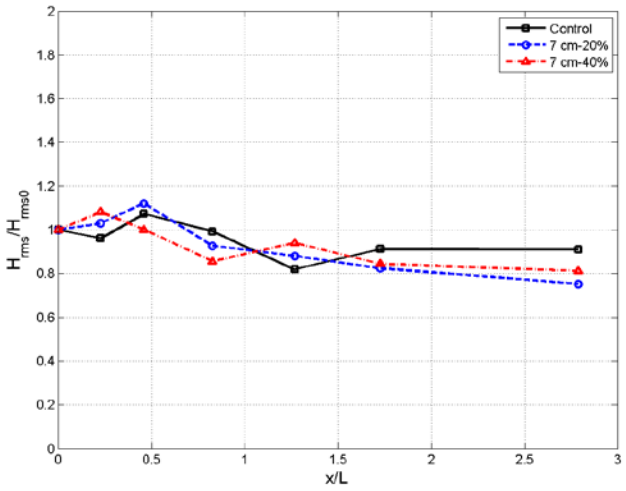

Figure 37. Normalized wave heights for different stem spacing standard deviations, [h_{veg}=29.2 cm, T=1.6 s]

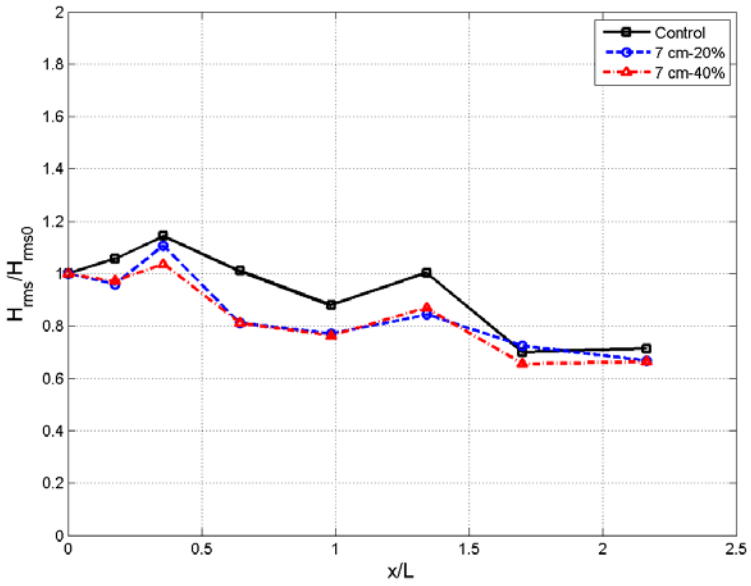

Figure 38. Normalized wave heights for different stem spacing standard deviations, [h_{veg}= 29.2 cm, T=2.0 s]

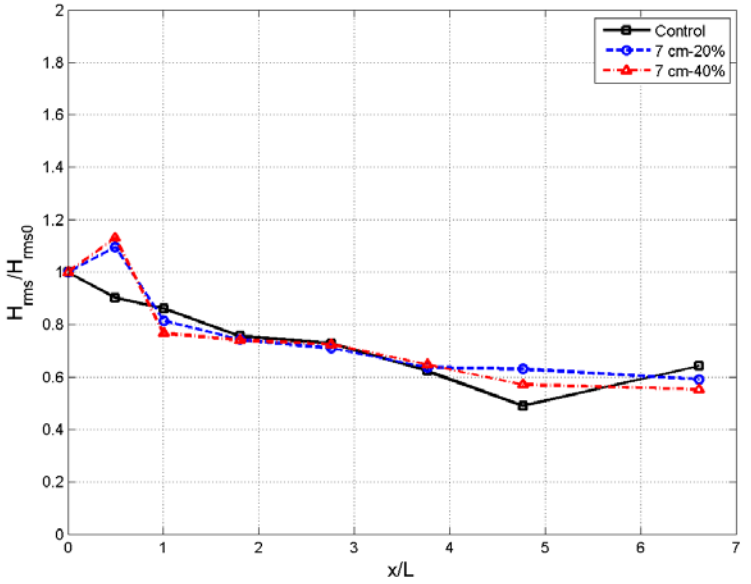

Figure 39. Normalized wave heights for different stem spacing standard deviations, [h_{veg}=17.2 cm, T=1.0 s]

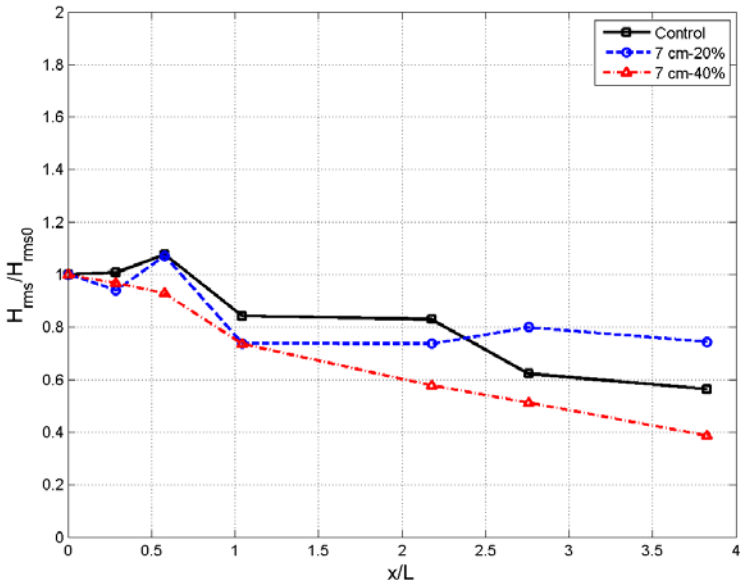

Figure 40. Normalized wave heights for different stem spacing standard deviations, [h_{veg}=17.2 cm, T=1.6 s]

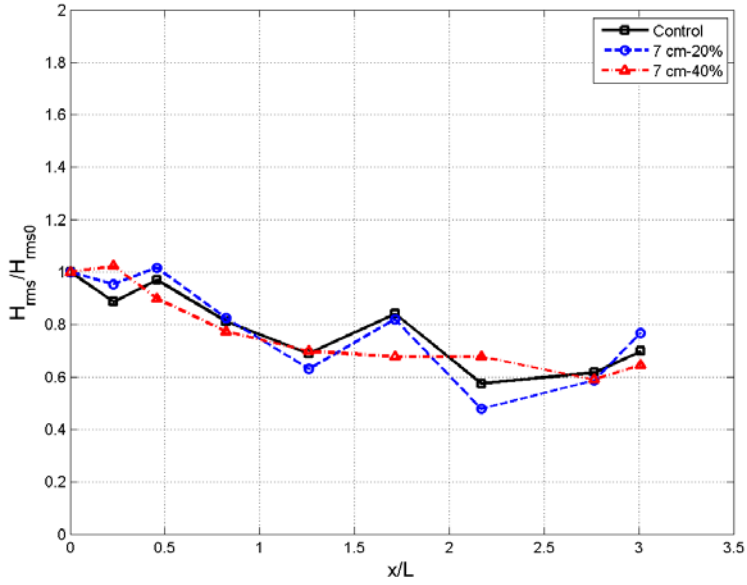

Figure 41. Normalized wave heights for different stem spacing standard deviations, [h_{veg}=17.2 cm, T=2.0 s]

A summary of the average percent reduction in wave height per wavelength for all tested hydrodynamic and vegetation conditions for h_{veg}=29.2 cm and 17.2 cm is presented in Table 8.

Table 8. Average percent reduction in wave height for flume

h_{veg} (cm)	T (s)	H_{wm} (cm)	Δs (cm)	σ (cm, % of Δs)	Average percent difference in wave height per wave length
29.2	1.0	7.3	-	-	4.7%
			7	1.4 (20%)	2.7%
				2.8 (40%)	8.0%
	1.6	6.4	-	-	3.2%
			7	1.4 (20%)	9.0%
				2.8 (40%)	6.8%
	2.0	4.8	-	-	13.4%
			7	1.4 (20%)	15.3%
				2.8 (40%)	15.7%
17.2	1.0	5.5	-	-	5.4%
			7	1.4 (20%)	6.2%
				2.8 (40%)	6.8%
	1.6	4.8	-	-	11.5%
			7	1.4 (20%)	6.8%
				2.8 (40%)	16.2%
	2.0	3.7	-	-	10.0%
			7	1.4 (20%)	8.0%
				2.8 (40%)	11.6%

In agreement with the experiments conducted in the Haynes Coastal Engineering Laboratory, the amount of wave dissipation was found to be dependent on stem spacing standard deviation despite not having a continuous shoaling bottom, as can be seen in Figure 42. The array with a 40% stem spacing deviation dissipated more energy than the

20% deviation array for all hydrologic conditions except for h_{veg}=29.2 cm and T=1.6 s. As previously mentioned, if the stems are more randomly arranged, there is more drag on downstream cylinders due to less wake sheltering as well as a possible increase in the turbulence scale such that greater wave attenuation is expected

For both experiments, it is worth mentioning that clearly in some of the datasets there is experimental error that resulted due to physical model construction flaws as well as gauge errors. Several of these errors occurred in the control measurements, which made identifying and comparing wave trends difficult in datasets where artificial vegetation was present. However, the common occurrence of overall trends in the data, especially greater wave attenuation due to larger stem spatial variation, lends confidence to the data. Simulating these wave trends with a one-dimensional model based on linear wave theory to identify the general influence of relative stem height, stem density, and stem spacing standard deviation on the bulk drag coefficient merits examination.

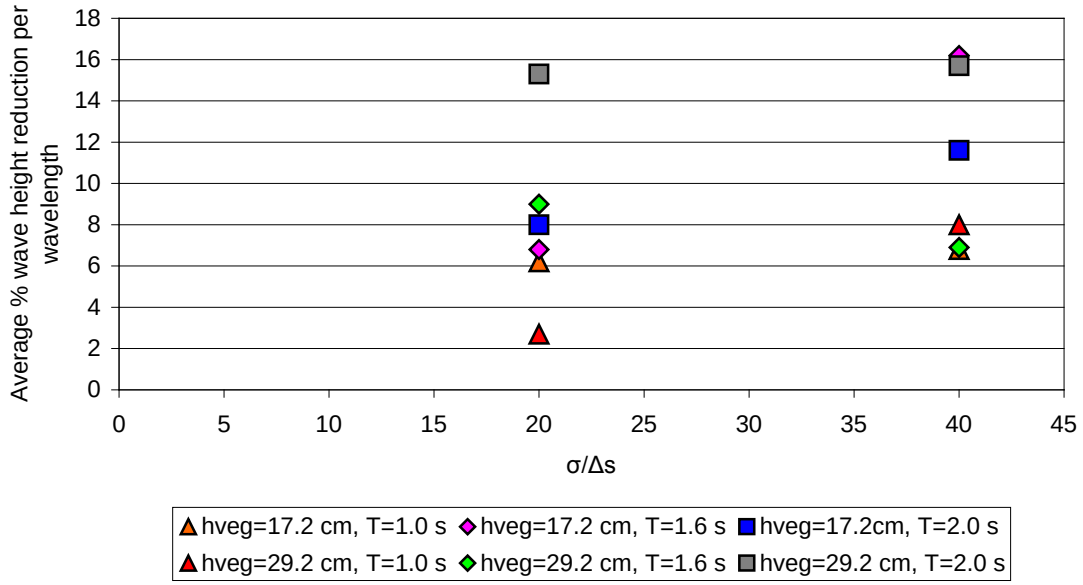

Figure 42. Average percent wave height reduction versus normalized spatial variation for flume

CHAPTER V

MODELING WAVE TRANSFORMATION OVER VEGETATION USING LINEAR WAVE THEORY

5.1. Introduction to One-dimensional Linear Wave Theory Model

5.1.1. Model Formulation

The formulation for wave dissipation due to vegetation developed by *Dalrymple et al.* (1984) was implemented into a one-dimensional, spectral wave transformation model in order to simulate the experimental results. The model tracks the energy associated with one frequency, in this case the frequency associated with the peak period given that the waves in the experiments were monochromatic, where energy density is calculated as:

$$E = \frac{1}{8}\rho g H_{rms}^2 \tag{5.1}$$

The governing equations of the model are based on linear theory, and dissipation is accounted for through reductions in wave energy. The required inputs are incident wave height H_0, wave period T, stem diameter d, stem density N, and stem length l_s. In order to simulate the results, the best fit between measured and predicted wave heights is obtained using the least-squares method where C_D is the single calibration parameter.

The model accounts for wave shoaling, wave breaking, and vegetation-induced dissipation. Assuming no refraction, wave shoaling is calculated from the conservation of energy equation by the following where *i* indicates an index:

$$E_i = E_{(i-1)}\left(\frac{C_{g_{(i-1)}}}{C_{g_i}}\right) \tag{5.2}$$

Wave breaking is determined using the simple model developed by *Battjes and Janssen* (1978) for random waves. Although the waves here are considered monochromatic, the basic assumption of this model is for each depth h there is a maximum possible wave height H_b such that all breaking or broken waves at that location are equal to H_b. From this concept, *Battjes and Janssen* (1978) developed a term Q_b which represents the fraction of breaking or broken waves at any one point, and it is through this term that the model primarily accounts for changes in depth. The equation for Q_b is provided below:

$$\frac{1-Q_b}{\ln Q_b} = -\left(\frac{H_{rms}}{H_b}\right)^2 \tag{5.3}$$

where H_b is taken as:

$$H_b = \kappa h \tag{5.4}$$

and κ is the breaker index indicating at which fraction of the total depth wave breaking occurs. The process to solve the transcendental equation for Q_b was obtained from Delft University of Technology's third-general wave model Simulating Wave Nearshore (SWAN) under the terms of the GNU General Public License. The energy dissipation rate in a broken wave is estimated from the bore dissipation in a bore of corresponding height as seen below:

$$\left\langle \varepsilon_B \right\rangle = \frac{1}{4}\rho g f \frac{H^3}{h} \tag{5.5}$$

By applying this equation to broken waves only where the probability of occurrence at a specific location is equal to Q_b, the following equation for wave dissipation due to wave breaking was implemented:

$$\langle \varepsilon_B \rangle = -\frac{1}{4} Q_b \rho g f H_b^2 \tag{5.6}$$

where H_b/h is assumed order one in shallow water and can be dropped.

A simulation was completed with a simple bathymetry in order to check the general behavior of the model. A plot of the wave transformation and Q_b for H_0=1 m and T=5.0 s is shown below in Figure 43 and Figure 44, in that order.

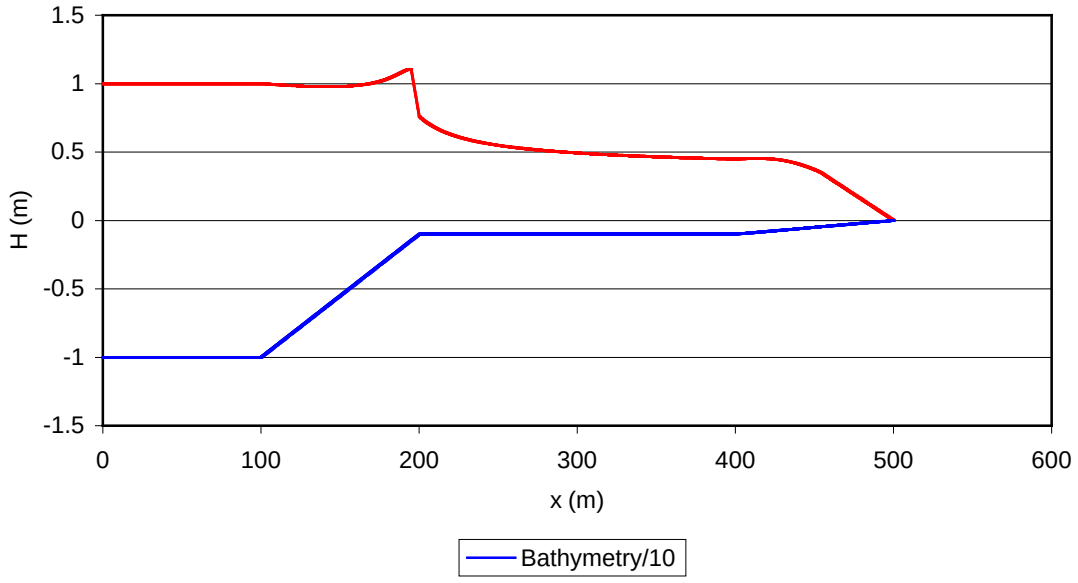

Figure 43. Modeling wave height over simple bathymetry

The model realistically captures the wave transformation as waves propagate over the bathymetry. As the waves encounter the slope, the model predicts shoaling and

then gradual breaking afterwards as the waves continue to propagate towards the shoreline. Closer to the shoreline wave breaking is again accelerated. This transformation of the waves is also reflected in the behavior of Q_b. The increases in Q_b mirror the wave height reductions due to shallower water as seen in Figure 43 while at the shoreline Q_b=1, signifying all the waves are broken at that location.

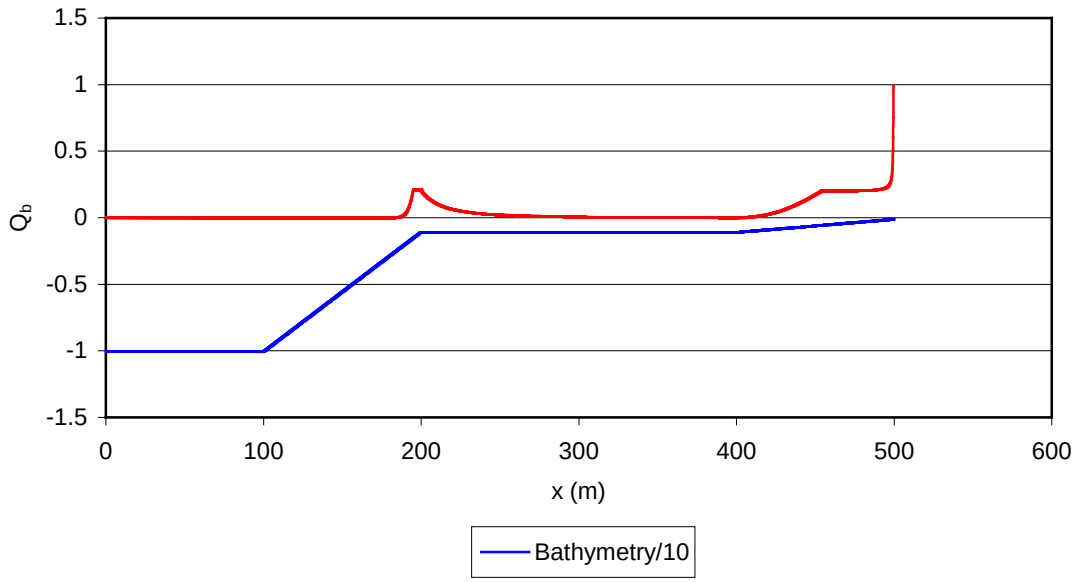

Figure 44. Q_b over simple bathymetry

After model yielded realistic wave behavior, a vegetation dissipation term was implemented. The equation for wave energy dissipation due to vegetation derived by *Dalrymple et al.* (1984) in terms of wave amplitude is the following:

$$\frac{\partial(EC_g)}{\partial x} = -\frac{2}{3\pi}\rho C_D N d\left(\frac{gk}{\omega}\right)^3 \frac{\left(\sinh^3 kl_s + 3\sinh kl_s\right)}{3k\cosh^3 kh} A^3 \qquad (5.7)$$

The equation was simply analytically integrated in order to obtain the change in wave energy as the following:

$$E_i = \left(\frac{-2}{\frac{\lambda}{C_g} dx - \frac{2}{\sqrt{E_{i-1}}}} \right)^2 \quad \text{where} \tag{5.8}$$

$$\lambda = \frac{-2}{3\pi} \rho C_D dN \left(\frac{kg}{2\omega} \right)^3 \frac{(\sinh^3 kl_s + 3\sinh kl_s)}{3k \cosh^3 kh} \left(\frac{8}{\rho g} \right)^{3/2} \tag{5.9}$$

This allowed the model to calculate the wave energy after vegetation-induced losses as a function of the energy at a previous calculation point.

5.1.2. Sensitivity Analysis of Input Parameters

Once general model behavior was verified, the sensitivity of the vegetation dissipation term to hydrodynamic conditions and vegetation characteristics was addressed. This was completed by altering the variable of interest while keeping all other inputs constant.

Looking first at hydrodynamic conditions, the first parameter varied was the incident wave height H_0. Table 9 presents the input parameters while the results are presented in Figure 45. As expected, a larger incoming wave is dissipated more by vegetation than a smaller wave. This was anticipated since wave height is present to the third power in the *Dalrymple et al*. (1984) formulation.

Table 9. Input parameters for sensitivity to incident wave height

Wave parameters		Vegetation characteristics			
H_0 (cm)	T	C_D	d (m)	N (stems/m^2)	l_s/h
5-40	2.0	0.1	0.004	250	0.3

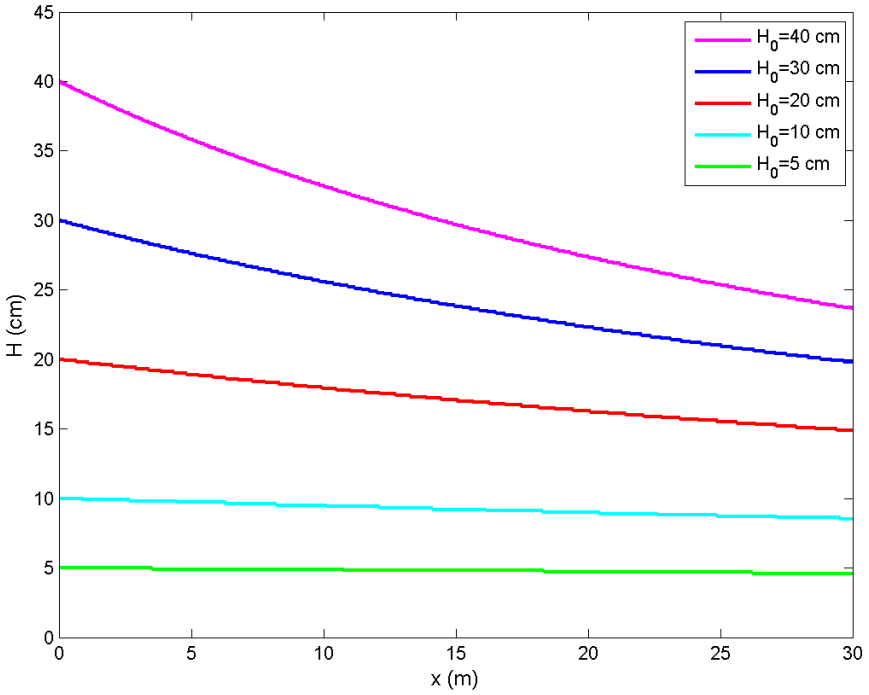

Figure 45. Sensitivity of vegetation dissipation to incident wave height, [T=2.0 s, C_D=0.1, d=0.004 m, N=250 stems/m^2, l_s/h=0.3]

The second parameter investigated was wave period, represented in Table 10 as the wavenumber times the water depth (kh). This representation was selected in order to investigate the wave period as a function of water depth, which determines whether a wave is within the shallow-water ($kh<\pi/10$), the intermediate-water ($\pi/10<kh<\pi$), or the deepwater range ($kh\geq\pi$). As can be seen in Figure 46, deepwater waves are less affected

by vegetation than shallow-water waves.

Table 10. Input parameters for sensitivity to wave period

Wave parameters		Vegetation characteristics			
H_0 (cm)	kh	C_D	d (m)	N (stems/m^2)	l_s/h
30	0.25-4.03	0.1	0.004	250	0.3

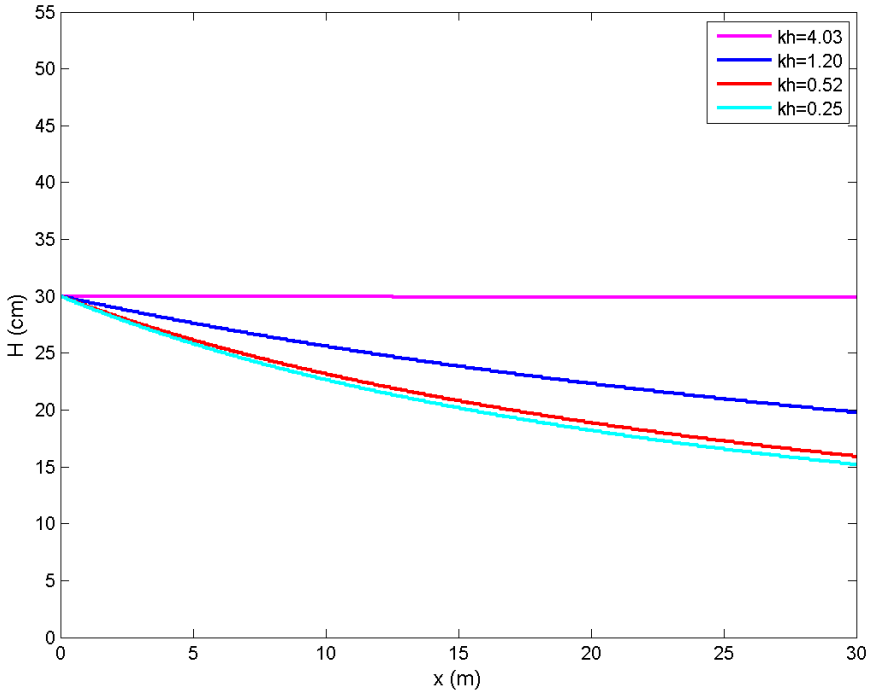

Figure 46. Sensitivity of vegetation dissipation to wave period, [H_0=30 cm, C_D=0.1, d=0.004 m, N=250 stems/m^2, l_s/h=0.3]

Shallow and deepwater waves have different particle trajectories, and these trajectories affect the amount of drag and, thus, the amount of wave dissipation. Diagrams of the particle trajectories for shallow and deepwater waves are presented in

Figure 47. A deepwater wave's particle path is a radius that decays exponentially with particle motion at the bottom being nearly negligible. The shallow-water wave's particle path experiences the same horizontal excursion but a decreasing vertical excursion until the bottom where no vertical motion is present. Looking at these trajectories, it is apparent that bottom features, in this case vegetation, will affect shallow-water waves more than deepwater waves.

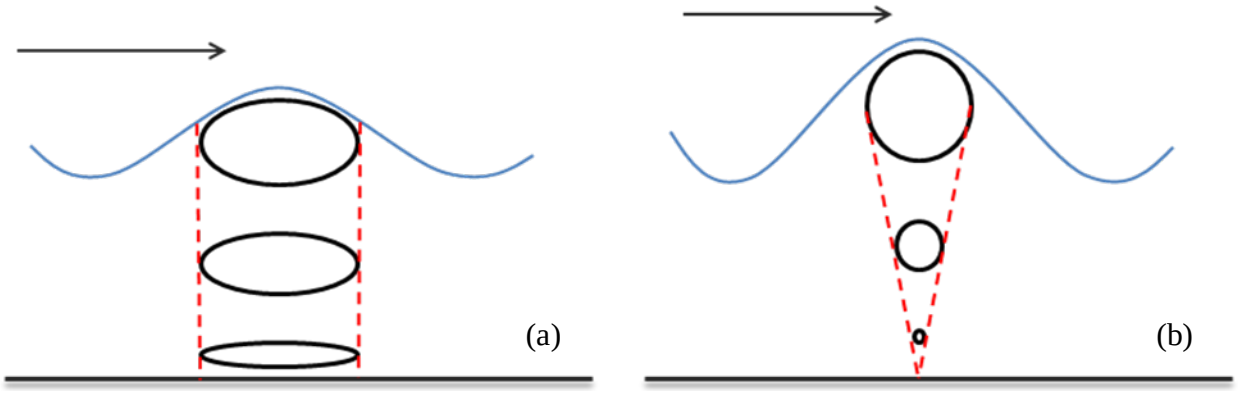

Figure 47. Particle trajectories for shallow-water (a) and deepwater (b) waves

The sensitivity of the model to vegetation characteristics, including the relative stem height and bulk drag coefficient, was also explored. Using the input parameters in Table 11, it was found that as stems occupy a larger portion of the water column, wave dissipation increases. These results can be seen in Figure 48.

Table 11. Input parameters for sensitivity to relative vegetation height

Wave parameters		Vegetation characteristics			
H_0 (cm)	T	C_D	d (m)	N (stems/m^2)	l_s/h
30	2.0	0.1	0.004	250	0.25-1.0

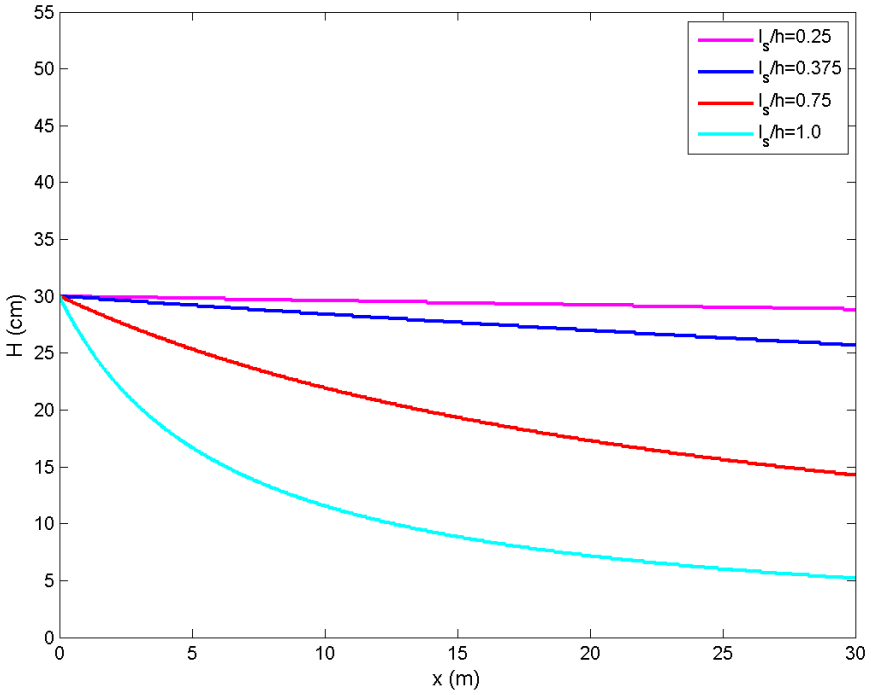

Figure 48. Sensitivity of vegetation dissipation to relative vegetation height, [H_0=30 cm, T=2.0 s, C_D=0.1, d=0.004 m, N=250 stems/m^2]

Again, this is because the highest wave particle velocities near the wave crest are impeded as the stems approach the surface of the water. When the stems are deeply submerged, only slower wave velocities are experienced and hence little drag is generated on these stems. As the water depth decreases, the stems remain submerged but occupy more of the water column and begin to interfere with greater wave velocities,

generating more drag as higher velocities are lowered. This drag generation results in a gradual increase in wave dissipation. Finally, as the vegetation protrudes from the water level and becomes emergent, there is a significant increase in dissipation since the highest wave particle velocities are now considerably impeded and drag is substantial, translating to the greatest amount of wave attenuation. A simple illustration of this interaction for a near-emergent and emergent condition is presented in Figure 49.

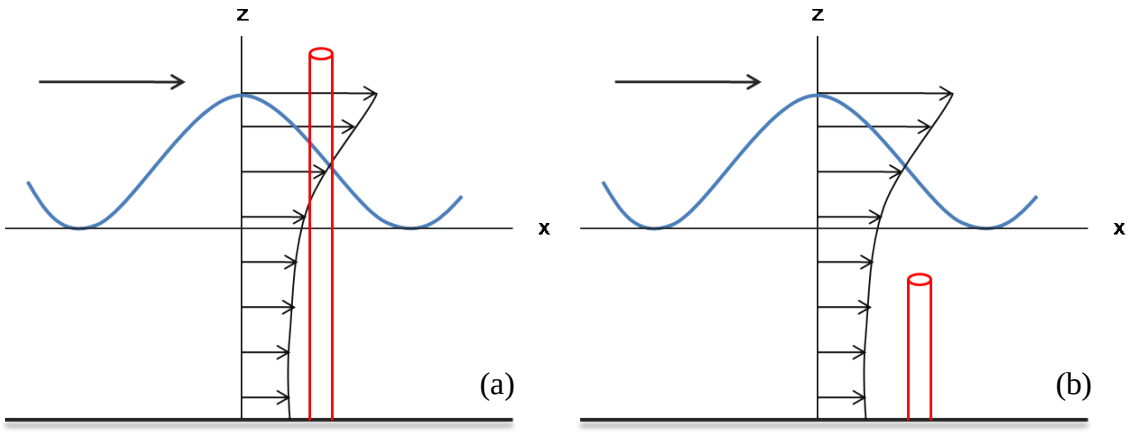

Figure 49. Interactions of particle velocities with emergent (a) and submerged (b) stems

In *Dalrymple et al.*'s (1984) vegetation dissipation term, the bulk drag coefficient C_D, stem density N, and stem diameter d are linearly multiplied. Therefore, a change in any one of these parameters influences the model by the same extent. For example, as seen in Figure 43, wave dissipation increases as the bulk drag coefficient increases. The model would react to a similar way to an increase in density as well as a wider stem diameter. The inputs are supplied in Table 12 with the results presented in Figure 50.

Table 12. Input parameters for sensitivity to bulk drag coefficient

Wave parameters		Vegetation characteristics			
H_0 (cm)	T	C_D	d (m)	N (stems/m^2)	l_s/h
30	2.0	0.0-1.0	0.004	250	0.3

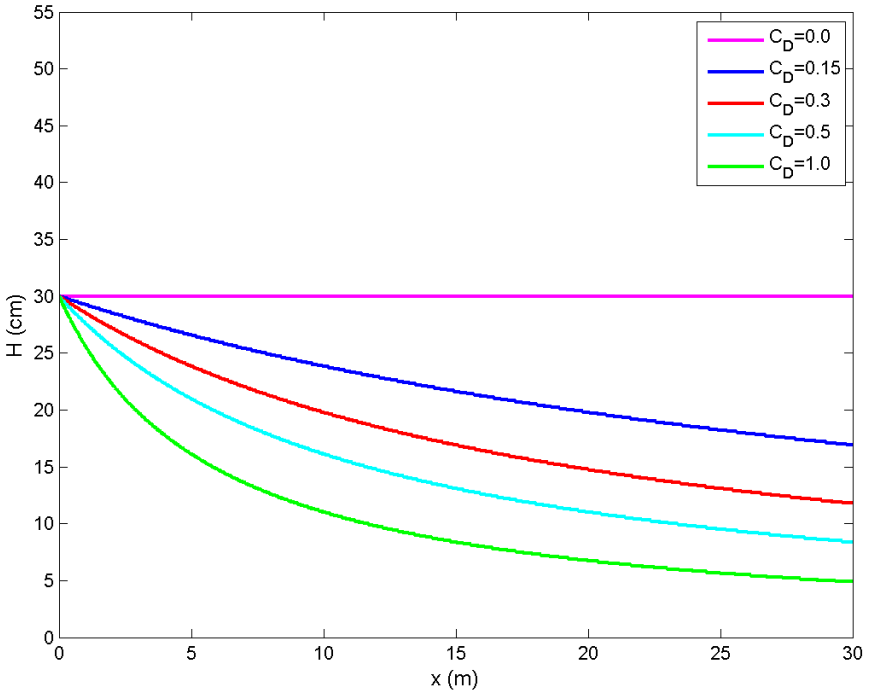

Figure 50. Sensitivity of vegetation dissipation to bulk drag coefficient, [H_0=30 cm, T=2.0 s, d=0.004 m, N=250 stems/m^2, l_s/h=0.3]

5.2. Modeling of Bulk Drag Coefficient

Although wave breaking was discouraged to avoid complicating the study, wave breaking occurred in both sets of experiments. Small spilling breakers were observed in the Haynes Coastal Engineering Laboratory, and spilling breakers sometimes occurred prematurely in the flume because of instability effects resulting from the glass walls.

Therefore, prior to modeling the vegetative conditions, the breaker index was calibrated for each wave condition by minimizing the least squares error between measured and predicted wave heights for the control wave conditions. The values of the calibrated breaker indices (κ_{cal}) are summarized below in Table 13. Examples of the predicted wave heights versus the measured wave heights for the Haynes Coastal Engineering Laboratory and the two-dimensional wave flume are presented in Figure 51 and 52, respectively. The remaining calibrated breaker index plots for each control condition can be referenced in Appendix A.

Table 13. Calibrated breaker indices

Haynes Coastal Engineering Laboratory			
h_{veg} (cm)	H_{wm} (cm)	T (s)	κ_{cal}
60	28.0	1.2	0.619
	28.0	2	0.187
40	28.0	1	1.046
	28.0	2	0.558
Two-dimensional flume			
h_{veg} (cm)	H_{wm} (cm)	T (s)	κ_{cal}
29.2	7.4	1.0	0.346
	6.8	1.6	0.237
	5.3	2.0	0.392
17.2	5.2	1.0	0.284
	4.8	1.6	0.255
	3.9	2.0	0.198

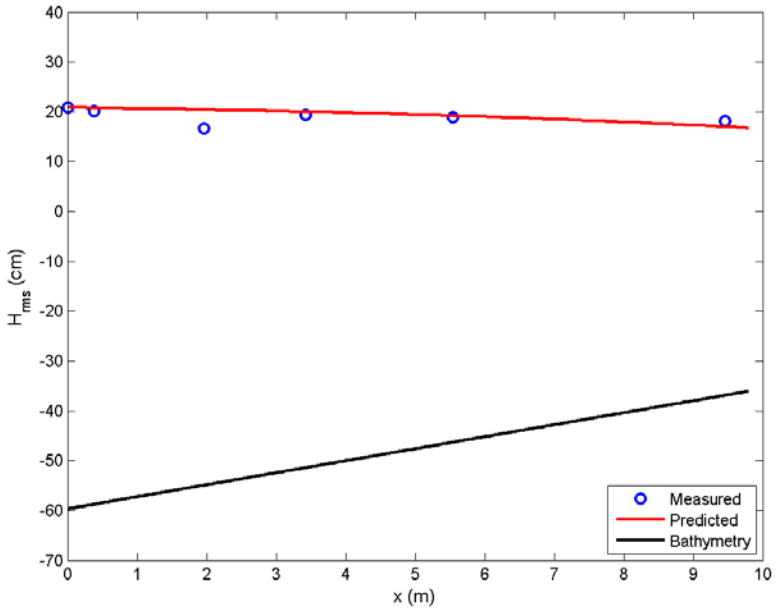

Figure 51. Calibrated breaker index, [h_{veg}=60 cm, H_{wm}=28.0 cm, T=1.2 s, κ_{cal}=0.619]

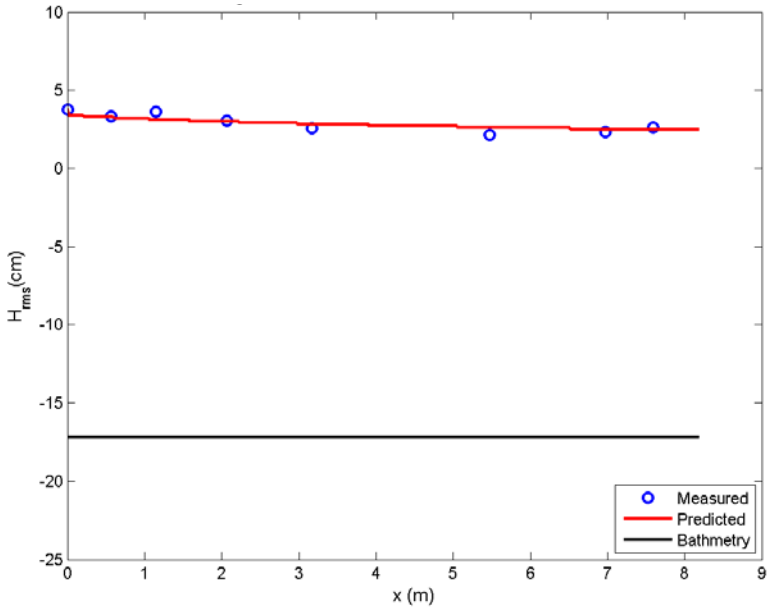

Figure 52. Calibrated breaker index, [h_{veg}=17.2 cm, H_{wm}=3.9 cm, T=2.0 s, κ_{cal}=0.198]

After calibrating the breaking index, the influence of relative stem height, stem density, and stem spacing deviation was examined by calibrating the bulk drag coefficient using experimental results. Like the breaker index, C_D was calibrated using the least squares method. Table 14 summarizes the calibrated drag coefficients (C_{Dcal}) for the Haynes Coastal Engineering Laboratory while Figure 53 presents an example of predicted wave heights versus measured wave heights. Additional plots of model results for the remaining wave conditions and vegetation fields are available in Appendix B.

Table 14. Vegetation field C_{Dcal} for Haynes Coastal Engineering Laboratory

h_{veg} (cm)	H_{wm} (cm)	T (s)	C_{Dcal}				
			4 cm-40%	7 cm-20%	7 cm-40%	7 cm-60%	11 cm-40%
60	28.0	1.2	0.0	0.0	0.04	0.001	0.0
		2.0	0.0	0.0	0.0	0.0	0.0
40	28.0	1.0	0.012	0.005	0.133	0.092	0.162
		2.0	0.013	0.022	0.375	0.424	0.194

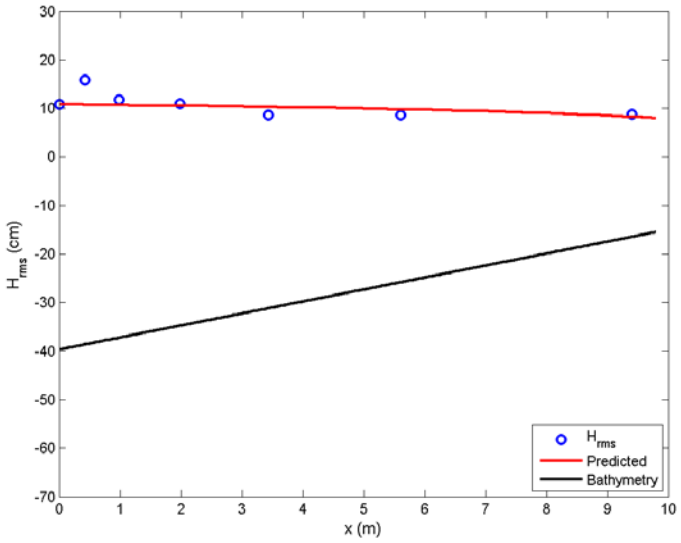

Figure 53. Predicted wave heights, [h_{veg}=40 cm, H_{wm}=28.0 cm, T=1.0 s, 4 cm-40%, C_{Dcal}=0.012]

As addressed in the experimental results section, the majority of the wave conditions for h_{veg}=60 cm experience very little, if any, attenuation and in some cases, wave height actually increases. This translated to a C_{Dcal}=0.0 for the majority of the wave conditions because the little dissipation that did occur is captured by wave breaking. An example of a plot where C_{Dcal}=0.0 is show below in Figure 54.

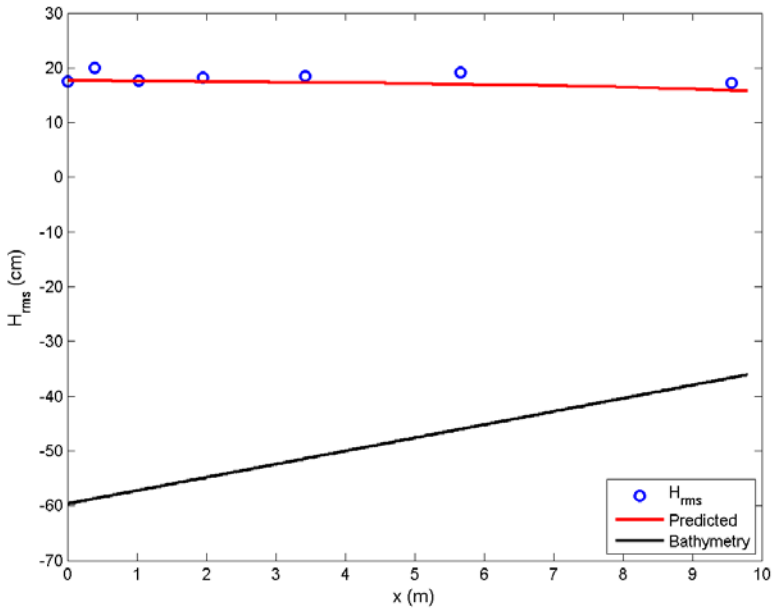

Figure 54. Predicted wave heights, [h_{veg}=60 cm, H_{wm}=28.0 cm, T=1.2 s, 7 cm-20%, C_{Dcal}=0.0]

Since C_{Dcal}=0.0 or approached that for every vegetation field, the vegetation possibly had little to no dissipative affect on the propagating waves due to being too deeply submerged, and if high enough density, actually caused wave shoaling. On the contrary, C_{Dcal} values for h_{veg}=40 cm are greater than zero, indicating vegetation-induced wave damping occurred. In agreement with *Mendez and Losada* (2004), the vegetation field

bulk drag coefficient is highly dependent on the ratio of stem length to water depth where higher l_s/h ratios translate into larger coefficient values .

Unfortunately, this eliminates h_{veg}=60 cm from any further analysis regarding influence of density and spacing uniformity, leaving only two wave conditions for the density analysis. A plot of the C_{Dcal} versus **a**d for h_{veg}=40 cm is presented in Figure 55.

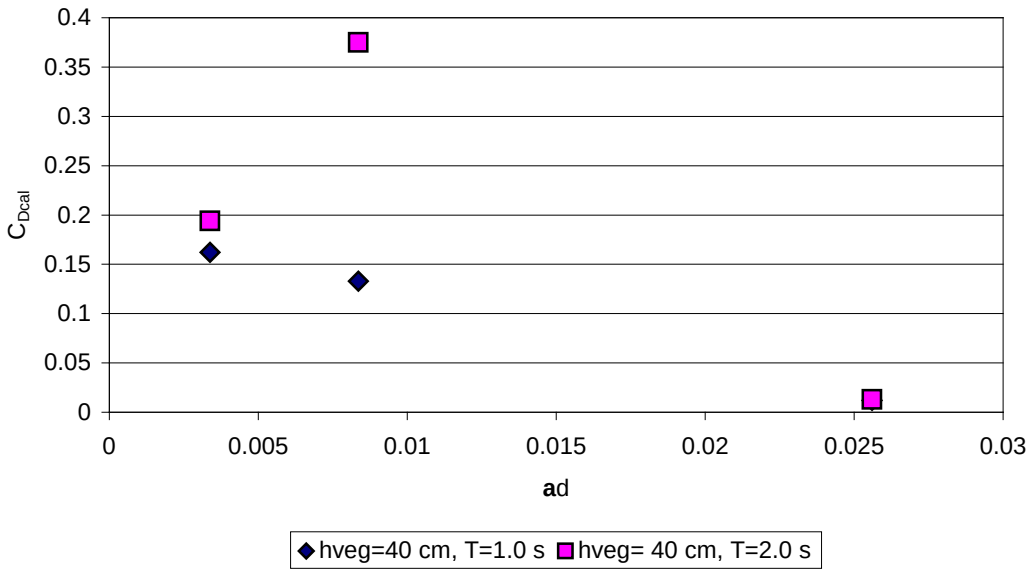

Figure 55. C_{Dcal} versus **a**d, [h_{veg}=40 cm]

Based on the concept of wake sheltering from *Nepf* (1999), it was expected C_{Dcal} would decrease with higher density, represented by a higher **a**d. This hypothesis is observed for T=1.0 s. However, for T=2.0 s, C_{Dcal} follows the anticipated trend except for the intermediate density array where C_{Dcal} is much higher than that of the lowest and highest density. It is difficult to form a conclusive statement regarding the influence of stem

density on the vegetation field bulk drag coefficient within this thesis without additional wave conditions, but it is anticipated the wake sheltering concept should hold if further experiments were conducted. The C_{Dcal} associated with the intermediate density appears unusually high when compared to other C_{Dcal} values so it is possible this value could be an anomaly.

Table 15 summarizes the calibrated bulk drag coefficient for the two-dimensional wave flume with an example of modeling results presented in Figure 56. Model results for other tested conditions for the two-dimensional flume are available in Appendix B.

Table 15. Vegetation field C_{Dcal} for two-dimensional flume

h_{veg} (cm)	H_{wm} (cm)	T (s)	C_{Dcal}	
			7 cm-20%	7 cm-40%
29.2	7.4	1.0	0.042	0.111
	6.8	1.6	0.021	0.013
	5.3	2.0	0.07	0.102
17.2	5.2	1.0	0.063	0.066
	4.8	1.6	0.0	0.087
	3.9	2.0	0.089	0.018

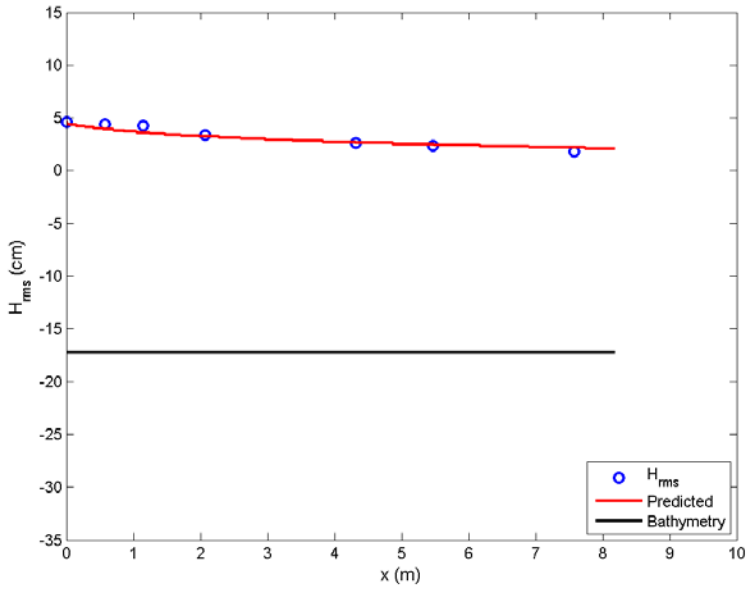

Figure 56. Predicted wave heights, [h_{veg}=17.2 cm, H_{wm}=4.8 cm, T=1.6 s, 7 cm-20%, C_{Dcal}=0.087]

The results for the Haynes Coastal Engineering Laboratory and two-dimensional wave flume will be presented jointly to investigate the influence of spacing uniformity on C_{Dcal}. The values of C_{Dcal} versus normalized stem spacing standard deviation for the Haynes Coastal Engineering Laboratory and flume experiments are presented in Figure 57 and Figure 58, respectively. The value of C_{Dcal} increased with higher normalized standard deviation for the majority of the conditions, agreeing with the marsh-scale wave height attenuation results obtained from the experiments. As stem spacing becomes more random, fewer cylinders are inline and may clump together such that the bulk drag coefficient increases due to less wake sheltering effects on individual downstream stems or turbulence is generated at the clump diameter rather than the stem diameter. Given that the bulk drag coefficient is a value for the average drag within the vegetation field, a

larger bulk drag coefficient translates into greater wave attenuation.

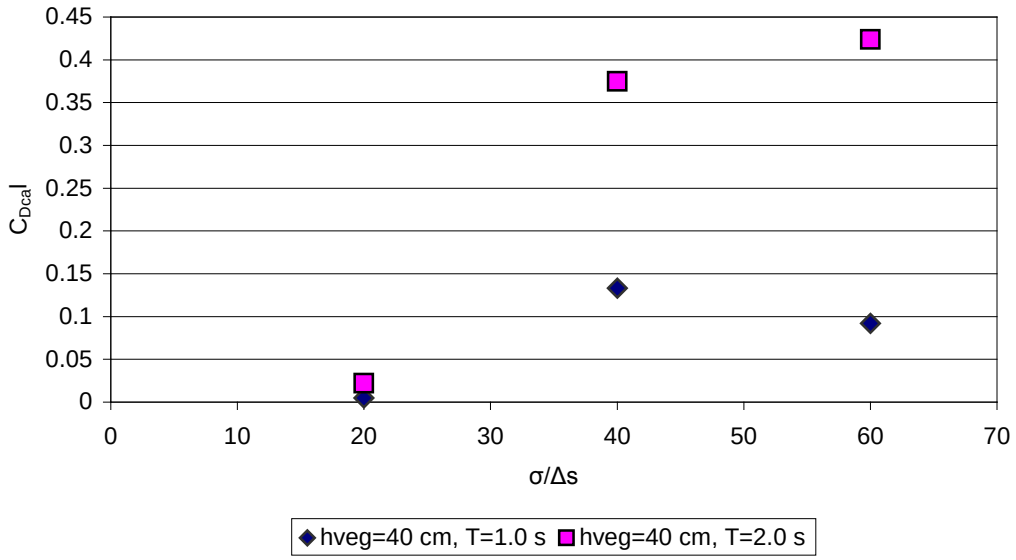

Figure 57. C_{Dcal} versus normalized stem spacing standard deviation for basin

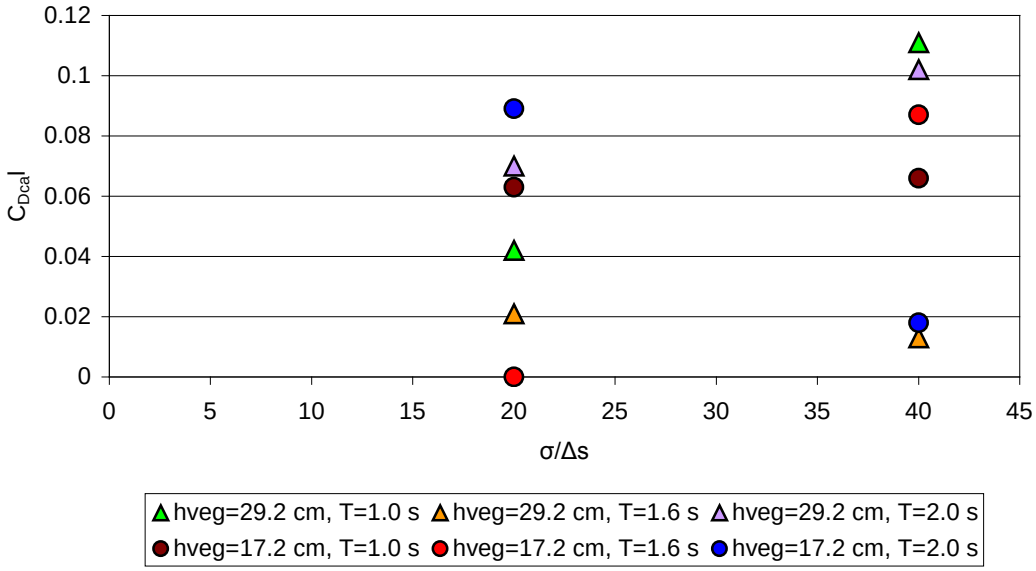

Figure 58. C_{Dcal} versus normalized stem spacing standard deviation for flume

In summary, the parameters investigated within this thesis (stem length to water depth ratio, stem density, and stem spacing standard deviation) affect the vegetation field bulk drag coefficient as well as the total wave attenuation. While the bulk drag coefficient and total wave attenuation both increase with higher l_s/h ratios and larger stem spacing standard deviation, the opposite relationship is seen with stem density whereby higher densities result in a lowering of the bulk drag coefficient but generally greater wave attenuation. This occurs because the relative decrease in the bulk drag coefficient is less than the relative increase in stem density such that the total drag increases with stem density.

CHAPTER VI

CONCLUSIONS

6.1. Conclusions

Experiments were conducted in the three-dimensional basin at the Haynes Coastal Engineering Laboratory and a two-dimensional wave flume in order to assess the influence of relative vegetation height, stem density, and stem spacing uniformity on wave dissipation. For both experiments, the amount of wave dissipation was highly dependent on the stem length to water depth ratio. As stems occupy more of the water column and approach l_s/h=1.0, less energy is transmitted through the vegetation field, directly translating into reduced wave heights. Emergent conditions are expected to dissipate the most wave energy because the plant stems occupy the entire water column and slow the highest wave particle velocities, generating the most drag. Wave attenuation was also found to be dependent on stem spacing, and thus, stem density. For h_{veg}=40 cm, the sparser vegetation fields resulted in the least amount of attenuation followed by the highest density while the intermediate density dissipated the most amount of wave energy. While it was originally anticipated that wave attenuation would continue to increase with increasing density, the denser array at 625 stems/m^2 appears to reach a maximum threshold where the wave attenuation is reduced due to flow possibly being diverted over the field rather than through it. Applying this to field conditions, healthy wetlands would be more efficient at dissipating wave energy than unhealthy wetlands due to a higher stem density, as long as the density did not exceed an unnatural maximum threshold. Lastly, spacing uniformity also influences the amount of wave

dissipation. As standard deviation of spacing increases, wave dissipation also increases. This is believed to result from wake sheltering, an interaction between upstream and downstream cylinders whereby upstream cylinders reduce the drag on downstream cylinders due to a reduced flow velocity. Higher standard deviations mean the placement of the stems is more random, which in turn lessens the probability of stems being aligned, increases grouping, and lowers the probability of wake sheltering on individual downstream stems. Another hypothesis for this dependence is larger-scale wakes are generated at the stem clump diameter rather than the individual stem diameter. For both hypotheses, drag on downstream stems increases with less wake sheltering and therefore result in greater wave attenuation at the marsh-scale.

A one-dimensional model based on linear theory was used to replicate the experiments by implementing a vegetation dissipation term developed by *Dalrymple et al.* (1984). Relative vegetation height and stem spacing standard deviation affected the vegetation field bulk drag coefficient and total wave attenuation in the same manner. In agreement with the experiments, the calibrated values of the bulk drag coefficient increased with higher l_s/h ratios and higher stem spacing standard deviations. Under the most submerged condition, C_{Dcal} was approximately 0.0 for all vegetation fields, suggesting the little dissipation that did occur resulted from wave breaking. As expected, a decrease in C_{Dcal} for higher densities was observed in one out of two wave conditions; however, the relative increase in density is greater than the relative decrease in the bulk drag coefficient so greater attenuation is generally expected with a higher density.

6.2. Recommendations

Recommendations for future research are focused on improving the understanding of wave transformations through emergent and submerged vegetation as well as more realistically modeling these transformations. Ideas for future research based on the context of this thesis are the following:

- Derive and implement a vegetation dissipation term that accounts for stem spatial variation.
- Conduct laboratory measurements on a wider range of vegetation characteristics, such as wider diameters, increased flexibility, and simulating leafy parts. This study focuses on one diameter wooden cylinders, and it would be interesting to see how flexibility and leaf drag would influence wave attenuation.
- Investigate the potential of wave attenuation to decrease after stem density exceeds some maximum threshold to verify the hypothesis presented herein.
- Investigate the influence of stem spatial distribution by comparing the wave attenuation over random arrays and patches of stems.
- Parameterize the drag coefficient as a function of vegetation characteristics to allow estimation of wave damping for future practical engineering purposes.

REFERENCES

Asano, T., H. Deguchi, and N. Kobayashi (1992), Interactions between water waves and vegetation, in *Proceedings of the 23rd International Conference on Coastal Engineering,* edited by B.L. Edge, pp. 2710-2723, American Society of Civil Engineers, Venice, Italy.

Asano, T., S. Tsutsui, and T. Sakai (1988), Wave damping characteristics due to seaweed, in *Proceedings of the 35th Coastal Engineering Conference in Japan,* pp. 138-142, Japanese Society of Civil Engineers, Matsuyama, Japan (in Japanese).

Augustin, L.N. (2007), Laboratory experiments and numerical modeling of wave attenuation through artificial vegetation, M.S. thesis, Texas A&M University, College Station, Texas.

Battjes, J.A., and J. P. F.M Janssen (1978), Energy loss and set-up due to breaking of random waves, in *Proceedings of the 16th International Conference on Coastal Engineering,* pp. 569-587, American Society of Civil Engineers, Hamburg, Germany.

Camfield, F.E. (1977), A method for estimating wind-wave growth and decay in shallow water with high values of bottom friction, *Coastal Engineering Technical Aid No. 77-6,* United States Army Corps of Engineers, Fort Belvoir, Virginia.

Code of Federal Regulations, Title 40: Protection of the Environment, Subchapter H, Section 230.3(t), Office of the Federal Register, Washington D.C.

Cooper, N.J. (2005), Wave dissipation across intertidal surfaces in the Wash Tidal Inlet, Eastern England, *Journal of Coastal Research, 21*(1), 28-40.

Dalrymple, R.A., J. T. Kirby, and P.A. Hwang (1984), Wave diffraction due to areas of energy dissipation, *Journal of Waterway, Port, Coastal, and Ocean Engineering, 110*(1), 67-79.

Dean, R.G. (1979), Wetland functions and values: the state of our understanding, effects of vegetation on shoreline erosional processes, in *Proceedings of the National Symposium on Wetlands,* pp. 415-426, American Water Resources Association, Lake Buena Vista, Florida.

Dean, R.G., and C.J. Bender (2006), Static wave setup with emphasis on damping effects by vegetation and bottom friction, *Coastal Engineering, 53,* 149-156.

Dean, R.G., and R.A. Dalrymple (1984), *Water Wave Mechanics for Engineers and Scientists,* World Scientific Publishing, Hackensack, New Jersey.

Dean, R.G., and R.A. Dalrymple (2004), *Coastal Processes with Engineering Applications*, Cambridge University Press, New York.

Dubi, A. (1995), Damping of water waves by submerged vegetation: A case study on *Laminaria hyperborea*, Ph. D thesis, University of Trondheim, Trondheim, Norway.

Elwany, M.H.S., W. O'Reilly, R.T. Guza, and R.E. Flick (1995), Effects of southern California kelp beds on waves, *Journal of Waterway, Port, Coastal, and Ocean Engineering, 121*(2), 143-150.

Feagin, R.A., J.L. Irish, I. Möller, A.M. Williams, and M.E. Mousavi (in review), Short communication: engineering properties of wetland plants with application to wave attenuation, *Coastal Engineering*.

Fonseca, M.S., and J.A. Cahalan (1992), A preliminary evaluation of wave attenuation by four species of seagrass, *Estuarine, Coastal, and Shelf Science, 35*, 565-576.

Goring, D.G., and V.I. Nikora (2002), Despiking acoustic Doppler velocimeter data, *Journal of Hydraulic Engineering, 128*(1), 117-126.

Kadlec, R.H. (1990), Overland flow in wetlands: vegetation resistance, *Journal of Hydraulic Engineering, 116*(5), 691-706.

Kobayashi, N., A.W. Raichle, and T. Asano (1993), Wave attenuation by vegetation, *Journal of Waterway, Port, Coastal, and Ocean Engineering, 119*(1), 30-48.

Knutson, P.L., R.A. Brochu, W.N. Seelig, and M. Inskeep (1982), Wave damping in *Spartina alterniflora* marshes, *Wetlands, 2*(1), 87-104.

Lima, S.F., C.F. Neves, and N. Rosauro (2006), Damping of gravity waves by fields of flexible vegetation, in *Proceedings of the 30th International Conference on Coastal Engineering*, edited by J.M. Smith, pp. 491-503, American Society of Civil Engineers, San Diego, California.

Løvås, S.M. (2000), Hydro-physical conditions in kelp forests and the effect on wave damping and dune erosion: A case study on *Laminari*a *hyperborea*, Ph. D. thesis, University of Trondheim, Trondheim, Norway.

Løvås, S.M., and A.Tørum (2000). Effect of submerged vegetation upon wave damping and run-up on beaches: A case study on *Laminaria hyperborean*, in *Proceedings of the 27th International Conference on Coastal Engineering*, edited by B.L. Edge, pp. 851-864, American Society of Civil Engineers, Sydney, Australia.

Mendez, F.J., and I.J. Losada (1999). Hydrodynamics induced by wind waves in a vegetation field, *Journal of Geophysical Research, 104* (C8), 18,383-18,396.

Mendez, F.J., and I.J. Losada (2004), An empirical model to estimate the propagation of random breaking and nonbreaking waves over vegetation fields, *Coastal Engineering, 51,* 103-118.

Möller, I. (2006), Quantifying saltmarsh vegetation and its effect on wave height dissipation: Results from a UK East coast saltmarsh, *Estuarine, Coastal, and Shelf Science, 69,* 337-35l.

Möller, I., and T. Spencer (2002), Wave dissipation over macro-tidal saltmarshes: Effects of marsh edge typology and vegetation change, *Journal of Coastal Research, SI36,* 506-521.

Möller, I., T. Spencer, J.R. French, D.J. Leggett, and M. Dixon (1999), Wave transformation over salt marshes: A field and numerical modelling study from North Norfolk, England, *Estuarine, Coastal, and Shelf Science, 49,* 411-426.

Morison, J.R., M.P. O'Brien, J.W. Johnson, and S. Schaaf (1950), The force exerted by surface waves on piles, *Petroleum Transactions, 189,* 149-154.

Natural Resources Conservation Service (2002), Smooth cordgrass plant fact sheet, date accessed, 30 April 2010, < http://plants.usda.gov/factsheet/pdf/fs_spal.pdf>.

Nepf, H.M. (1999), Drag, turbulence, and diffusion in flow through emergent vegetation, *Water Resources Research, 32*(2), 479-489.

Nepf, H.M. (2004), Vegetated flow dynamics, in *The Ecogeomorphology of Tidal Marshes*, edited by S. Fagherazzi, M. Marani, and L.K. Blum, pp. 137-163, American Geophysical Union, Washington, D.C.

Neumeier, U., and P. Ciavola (2004), Flow resistance and associated sedimentary processes in a *Spartina maritime* salt-marsh, *Journal of Coastal Research, 20*(2), 435-447.

Seymour, R.J. (1996), Discussion on "Effects of southern California kelp beds on waves", *Journal of Waterway, Port, Coastal, and Ocean Engineering, 122*(2), 207-208.

Sorensen, R.M. (2006), *Basic Coastal Engineering*, Springer Science, New York.

Texas A&M University (1981), Hydromechanics Laboratory Manual, obtained from the Civil Engineering Laboratory building on February 23, 3010.

Texas A&M University (2004), Haynes Coastal Engineering Laboratory, date accessed, 13 March 2010, < http://coastal.tamu.edu/facilities-shallowwater.html>.

Tiner, R.W., (1993), *Field Guide to Coastal Wetland Plants of the Southeastern United States,* The University of Massachusetts Press, Amherst, Massachusetts.

Türker, U., O. Yagci, and M.S. Kabdaşli (2006), Analysis of coastal damage of a beach profile under the protection of emergent vegetation, *Ocean Engineering, 33,* 810-828.

United States Environmental Protection Agency (2006), Economic Benefits of Wetlands, date accessed, 1 May 2010, < http://www.epa.gov/owow/wetlands/pdf/EconomicBenfits.pdf>.

APPENDIX A

CALIBRATED BREAKING INDICES

HAYNES COASTAL ENGINEERING LABORATORY

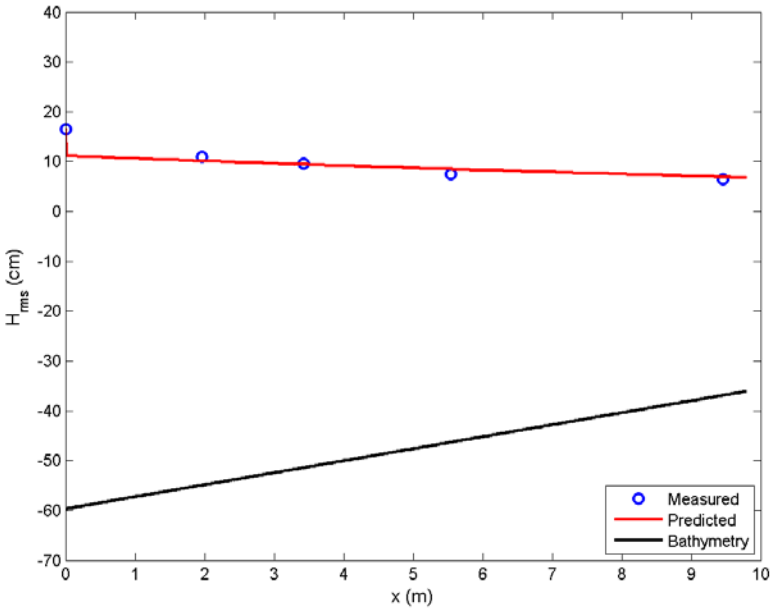

[h_{veg}= 60 cm, H_{wm}=28.0 cm, T=2.0 s, κ_{cal}=0.187]

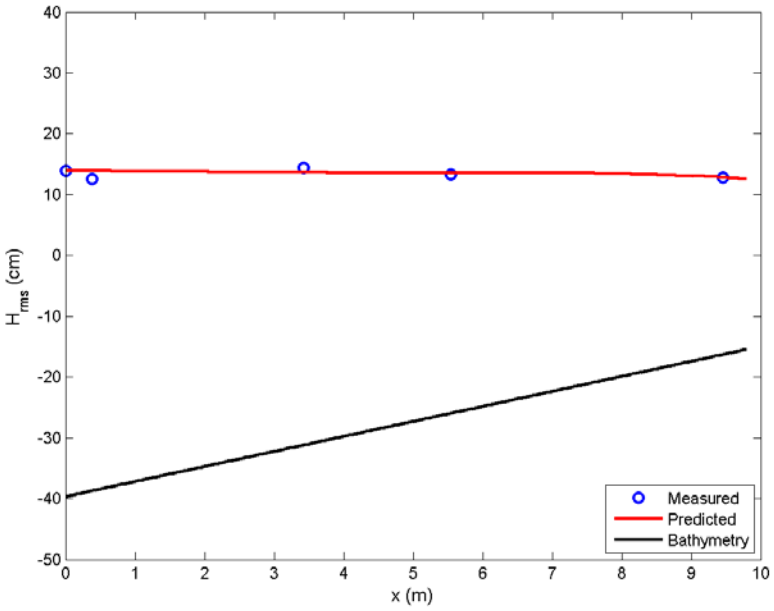

[h_{veg}=40 cm, H_{wm}=28.0 cm, T=1.0 s, κ_{cal} =1.046]

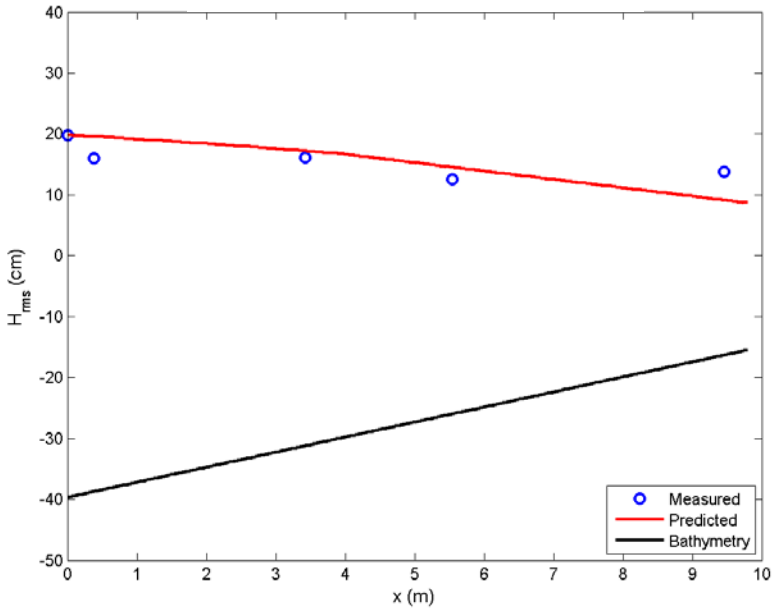

[h_{veg}=40 cm, H_{wm}=28.0cm, T=2.0 s, κ_{cal} =0.558]

TWO-DIMENSIONAL WAVE FLUME

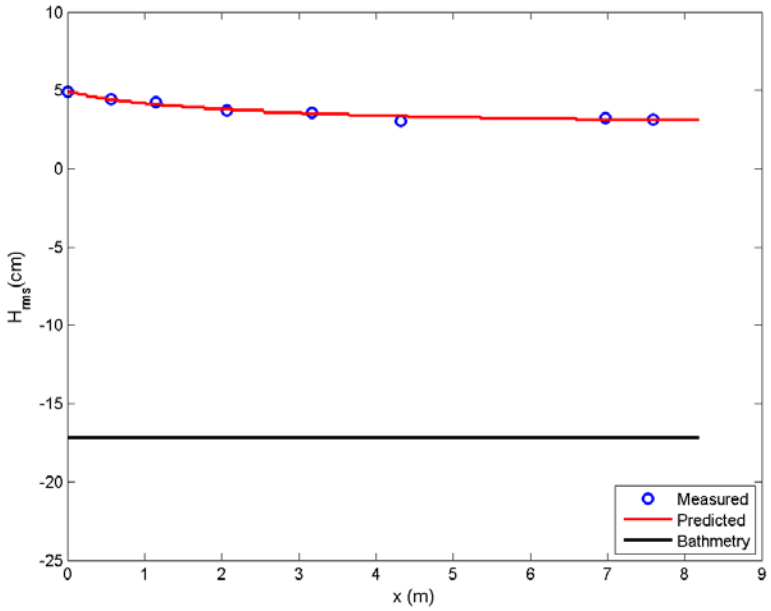

[h_{veg}=17.2 cm, H_{wm}=5.2 cm, T=1.0 s, κ_{cal}=0.284]

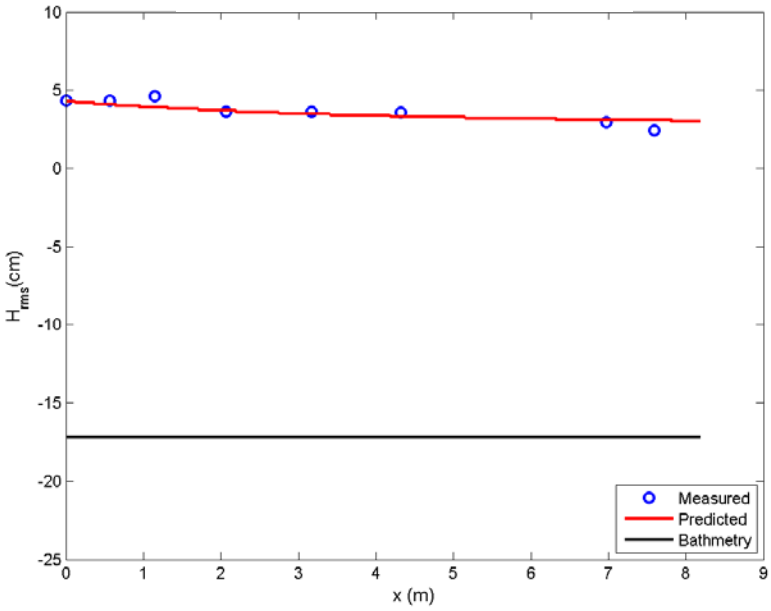

[h_{veg}=17.2 cm, H_{wm}=4.8 cm, T=1.6 s, κ_{cal}=0.255]

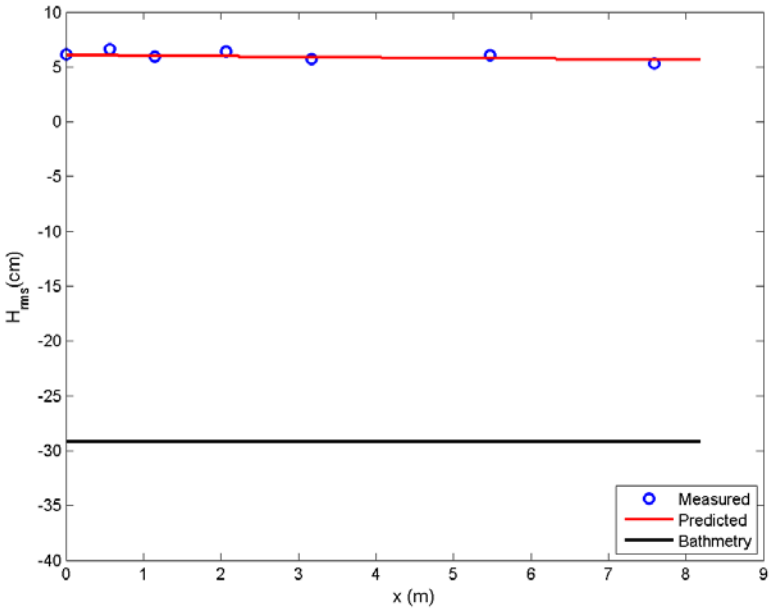

[h_{veg}=29.2 cm, H_{wm}=7.4 cm, T=1.0 s, κ_{cal}=0.346]

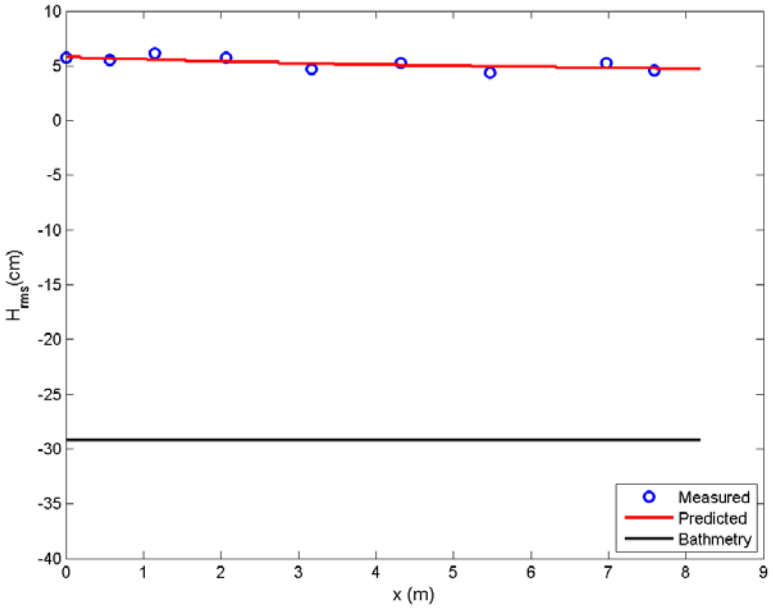

[h_{veg}=29.2 cm, H_{wm}=6.8 cm, T=1.6 s, κ_{cal}=0.237]

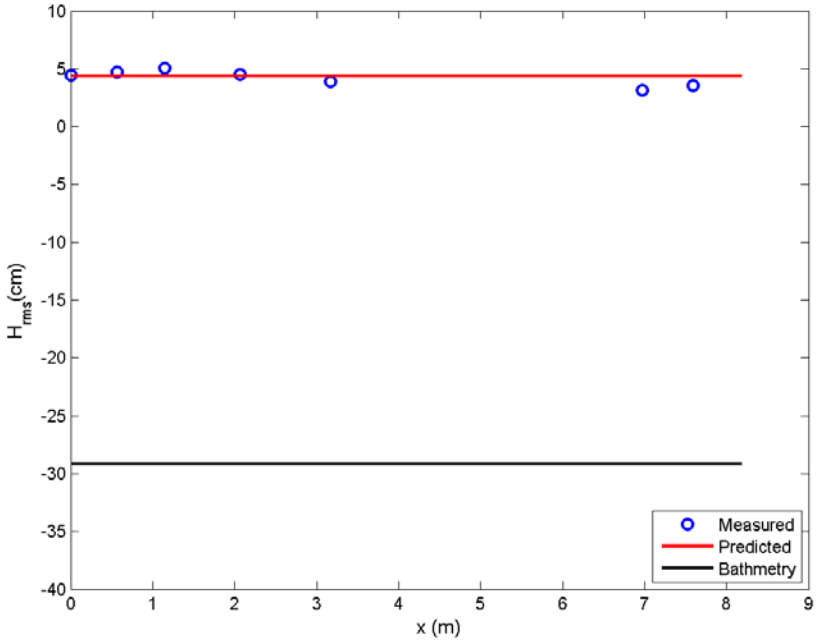

[h_{veg}=29.2 cm, H_{wm}=5.3 cm, T=2.0 s, κ_{cal}=0.392]

APPENDIX B

CALIBRATED BULK DRAG COEFFICIENTS

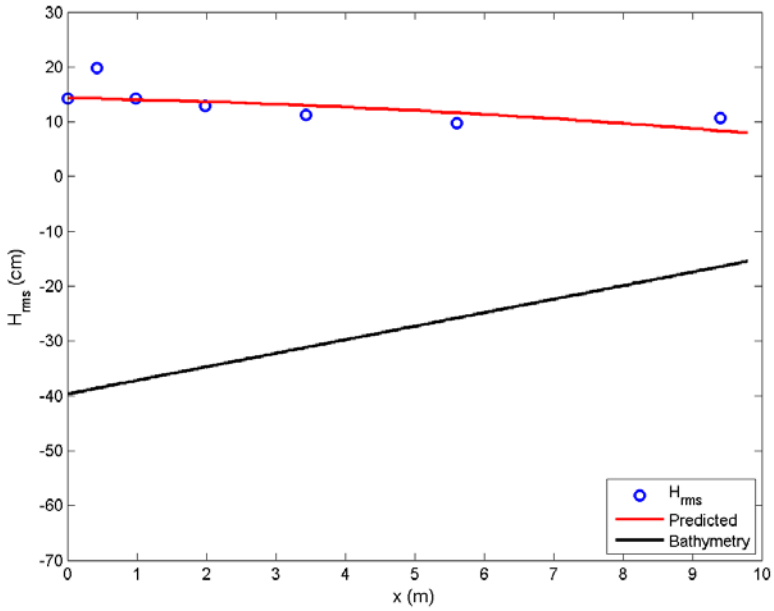

[h_{veg}=40 cm, H_{wm}=28.0 cm, T=2.0 s, 4 cm-40%, C_{Dcal}=0.013]

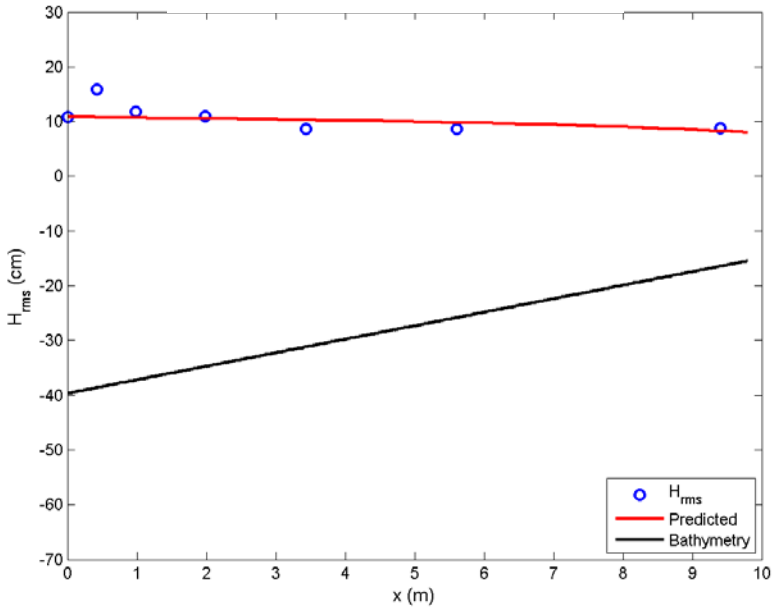

[h_{veg}=40 cm, H_{wm}=28.0 cm, T=1.0 s, 4 cm-40%, C_{Dcal}=0.012]

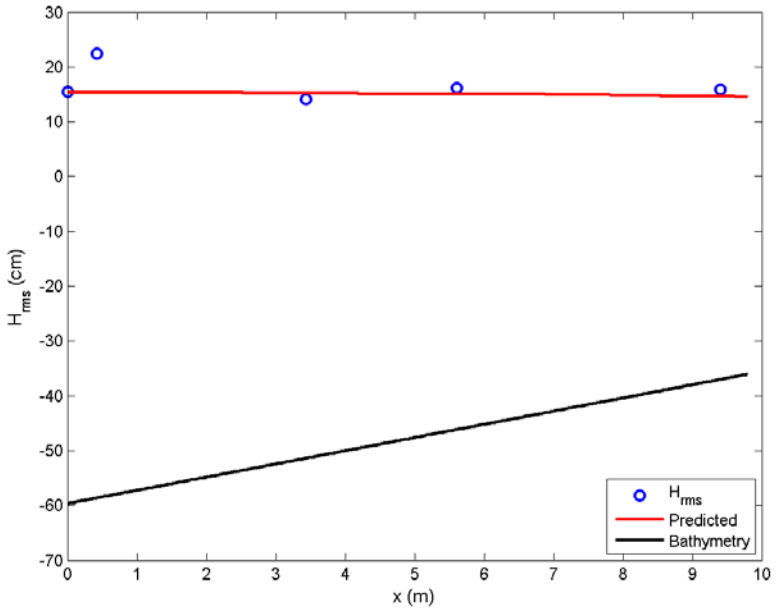

[h_{veg}=60 cm, H_{wm}=28.0 cm, T=1.2 s, 4 cm-40%, C_{Dcal}=0.0]

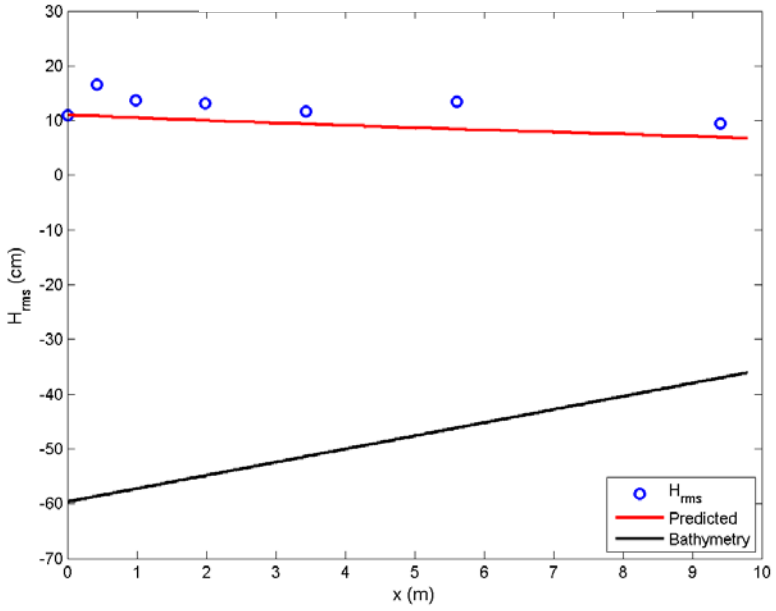

[h_{veg}=60 cm, H_{wm}=28.0 cm, T=2.0 s, 4 cm-40%, C_{Dcal}=0.0]

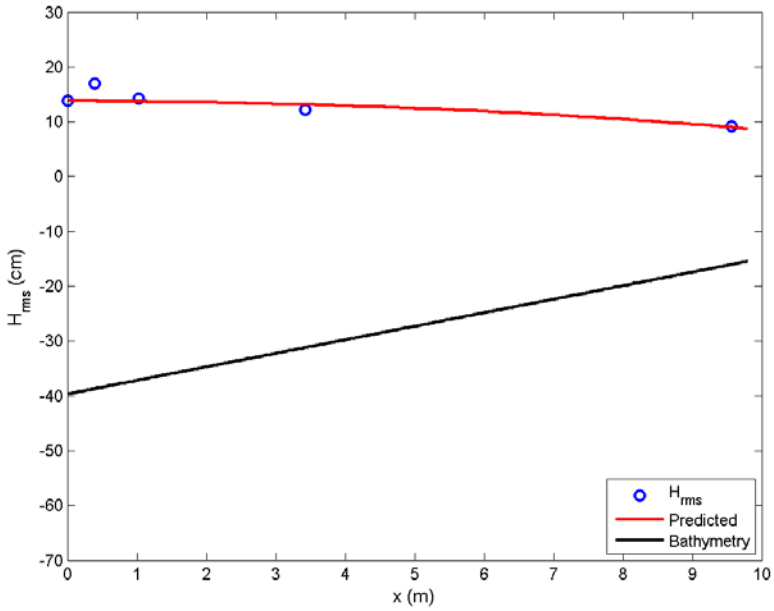

[h_{veg}=40 cm, H_{wm}=28.0 cm, T=2.0 s, 7 cm-20%, C_{Dcal}=0.022]

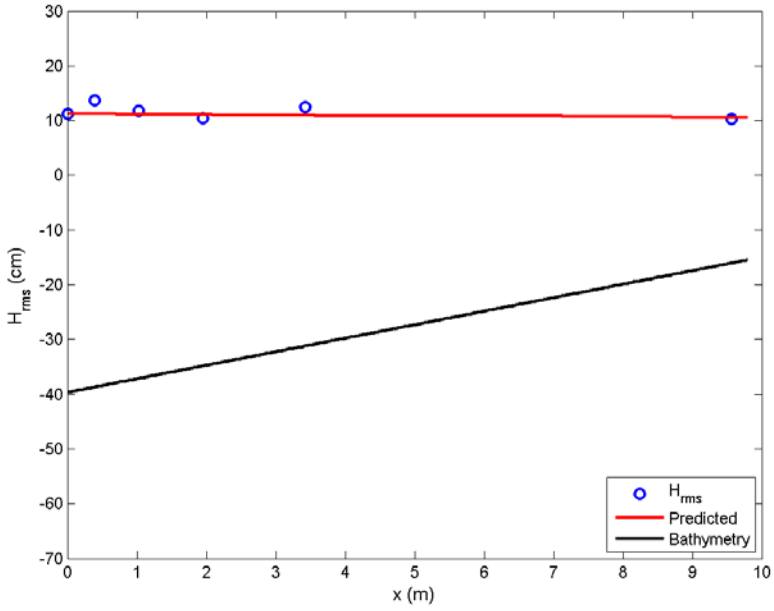

[h_{veg}=40 cm, H_{wm}=28.0 cm, T=1.0 s, 7 cm-20%, C_{Dcal}=0.005]

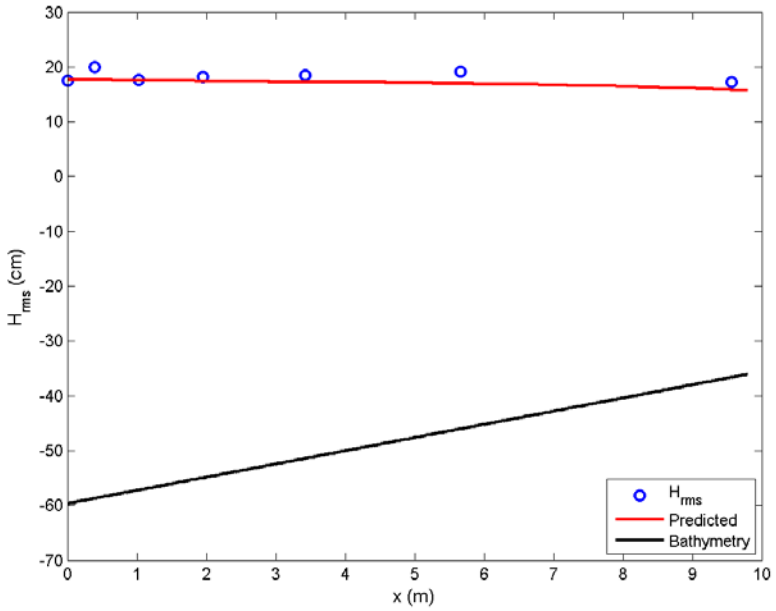

[h_{veg}=60 cm, H_{wm}=28.0 cm, T=1.2 s, 7 cm-20%, C_{Dcal}=0.0]

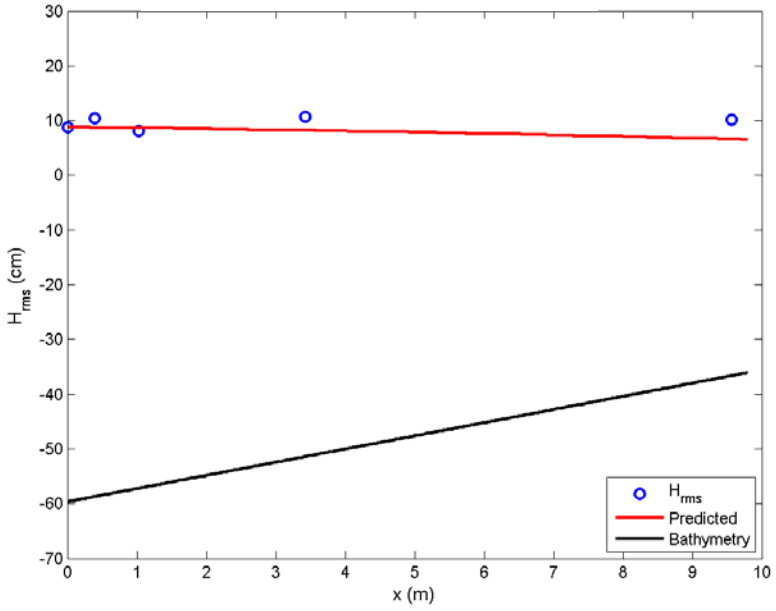

[h_{veg}=60 cm, H_{wm}=28.0 cm, T=2.0 s, 7 cm-20%, C_{Dcal}=0.0]

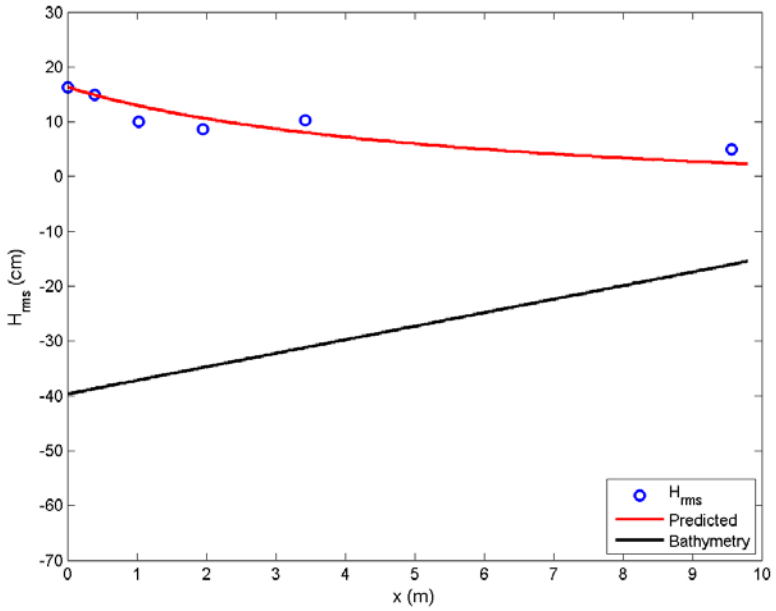

[h_{veg}=40 cm, H_{wm}=28.0 cm, T=2.0 s, 7 cm-40%, C_{Dcal}=0.375]

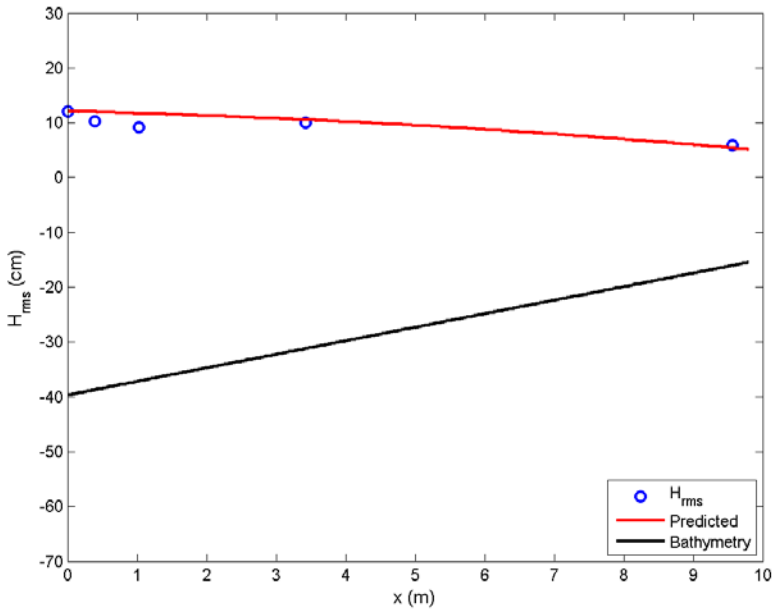

[h_{veg}=40 cm, H_{wm}=28.0 cm, T=1.0 s, 7 cm-40%, C_{Dcal}=0.133]

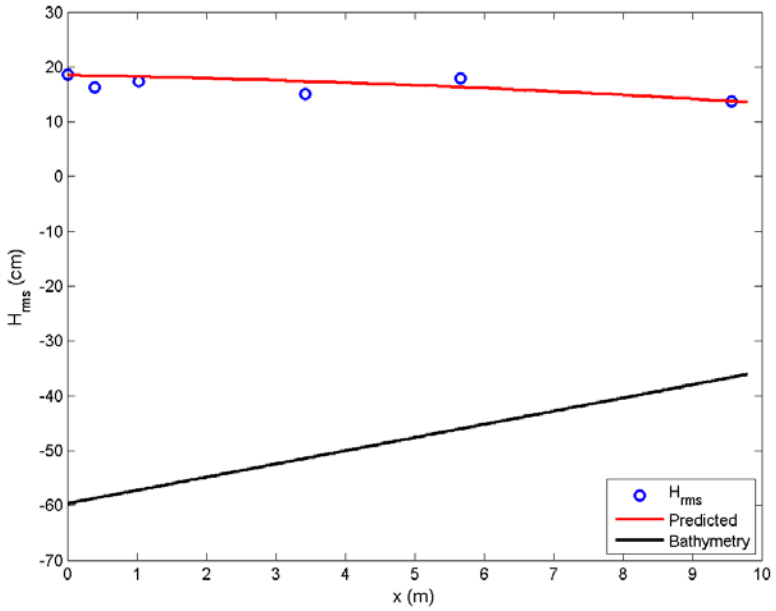

[h_{veg}=60 cm, H_{wm}=28.0 cm, T=1.2 s, 7 cm-40%, C_{Dcal}=0.04]

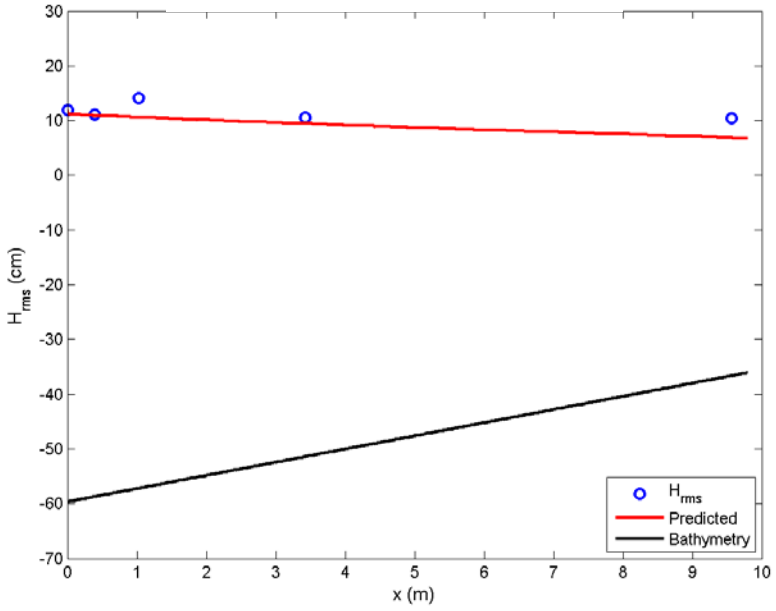

[h_{veg}=60 cm, H_{wm}=28.0 cm, T=2.0 s, 7 cm-40%, C_{Dcal}=0.0]

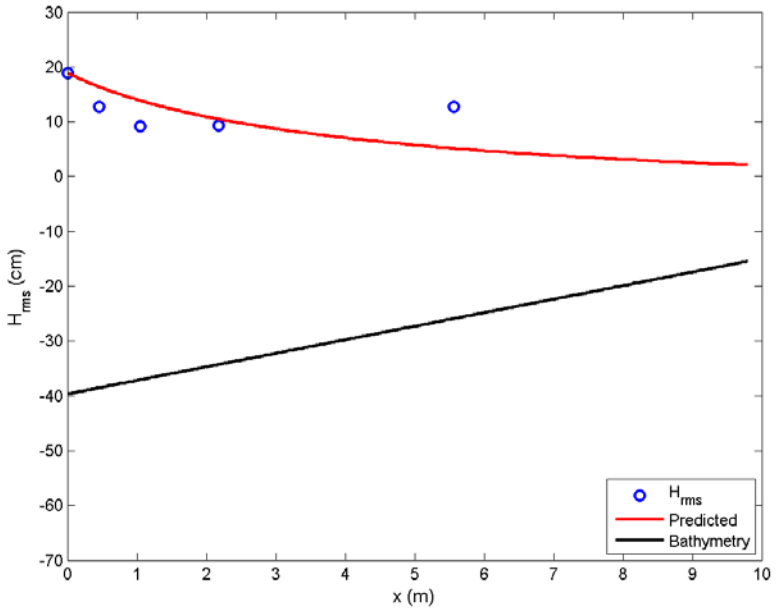

[h_{veg}=40 cm, H_{wm}=28.0 cm, T=2.0 s, 7 cm-60%, C_{Dcal}=0.424]

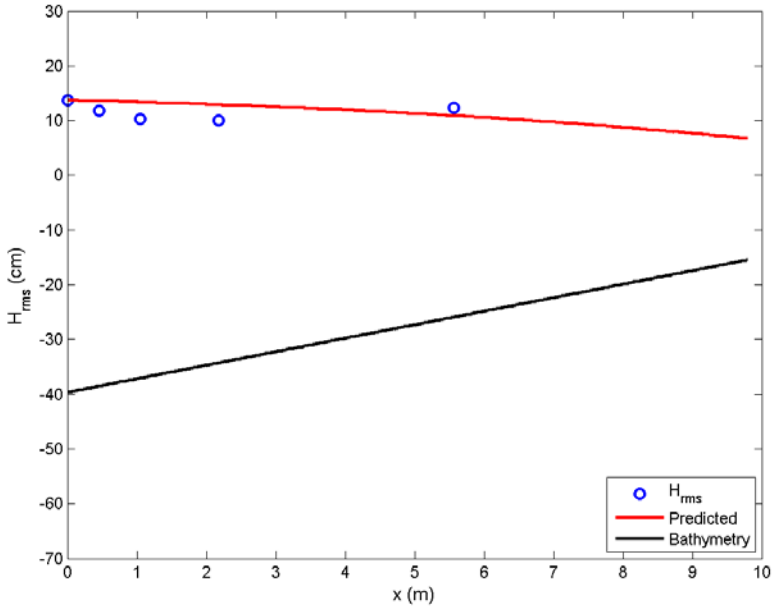

[h_{veg}=40 cm, H_{wm}=28.0 cm, T=1.0 s, 7 cm-60%, C_{Dcal}=0.092]

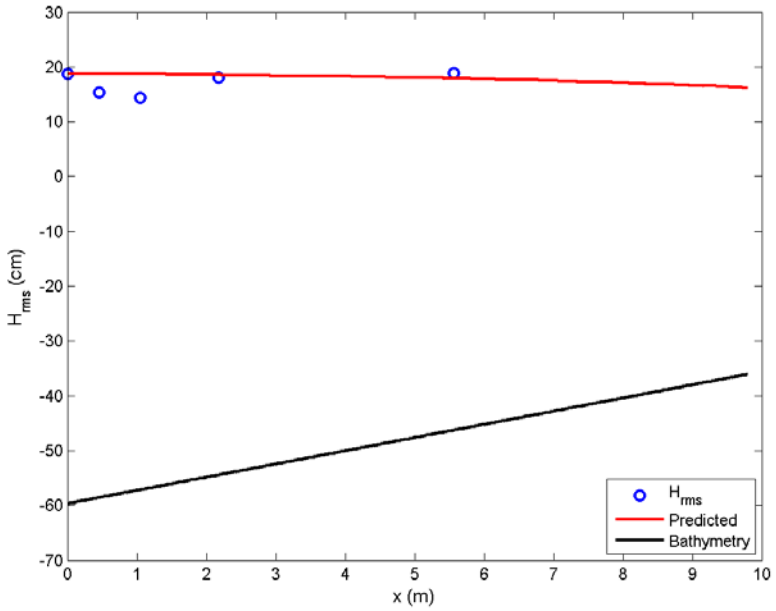

[h_{veg}=60 cm, H_{wm}=28.0 cm, T=1.2 s, 7 cm-60%, C_{Dcal}=0.0]

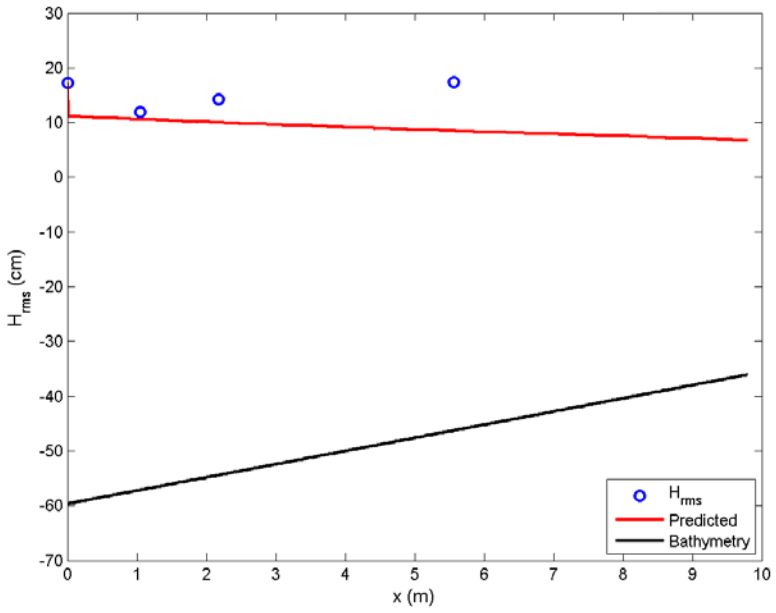

[h_{veg}=60 cm, H_{wm}=28.0 cm, T=2.0 s, 7 cm-60%, C_{Dcal}=0.0]

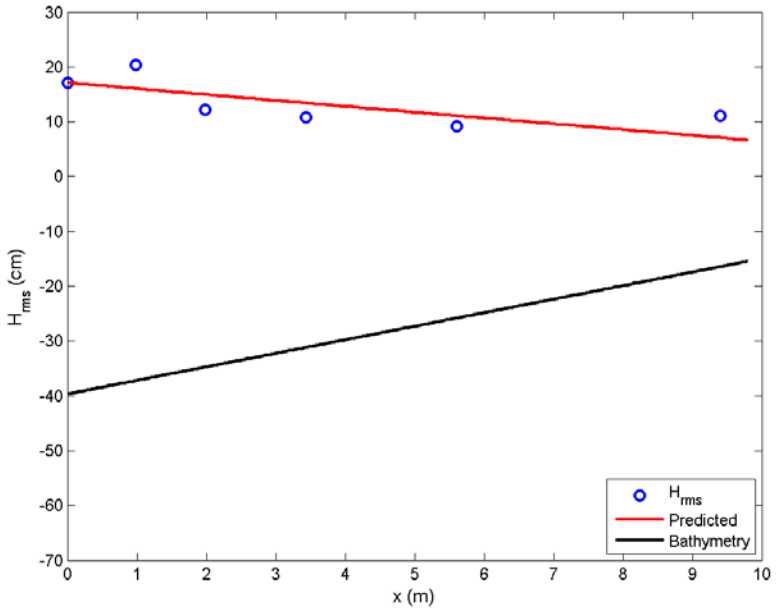

[h_{veg}=40 cm, H_{wm}=28.0 cm, T=2.0 s, 11 cm-40%, C_{Dcal}=0.194]

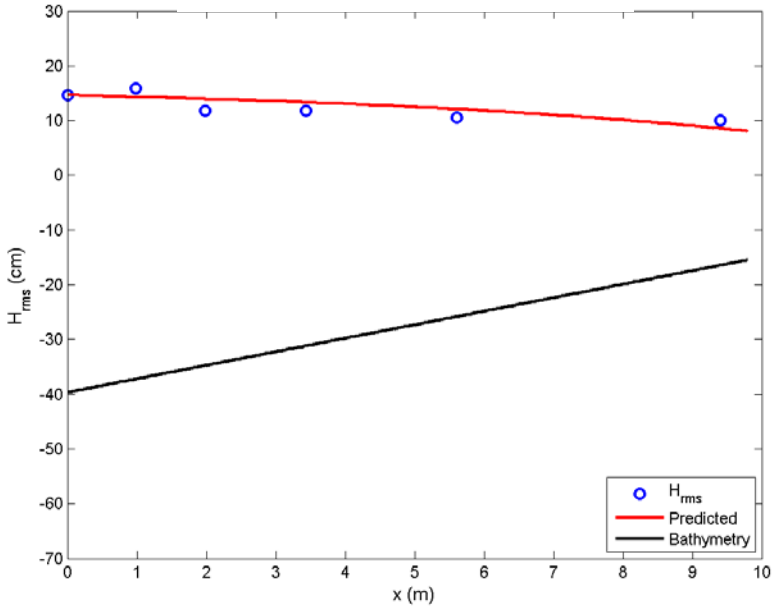

[h_{veg}=40 cm, H_{wm}=28.0 cm, T=1.0 s, 11 cm-40%, C_{Dcal}=0.162]

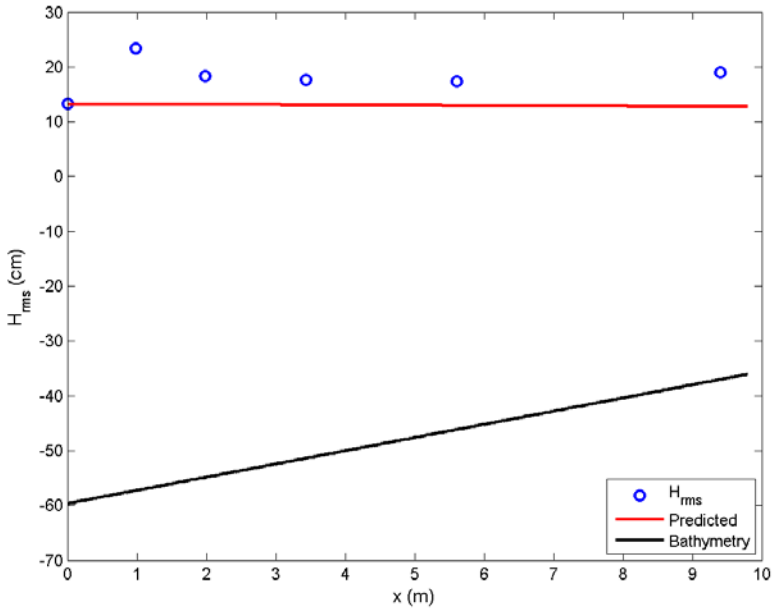

[h_{veg}=60 cm, H_{wm}=28.0 cm, T=1.2 s, 11 cm-40%, C_{Dcal}=0.0]

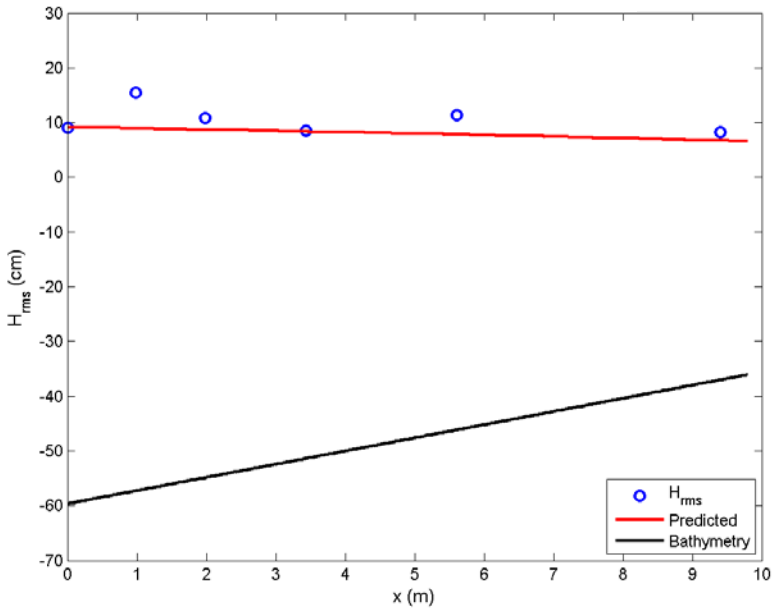

[h_{veg}=60 cm, H_{wm}=28.0 cm, T=2.0 s, 11 cm-40%, C_{Dcal}=0.0]

TWO-DIMENSIONAL WAVE FLUME

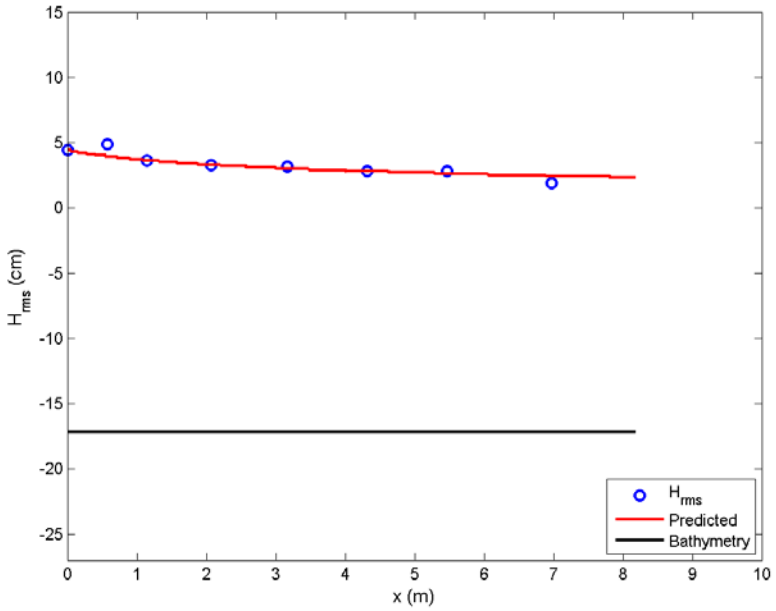

[h_{veg}=17.2 cm, H_{wm}=5.2 cm, T=1.0 s, 7 cm-20%, C_{Dcal}=0.063]

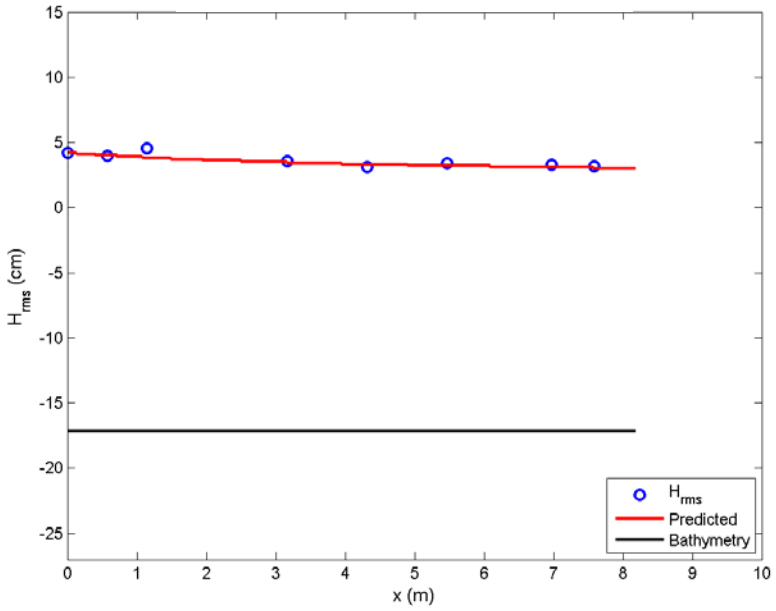

[h_{veg}=17.2 cm, H_{wm}=4.8 cm, T=1.6 s, 7 cm-20%, C_{Dcal}=0.0]

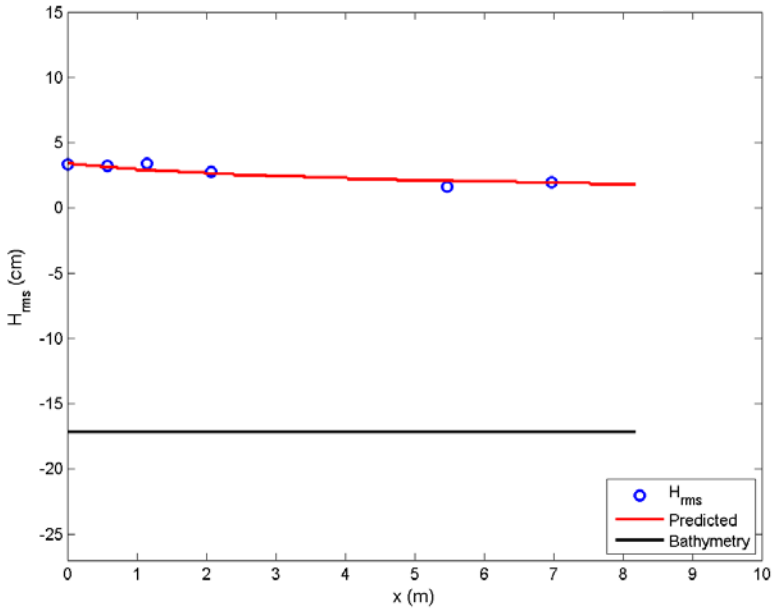

[h_{veg}=17.2 cm, H_{wm}=5.2 cm, T=2.0 s, 7 cm-20%, C_{Dcal}=0.089]

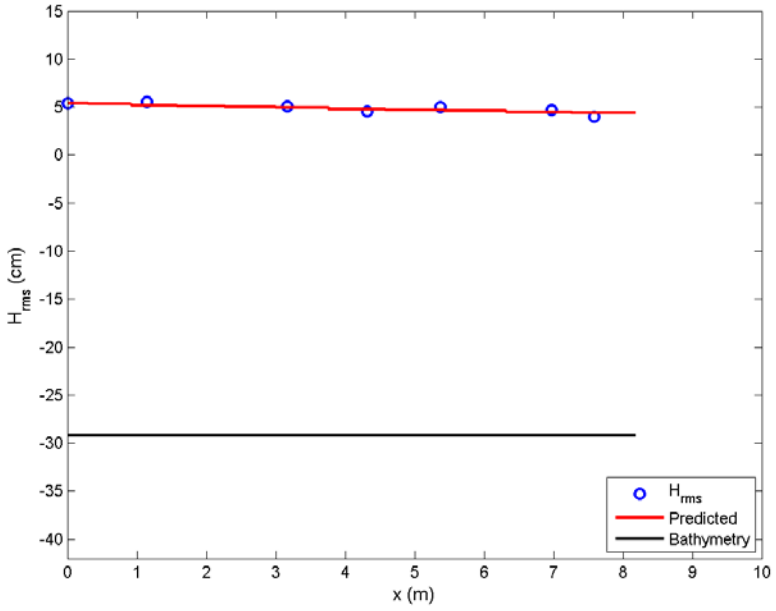

[h_{veg}=29.2 cm, H_{wm}=7.4 cm, T=1.0 s, 7 cm-20%, C_{Dcal}=0.042]

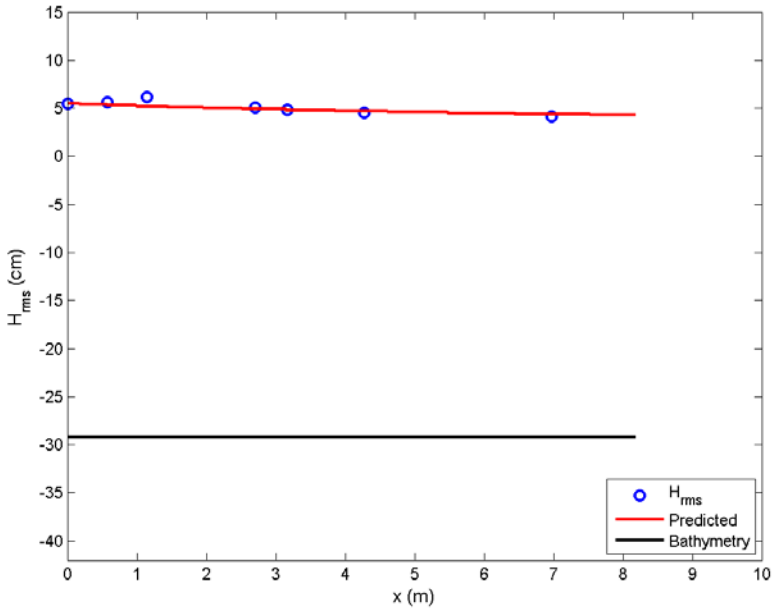

[h_{veg}=29.2 cm, H_{wm}=6.8 cm, T=1.6s, 7 cm-20%, C_{Dcal}=0.021]

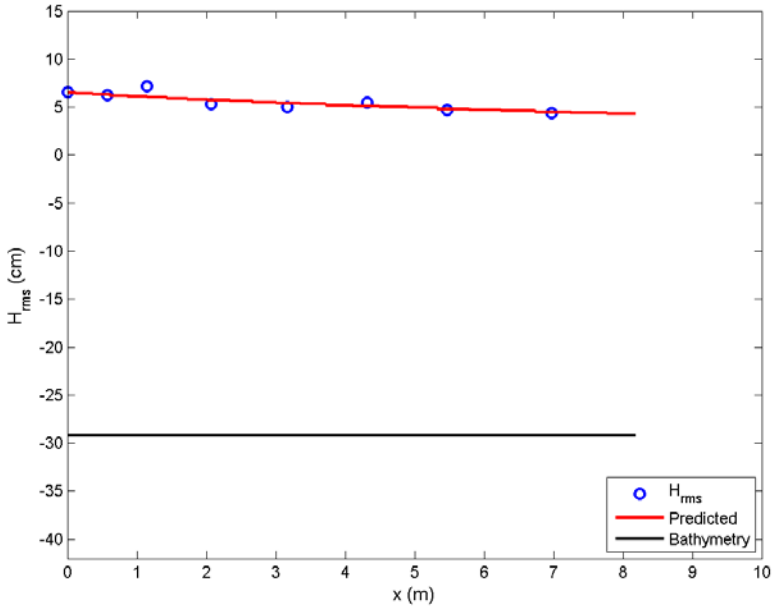

[h_{veg}=29.2 cm, H_{wm}=5.3 cm, T=2.0s, 7 cm-20%, C_{Dcal}=0.07]

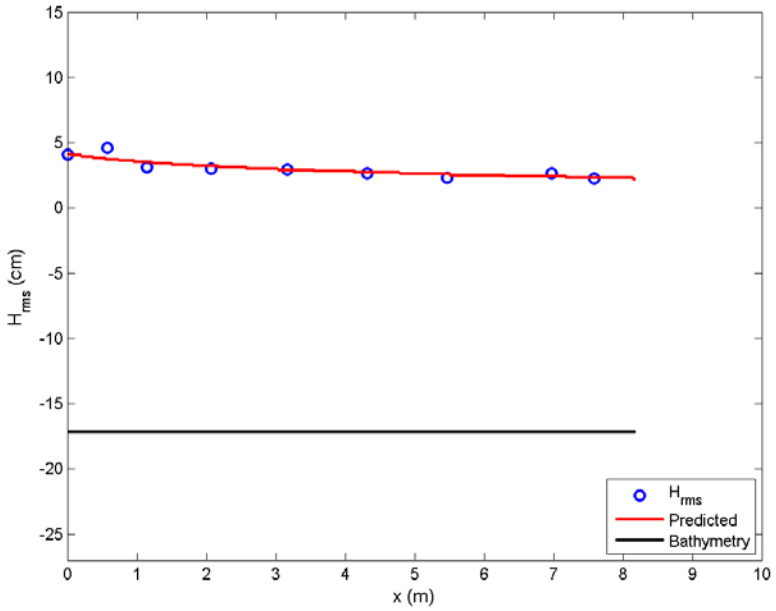

[h_{veg}=17.2 cm, H_{wm}=5.2 cm, T=1.0s, 7 cm-40%, C_{Dcal}=0.066]

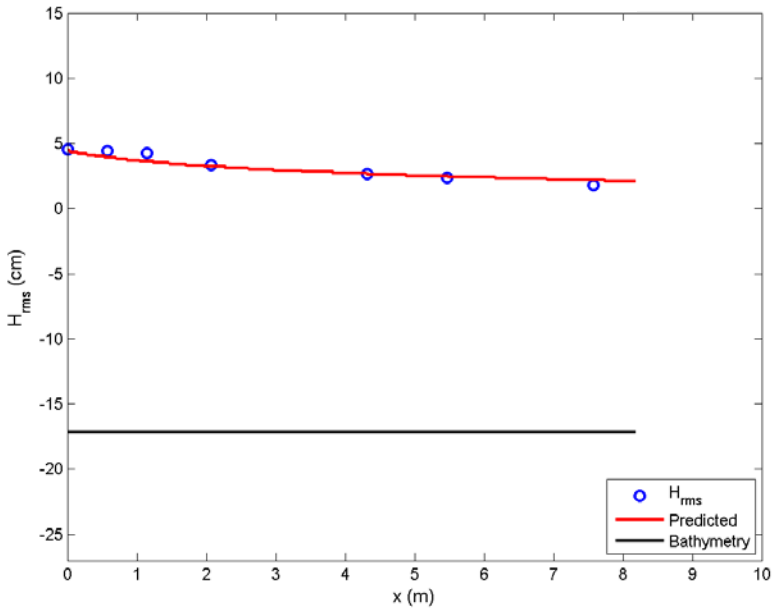

[h_{veg}=17.2 cm, H_{wm}=4.8 cm, T=1.6 s, 7 cm-40%, C_{Dcal}=0.087]

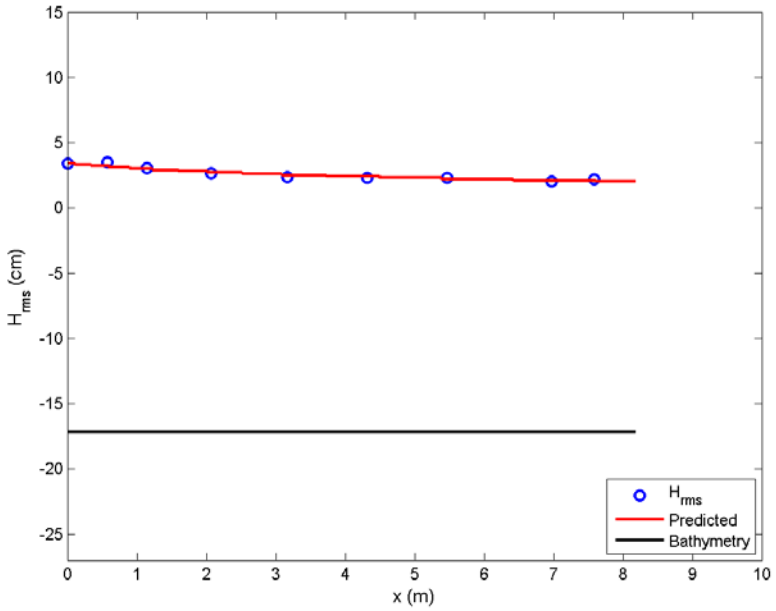

[h_{veg}=17.2 cm, H_{wm}=3.9 cm, T=2.0 s, 7 cm-40%, C_{Dcal}=0.019]

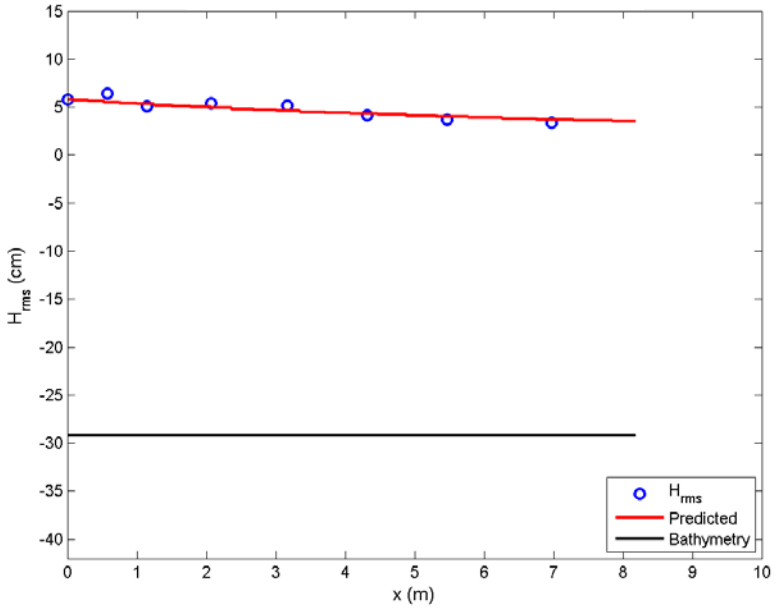

[h_{veg}=29.2 cm, H_{wm}=7.4 cm, T=1.0 s, 7 cm-40%, C_{Dcal}=0.111]

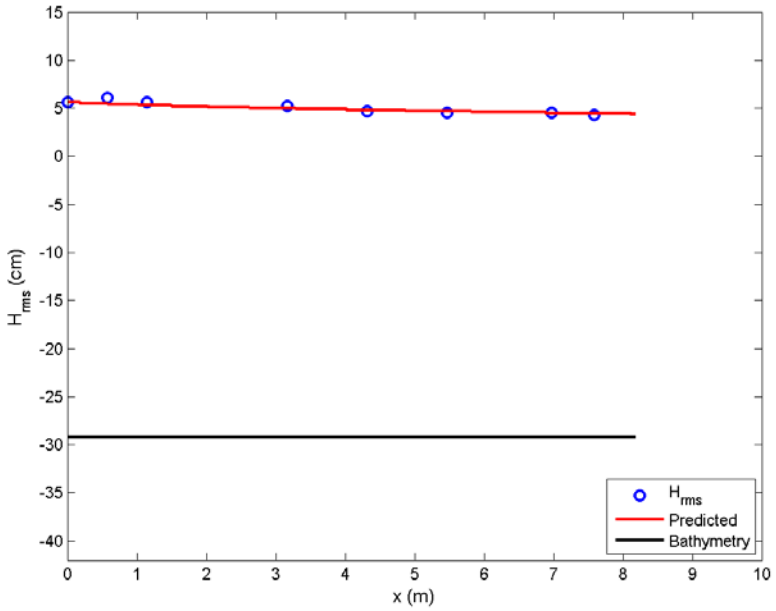

[h_{veg}=29.2 cm, H_{wm}=6.8 cm, T=1.6 s, 7 cm-40%, C_{Dcal}=0.013]

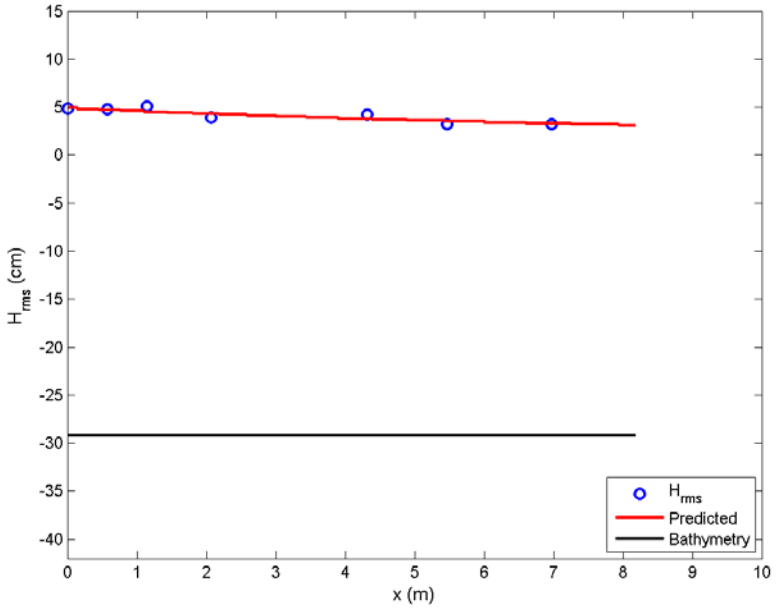

[h_{veg}=29.2 cm, H_{wm}=5.3 cm, T=2.0 s, 7 cm-40%, C_{Dcal}=0.103]

VITA

Name:	Mary Elizabeth Anderson
Email Address:	maryanderson64@gmail.com
Education:	B.S., Biological Engineering Mississippi State University, Mississippi State, MS (2008) M.S., Ocean Engineering Texas A&M University, College Station, TX (2010)
Mailing Address:	Head, Ocean Engineering Program Coastal and Ocean Engineering Division Department of Civil Engineering Texas A&M University 3136 TAMU College Station, TX 77843-3136